Western University
Scholarship@Western

Digitized Theses | Digitized Special Collections

1974

Observations Of Travelling Ionospheric Disturbances At London, Canada Using Phase-interferometry Of Solar Radio-emissions

John Litva

Follow this and additional works at: https://ir.lib.uwo.ca/digitizedtheses

Recommended Citation
Litva, John, "Observations Of Travelling Ionospheric Disturbances At London, Canada Using Phase-interferometry Of Solar Radio-emissions" (1974). *Digitized Theses*. 740.
https://ir.lib.uwo.ca/digitizedtheses/740

This Dissertation is brought to you for free and open access by the Digitized Special Collections at Scholarship@Western. It has been accepted for inclusion in Digitized Theses by an authorized administrator of Scholarship@Western. For more information, please contact tadam@uwo.ca, wlswadmin@uwo.ca.

National Library of Canada

Cataloguing Branch
Canadian Theses Division

Ottawa, Canada
K1A 0N4

Bibliothèque nationale du Canada

Direction du catalogage
Division des thèses canadiennes

NOTICE

The quality of this microfiche is heavily dependent upon the quality of the original thesis submitted for microfilming. Every effort has been made to ensure the highest quality of reproduction possible.

If pages are missing, contact the university which granted the degree.

Some pages may have indistinct print especially if the original pages were typed with a poor typewriter ribbon or if the university sent us a poor photocopy.

Previously copyrighted materials (journal articles, published tests, etc.) are not filmed.

Reproduction in full or in part of this film is governed by the Canadian Copyright Act, R.S.C. 1970, c. C-30. Please read the authorization forms which accompany this thesis.

THIS DISSERTATION
HAS BEEN MICROFILMED
EXACTLY AS RECEIVED

AVIS

La qualité de cette microfiche dépend grandement de la qualité de la thèse soumise au microfilmage. Nous avons tout fait pour assurer une qualité supérieure de reproduction.

S'il manque des pages, veuillez communiquer avec l'université qui a conféré le grade.

La qualité d'impression de certaines pages peut laisser à désirer, surtout si les pages originales ont été dactylographiées à l'aide d'un ruban usé ou si l'université nous a fait parvenir une photocopie de mauvaise qualité.

Les documents qui font déjà l'objet d'un droit d'auteur (articles de revue, examens publiés, etc.) ne sont pas microfilmés.

La reproduction, même partielle, de ce microfilm est soumise à la Loi canadienne sur le droit d'auteur, SRC 1970, c. C-30. Veuillez prendre connaissance des formules d'autorisation qui accompagnent cette thèse

LA THÈSE A ÉTÉ
MICROFILMÉE TELLE QUE
NOUS L'AVONS REÇUE

OBSERVATIONS OF TRAVELLING IONOSPHERIC DISTURBANCES AT LONDON, CANADA USING PHASE INTERFEROMETRY OF SOLAR RADIO EMISSIONS

by

John Litva

Department of Physics

Submitted in partial fulfillment

of the requirements for the degree of

Doctor of Philosophy

Faculty of Graduate Studies

The University of Western Ontario

London, Canada

December 1973

© John Litva

ABSTRACT

A new technique for observing travelling ionospheric disturbances (TIDS) and determining their parameters is presented. It consists of the measurement of TID induced phase (angle of arrival) and amplitude variations of radio waves which propagated through the ionosphere from localized regions of enhanced emission on the sun. These measurements were made with solar radio interferometers operating on a frequency of 51.7 MHz. Theoretical expressions are derived which permit one to determine the following TID parameters from the interferometer measurements:

(a) speed

(b) line of travel

(c) period

(d) wavelength

(e) height

(f) tilt

(g) electron number density perturbations

Some observations of TIDS made at London, Canada are presented. They show good evidence of TID wave trains consisting of 15 to 18 wave cycles, whereas a survey of past observations suggests that at most four cycles have been observed in TID wave trains. The angular deflections of the solar line of sight at 51.7 MHz were measured to be between ±6 to ±28 minutes of arc - in one case it was a remarkable ±50 minutes of arc - corresponding electron number density perturbations are calculated to be of the order of 1 to 2 percent. The observed variations in amplitude corresponding to the larger angle-of-arrival scintillations were about 5 dB.

The solar radio interferometer used to measure the angle-of-arrival deviations is shown to be a sensitive instrument for detecting TIDs in the ionosphere; capable of detecting TIDs with electron number density perturbations as low as one percent or less. The TIDs were observed as quasi-periodic scintillations in the angle-of-arrival of radio-waves emitted by localized disturbed regions on the solar disk. It is shown that the speed, line of travel, period and wavelength of the TIDs can be deduced from the manner in which the period and magnitude of the observed scintillations vary with time. The speed of the TIDs as a function of height is also determined by correlating the degree of amplitude fading due to defocusing and focusing effects with the maximum observed rate of change of angle-of-arrival.

Theoretical expressions are derived for determining the angle-of-arrival of signals from one and two sources using a swept lobe interferometer. Experimental results showing deviations in the angle-of-arrival of a signal from the radio source Cassiopeia A are given and shown, by application of the two source theory, to be caused by interference with a signal from the radio source Cygnus A. In addition results are given of a laboratory simulation of an interferometer system monitoring two sources. These again show good agreement with theory. A lengthy digression is made based on the two source theory to show that the measured quasi-periodic scintillations were not produced by a mechanism other than TIDs.

The sun, when emitting rf energy at an enhanced level, is shown to be an effective source for detecting TIDs. In effect, it tends

to select time intervals, for the observer, when there is a good likelihood of TIDs being present in the ionosphere. TIDs tend to be present when the ionosphere is disturbed and the ionosphere tends to be disturbed when the sun is disturbed. The fact that the sun radiates at an enhanced level, only at times when it is in a disturbed state, completes this cause effect relationship. On the other hand it is not an effective source for obtaining synoptic measurements because measurements are possible only on those infrequent occasions when the sun is radiating at an enhanced level.

The TIDs were observed on 18 days and were primarily of two types; one with a period of approximately 6 minutes, the other with the period of 21 minutes. The former travelled with the speed of about 200 km/hr and a corresponding wavelength of 20 km. The speed of the latter was between 800 and 2000 km/hr and the corresponding wavelength between 300 and 700 km; they also had a preferred line of travel which was orientated north-south. There is some evidence also of a TID with a wave period between 60 and 65 minutes. It is shown that the properties and parameters of the observed TIDs using the angle of arrival technique developed herein are consistent with observations of TIDs conducted by other workers using a variety of experimental techniques. Wave trains which are up to four times as long as the largest previously observed were observed and are documented in this thesis. In addition their properties are shown to be in agreement with those predicted by the gravity wave theory.

ACKNOWLEDGEMENTS

TABLE OF CONTENTS

LIST OF FIGURES

LIST OF TABLES

LIST OF SYMBOLS

Φ	total phase difference
ϕ, Δ	true phase differences
ϕ', Δ'	apparent phase differences
n	an integer
λ	wavelength
d	antenna separation
θ	angle between radio signal and interferometer base-line
θ_N	angle of non-terrestrial radio signal with respect to base-line
θ_S	angle between a ray from the center of the sun and the interferometer base-line
ϕ_N	phase between non-terrestrial signal received at the two interferometer antennas
θ_{SN}	angle-of-arrival $\equiv \theta_S - \theta_N$
t	time
e_1, e_1', e_1'', e_2''	rf voltage amplitudes
ω_1	angular radio frequency
Ψ	angular audio frequency of phase shifter
ϵ_1, ϵ_2	phase delays caused by cables and electronics
E_I, E_{II}	rf voltages
E_α, E_α'	resultant rf voltages
α_1, α_2	ratios of two rf voltage amplitudes
A, A_2, A_3	amplitudes of resultant rf voltages
A_1, A_{31}	audio voltages (Interferometer signals)

A_o	amplitude of the sum of two audio voltages
A_{op}	maximum (peak) audio voltage amplitude
A_{om}	minimum audio voltage amplitude
a_n, b_n	Fourier amplitude coefficients
F_n	resultant Fourier amplitude coefficient
ϕ_n	Fourier phase coefficient
ξ, ξ_1, ξ_2	amplitudes of audio voltages
β	random phase difference between two rf signals
θ_1, θ_2	phase variables for resultant voltages
γ	resultant phase variable
p, r	ratios of two rf voltage amplitudes
$\delta\phi$	phase perturbation
c	reduced amplitude
T_1, T_2, τ	time (periods)
α	right ascention
δ	declination
z	zenith angle of the sun
r	radius of the earth
D	height of ionosphere above the earth
B	distance between observer and solar ray intersection point in the ionosphere
δ	angle formed at the center of the earth
h	altitude of the sun
DEC	declination of the sun
HA	hour angle of the sun
Az	azimuthal angle of point of intersection of the ionosphere with the solar ray

S	co-latitude of intersection point
t	hour angle of intersection point
LAT(R)	latitude of intersection point
LONG(R)	longitude of intersection point
V	intersection point velocity
U	TID velocity
U'	TID velocity modified by motion of the solar line of sight
α_U	azimuthal angle of TID velocity vector
α_V	azimuthal angle of interesection point velocity vector
T'	apparent TID period
λ_t	TID wavelength
μ	refractive index
b	$\equiv 1.6 \times 10^3$ (MKS)
N	local number density of free electrons
e	charge of an electron
m	mass of an electron
ε_0	permittivity of free space
τ	angular deflection
ℓ	distance measured along ray trajectory
u	distance measured at right angles to ray trajectory
$\Delta\phi_1, \Delta\phi_2$	phase scintillations for wide and narrow E-W interferometers
$\Delta\phi_3$	phase scintillations for N-S interferomters
$\Delta\theta_{1,2}$	perturbation to θ for wide and narrow E-W interferometers
$\Delta\theta_3$	perturbation to θ for the N-S interferometer
ξ	horizontal electron number density gradient

TS	azimuth of projection of solar line of sight onto observers horizon plane
ζ	spherical angle
$F_{1,2}$	response of E-W interferometer
F_3	response of N-S interferometer
X_N, Z_N	axes of a cartesian coordinate system used to depict interferometer constant phase surfaces
e	constant ≡ 0.3098 also, angle solar ray makes with the ground
r	distance between observer and ionospheric intersection point (plane earth approximation)
H	height of intersection point
θ	angular deflection of the solar ray
ds	an element of distance measured in the ionosphere
dp, dx	elements of distance measured along the ground
E_o, E_x	radio energy densities along the ground
K	constant ≡ H/U'
P	flux density
X	recorded amplitude deflection
a	slope of amplitude calibration curve
b	y-axis intercept of calibration curve

The author of this thesis has granted The University of Western Ontario a non-exclusive license to reproduce and distribute copies of this thesis to users of Western Libraries. Copyright remains with the author.

Electronic theses and dissertations available in The University of Western Ontario's institutional repository (Scholarship@Western) are solely for the purpose of private study and research. They may not be copied or reproduced, except as permitted by copyright laws, without written authority of the copyright owner. Any commercial use or publication is strictly prohibited.

The original copyright license attesting to these terms and signed by the author of this thesis may be found in the original print version of the thesis, held by Western Libraries.

The thesis approval page signed by the examining committee may also be found in the original print version of the thesis held in Western Libraries.

Please contact Western Libraries for further information:
E-mail: libadmin@uwo.ca
Telephone: (519) 661-2111 Ext. 84796
Web site: http://www.lib.uwo.ca/

CHAPTER I

INTRODUCTION

A number of observations of travelling ionospheric disturbances (TIDs) at various locations in both hemispheres have been reported in the last three decades. This thesis describes observations of TIDs located in a region of the ionosphere between latitudes 35^{o}N and 40^{o}N and between longitudes 70^{o}W and 92^{o}W. The observations were made with a solar radio interferometer situated at London, Canada (43^{o}N, 81^{o}W).

1.1 TRAVELLING IONOSPHERIC DISTURBANCES (TIDs)

TIDs are electron density irregularities in the F region which have been observed to move over horizontal distances of thousands of kilometers. The disturbance consists of a periodic change of the electron density with horizontal distance. The velocity of the TID has been measured at many locations by many workers using a variety of techniques. Some of the techniques employed are vertical-incidence sounding (Pierce and Mimno, 1940; Wells and George, 1946), doppler radar (Georges, 1968; Chan and Villard, 1962), back-scatter radar (Tveten, 1961), in-situ satellite density measurements (Newton et al., 1969), three-station single-frequency ionosondes (Munro, 1958), Thomson radar (Thome, 1968; Vasseur and Waldteufel, 1969), Faraday rotation (Titheridge, 1963) and angle-of-arrival measurements (Lawrence and Jespersen, 1961; Vitkevich, 1958). Fig. 1 is a summary of a large number of the measurements of the horizontal velocity and the wavelength of TIDs. The higher

velocity TIDs tend to travel in the north-south direction while those with lower velocities have no preferred direction of travel. They have wavelengths from about 50 to 2000 kms and horizontal velocities from 180 to 2500 km/hr.

Recently Newton, et al. (1969) observed local changes in neutral density in the atmosphere located over the northern hemisphere. Their observations were obtained from density gauges located on the Explorer 32 satellite. Approximately 10% of these showed the occurrence of wave structure with average deviations in density of 10 to 20% from the background density. Waves were observed to be most prevalent at the higher latitudes near the auroral zone and were observed most frequently in the late evening and early morning hours. The horizontal wavelengths were reported to be between 130 km and 520 km. They were observed over the altitude range from 286 km (satellite perigee) to at least 510 km. The waves were interpreted as being gravity waves with a north-south direction of propagation.

1.2 GRAVITY WAVES

Hines (1960) suggested that TIDs are a manifestation of atmospheric gravity waves. These are the low-frequency counterpart of acoustic waves in an atmosphere with gravity. The general properties of these waves in an isothermal atmosphere were derived and applied to upper-atmospheric phenomena by Hines (1960).

When TIDs are represented by contours of constant electron density, it is found that they tend to be tilted or displaced forward from the vertical in the direction of motion (Thome, 1964). The

gravity wave theory suggests that this forward tilt of TID wavefronts is a consequence of a downward component of phase progression that accompanies an upward component of energy flux. This anisotropy is introduced by the preferred direction of the force of gravity. The energy sources are considered to be located below the mesosphere and not in the region where the TIDs are observed. The amplitude of gravity waves is small near the ground, but increases exponentially with height as the atmospheric density decreases.

Hines (1960) and Friedman (1966) have shown that gravity waves are ducted by the lower atmosphere and that some of the energy escapes and propagates upwards. As it propagates up through the F region it produces a wave structure in the ionosphere. This structure causes refraction, reflection or focussing of radio waves as seen by ground-based observers. As the gravity wave progresses upward past the peak of the F_2 layer the phase fronts are tilted upwards by dissipation of energy due to viscosity and heat conduction (Hines, 1968). There is a tendency for the frontal surfaces of TIDs to become nearly vertical for heights above about 300 km, (Chimonas and Hines, 1970).

1.3 PREVIEW

Measurement of the angle-of-arrival of a radio signal with a two-element interferometer is discussed in Chapter II. The angle-of-arrival of the incoming signal is made with respect to the interferometer base line and derived from a measurement of the difference in phase between signals arriving at the two antennas. The principle of the swept-lobe interferometer which was used to observe TIDs is described. The measurement of the angle-of-arrival from two sources is also described

in some detail. It will be shown that in this case the angle-of-arrival may undergo quasi-periodic scintillations due to the interference between the two. The characteristics of these scintillations are described in detail.

Chapter III indicates that TIDs can be detected and certain properties determined from angle-of-arrival measurements made on relatively intense localized sources on the solar disk, which appear on occasions when the sun is disturbed. The TIDs cause deviations in angle-of-arrival, or scintillations, due to the bending of the solar line-of-sight by horizontal gradients in refractive index associated with TIDs. The speed of a TID is obtained from the variation in the period of the scintillation and the direction of motion of a TID is obtained from the variation in the amplitude of the scintillation. It is also shown that the speed of the TIDs, as a function of height, can be obtained from the temporal variation of signal strength and rate of change of angle-of-arrival due to refraction of the solar radiation.

The scintillations in angle-of-arrival that were observed on a number of days and which are ascribed to TIDs are discussed in Chapter IV. The measurements were obtained with a compound interferometer with either two interferometers with different antenna separations on an east-west base line or one interferometer on an east-west base line and the other one on a predominantly north-south base line. Alternative interpretations of the observed scintillations are shown to be invalid. In particular, the principal alternative proposal which attributes the scintillations to interference between two sources is shown to be invalid. Two types of TIDs were detected

and their parameters are described. One type was observed to travel toward the equator, with a period of 21 minutes and a wavelength of the order of 400 km. The other was observed to travel along an east-west direction with a period of 6 minutes and a wavelength of 20 km. The wavefront tilt of the latter is deduced from the measurements and found to be 52° (± 20°). Both kinds of TIDs were, on at least one occasion, observed continuously for over 5 hours. The first type appears to be an F-region phenomenon and the other an E-region phenomenon.

In Chapter V it is shown that the properties and parameters of the observed TIDs are consistent with observations of TIDs conducted by other workers using a variety of experimental techniques. In particular they are consistent with observations of TIDs by previous experimenters using the angle-of-arrival technique. The new properties of TIDs reported in this thesis are; firstly, the TIDs were observed to contain three to five times the number of wave periods that have been reported to date, and secondly, the wave period was observed to be relatively constant throughout the wave train, suggesting the presence of one predominant spectral component.

It is also shown that the properties of the observed TIDs are consistent with those predicted by the gravity wave theory. This is significant because gravity waves are generally accepted as being responsible for producing TIDs.

CHAPTER II

MEASUREMENT OF THE ANGLE-OF-ARRIVAL OF SIGNALS FROM ONE AND TWO SOURCES WITH AN INTERFEROMETER

2.1 INTRODUCTION

Since the angle-of-arrival measurements reported in this thesis were obtained with a swept-lobe interferometer its operation is discussed in considerable detail. Theoretical expressions are derived for determining the angle-of-arrival of signals from one and two sources. Experimental results showing deviations in the angle-of-arrival of a radio signal from the radio source Cassiopeia A are given and shown, by application of the two source theory, to be caused by interference with a signal from the radio source Cygnus A. In addition, results are given of a laboratory simulation of an interferometer system monitoring two sources. These again show good agreement with theory. The results of this chapter form the theoretical justification for the TID interpretation of the measured deviations in angle-of-arrival of radio signals from the sun which are presented in Chapter IV.

2.2 MEASUREMENT OF ANGLE-OF-ARRIVAL FROM ONE SOURCE WITH AN INTERFEROMETER

Consider Fig. 2 where two antennas forming an interferometer are located at O and A along the base-line OY and separated by distance d. Two rays from a single source denoted by S are shown arriving at each antenna. The total phase difference Φ of the radiation arriving from the source at the two antennas may be expressed generally as:

$$\Phi = (2\pi n + \phi) = \frac{2\pi d}{\lambda} \cos\theta \qquad (1)$$

Where; ϕ = the measured phase difference in the range 0 to 2π

n = an integer in the range $-\frac{d}{\lambda} \leq n \leq \frac{d}{\lambda}$

λ = wavelength of the radiation

θ = the angle between the signal and interferometer base-line.

In this case of a non-terrestrial body, such as the sun, knowledge of its location allows for the calculation of angle θ_S between a ray from its center and the interferometer base-line and subsequent determination of n from Eq. 1. The angle θ_N of the non-terrestrial signal with respect to the interferomter base-line can then be determined from Eq. 1 and a measurement of ϕ_N where, ϕ_N is the phase between the non-terrestrial signal received at the two interferometer antennas. The angle θ_{SN} is defined by:

$$\theta_{SN} = \theta_S - \theta_N \qquad (2)$$

Both θ_N and θ_S are always positive and measured from the line OY. θ_{SN} as defined here may be both positive or negative. It is called the angle-of-arrival henceforth, and the measured values reported here form the principal data base for this thesis, augmented by measurements of the amplitude of the non-terrestrial signal.

2.3 PRINCIPLE OF THE SWEPT-LOBE INTERFEROMETER AND ONE SOURCE

A theoretical description of the operation of a fundamental swept-lobe interferometer with one source is given, based, in part, on that given by Winacott (1961).

Fig. 3a shows a block diagram of a basic swept-lobe interferometer. The two voltages $e_1 \sin\omega_1 t$ and $e_1 \sin(\omega_1 t + 2\pi n + \phi)$ are generated at antennas I and II respectively, by the incoming signal. The signal

from antenna II is phase shifted at the rate Ψ radians second by the phase shifter and also phase delayed a fixed amount ε_2 by the coaxial cable and electronic components between antenna II and the adder. Similarly the signal at the adder from antenna I is phase delayed by ε_2. In addition, the amplitudes of the signals at the adder will differ from those at the antennas due to attenuation and amplification along the signal paths. The appropriate values for the signals from antenna I and II at the adder E_I and E_{II} respectively, are given below.

$$E_I = e_1' \sin(\omega_1 t - \varepsilon_1) \tag{3}$$

$$E_{II} = e_1'' \sin(\omega_1 t + 2\pi n + \phi + \Psi t - \varepsilon_2) \tag{4}$$

Where $e_1' = \alpha_1 e_1$

$e_1'' = \alpha_2 e_1$

and α_1 and α_2 are constants.

The output signal E_a from the adder is the sum of the two input signals.

$$E_a = E_I + E_{II} \tag{5}$$

Now it will be shown that a signal with angular frequency Ψ and phase angle ϕ' can be obtained by rectification of the rf signal E_a given by Eq. 5. The amplitude of E_a as a function of the time follows from the vector diagram shown in Fig. 3b.

$$A(\Psi t) = \{(e_1')^2 + (e_1')^2 + 2e_1'e_2'' \cos(\Psi t + \phi')\}^{\frac{1}{2}} \tag{6}$$

where $\phi' = \phi + (\varepsilon_1 - \varepsilon_2)$

The function $A(\Psi t)$ when expressed in terms of a Fourier series takes the form:

$$A(\Psi t) = \frac{a_0}{2} + F_1\cos(\Psi t + \phi_1) + F_2\cos(2\Psi t + \phi_2) + \cdots + F_n\cos(n\Psi t + \phi_n) \tag{7}$$

where $F_n = (a_n^2 + b_n^2)^{1/2}$

$$\phi_n = \tan^{-1}\left[-\frac{b_n}{a_n}\right]$$

$$a_n = \frac{1}{\pi}\int_0^{2\pi} A(\psi t)\cos\ n\psi t\ d(\psi t)$$

$$b_n = \frac{1}{\pi}\int_0^{2\pi} A(\psi t)\ \sin n\psi t\ d(\psi t)$$

The amplitude F_1 and phase ϕ_1 of the fundamental spectral component of $A(\psi t)$ are obtained by solving for a_1 and b_1.

$$a_1 = \frac{1}{\pi}\int_0^{2\pi}\left[(e_1')^2 + (e_1'')^2 + 2e_1'e_1''\cos(\psi t + \phi')\right]^{1/2}\cos\psi t\ d(\psi t)$$

$$b_1 = \frac{1}{\pi}\int_0^{2\pi}\left[(e_1')^2 + (e_1'')^2 + 2e_1'e_1''\cos(\psi t + \phi')\right]^{1/2}\sin\psi t\ d(\psi t)$$

If the parameter of integration is changed by $y = \psi t + \phi'$ the expression for a_1 becomes

$$a_1 = \frac{\cos\phi'}{\pi}\int_{\phi'}^{2\pi + \phi'}\left[(e_1')^2 + (e_1'')^2 + 2e_1'e_1''\cos y\right]^{1/2}\cos y\ dy$$

$$+ \frac{\sin\phi'}{\pi}\int_{\phi'}^{2\pi + \phi'}\left[(e_1')^2 + (e_1'')^2 + 2e_1'e_1''\cos y\right]^{1/2}\sin y\ dy$$

The second term is identically equal to zero. Therefore the value of a_1 is given by,

$$a_1 = \xi\cos\phi'$$

where,

$$\xi = \frac{1}{\pi}\int_{\phi'}^{2\pi + \phi'}\left[(e_1')^2 + (e_1'')^2 + 2e_1'e_1''\cos y\right]^{1/2}\cos y\ dy$$

Similarly the value of b_1 can be shown to be

$$b_1 = -\xi \sin \phi'$$

The values of F_1 and ϕ_1 determined from a_1 and b_1 are,

$$F_1 = [\xi^2 \cos^2\phi' + \xi^2 \sin^2\phi']^{\frac{1}{2}} = \xi$$

and,

$$\phi = \tan^{-1}\left[\frac{\xi \sin\phi'}{\xi \cos\phi'}\right] = \phi'$$

Therefore the fundamental component of $A(\Psi t)$ is given by,

$$A_1(\Psi t) = \xi \cos (\Psi t + \phi') \qquad (8)$$

This component is extracted from the interferometer signal given by Eq. 5 following rectification by a narrow band-pass filter. It is compared in a phase meter with a signal generated by the phase shifter to obtain the value, ϕ', which is continuously recorded on a paper chart recorder. This value differs from the phase difference ϕ between the signals at the antennas in Fig. 3a by the constant phase angle $(\varepsilon_1 - \varepsilon_2)$. This phase error which is introduced by the cables and electronic components can be determined from observations on a radio star, such as Cassiopeia A. The output of the phase meter can then be corrected by this constant deviation in phase angle to give the correct phase angle ϕ. The amplitude of Eq. 8 is recorded on another chart and is proportional to the field strength of the received radiation. This proportionality follows from the expression for ξ when the values of e_1' and e_1'' are replaced by their equivalent values $\alpha_1 e_1$ and $\alpha_2 e_1$, respectively.

2.4 THE SWEPT-LOBE INTERFEROMETER AND TWO SOURCES

A theoretical description of the measurement of the angle-of-arrival from two independent noise sources with a rotating lobe interferometer is now presented. It will be shown that interference between the two sources causes perturbations to the measured phase and amplitude.

In Fig. 4a two signals of amplitude e_1 and e_2 are shown arriving at the antennas of the interferometer. The signals are from independent radio sources whose emissions are assumed to be noise like. The phase difference between the signals from the two sources at antenna I, β is a random function of time. On the other hand, the phases between the signals at antenna I and II from one source, ϕ and from the other source, Δ are due to their geometry with respect to the interferometer base-line.

Following the discussion in section 2.3 the signal at the adder from antenna I is

$$e_1' \sin(\omega_1 t - \varepsilon_1) + e_2' \sin(\omega_1 t + \beta - \varepsilon_1)$$

and from antenna II

$$e_1'' \sin(\omega_1 t + \phi + \Psi t - \varepsilon_2) + e_2'' \sin(\omega_1 t + \beta + \Delta + \Psi t - \varepsilon_2)$$

The modulated interferometer signal now takes the form

$$E'a = A_1 \sin(\omega_1 t \pm \Theta_1) + A_2 \sin(\omega_1 t + \Theta_2 + \beta) \qquad (9)$$

where

$$\Theta_1 = \cos^{-1} \frac{e'_1 + e''_1 \cos(\Psi t + \phi')}{A_1}$$

$$\Theta_2 = \cos^{-1} \frac{e_2' + e_2'' \cos(\Psi t + \Delta')}{A_2}$$

The values for the amplitude A_1 and A_2 of the two rf signals given by Eq. 9 follow from the vector diagrams in Fig. 4b

$$A_1 = [(e_1')^2 + (e_1'')^2 + 2e_1'e_1'' \cos(\Psi t + \phi')]^{1/2}$$

$$A_2 = [(e_2')^2 + (e_2'')^2 + 2e_2'e_2'' \cos(\Psi t + \Delta')]^{1/2}$$

where

$$\phi' = \phi + (\varepsilon_1 - \varepsilon_2)$$

$$\Delta' = \Delta + (\varepsilon_1 - \varepsilon_2)$$

Following addition of the two terms in Eq. 9 it takes the form

$$E'a = A_3 \sin(\omega_1 t + \Theta_3) \qquad (10)$$

where

$$A_3 = [A_1^2 + A_2^2 + 2A_1A_2 \cos(\beta \pm \Theta_2 \pm \Theta_1)]^{1/2}$$

$$\Theta_3 = \tan^{-1} \frac{A_1 \sin(\pm\Theta_1) + A_2 \sin(\pm\Theta_2 + \beta)}{A_1 \cos(\pm\Theta_1) + A_2 \cos(\pm\Theta_2 + \beta)}$$

A trigonometric change to the expression for A_3 gives

$$A_3 = [(A_1 + A_2)^2 - 4A_1A_2 \sin^2(\gamma/2)]^{1/2}$$

where

$$\gamma = \beta \pm \Theta_2 \pm \Theta_1.$$

The parameter A_3 can be expanded by the binomial theorem as follows;

$$A_{3_\gamma} = (A_1 + A_2) - \frac{2A_1A_2}{A_1 + A_2}\sin^2\frac{\gamma}{2} - \frac{2A_1^2A_2^2}{(A_1 + A_2)^3}\sin^4\frac{\gamma}{2}$$

$$- 4\frac{A_1^3A_2^3}{(A_1 + A_2)^5}\sin^6\frac{\gamma}{2} - 10\frac{A_1^4A_2^4}{(A_1 + A_2)^7}\sin^8\frac{\gamma}{2} \text{ -----} \qquad (11)$$

This series will converge, provided $A_1 \neq A_2$ when $\sin \frac{\gamma}{2} = 1$; in which case $A_3 = 0$. These rapid short lived excursions to zero will not affect the output of the detector because of its relatively long time constant. The parameter γ is a random function of time because one of the terms in its definition is a random function of time. Since all the terms following the first are a function of this variable they represent incoherent broad band signals and contribute to the noise level in the video channel before being passed through a narrow-band video filter.

Although it appears as though the terms following the first in Equation 11 will not contribute significantly to the fundamental coherent Fourier component of Equation 11 it is difficult to prove this mathematically. Since it is relatively easy to demonstrate this experimentally an experimental proof of this point was in fact carried out. This was performed in two ways; firstly, in Section 2.6 the phase and amplitude perturbations caused by interference between the two radio stars Cassiopeia A

and Cygnus A were shown to be consistent with the above contention and secondly in Section 27 the results of a laboratory simulation of the interferometer and two sources also verified this contention.

It thus now follows that the fundamental Fourier component of Equation 11 to the first order, at least, is given by

$$A_{31}(\Psi t) = \xi_1 \cos(\Psi t + \phi') + \xi_2 \cos(\Psi t + \Delta') \qquad (12)$$

This is the video signal that is passed through the band-pass filter and is simply the sum of the video signals that would be obtained with two swept-lobe interferometers observing separate sources. For the case of three or more sources Eq. 12 would contain further terms and its complexity would increase rapidly with the number of sources.

Calculation of the variation in phase and amplitude measured by the interferometer when observing two signals follows from Eq. 12 and Fig. 5 remembering that ξ_1 and ξ_2 are proportional to e_1 and e_2 respectively.

Let $e_2 = \eta e_1$

and $e = Ao/e_1$

where Ao = resultant of the addition of the two vectors e_1 and e_2 which are $(\Delta' - \phi')$ degrees out of phase

$\eta < 1$

The phase of A_0 with respect to e_1 denoted by $\delta\phi$ is also the phase perturbation of e_1 produced by e_2, which is given by

$$\delta\phi = \cos^{-1} \frac{1 + c^2 - \eta^2}{2c} \tag{13}$$

the reduced amplitude c is given by

$$c = [1 + \eta^2 + 2\eta\cos(\Delta' - \phi')]^{\frac{1}{2}} \tag{14}$$

The ratio peak or maximum to minimum A_0 denoted by A_{op} and A_{om} respectively is given by

$$\frac{A_{op}}{A_{om}} = \frac{1 + \eta}{1 - \eta} \tag{15}$$

A plot of $\delta\phi$ versus $(\Delta' - \phi')$ derived from Eqs. 13 and 14 for various values of η is given in Fig. 6 and the corresponding plot for c derived from Eq. 14 is given in Fig. 7. Both the phase and amplitude go through one cycle whenever $(\Delta' - \phi')$ progresses through 2π radians. For the larger values $\delta\phi$ is non-symmetric and has a marked "saw-tooth" shape. If the time (period) taken for ϕ' to change by 2π radians is T_1 and the time for Δ' to change by 2π radians is T_2 then the time (period) τ for $(\Delta' - \phi')$ to change by 2π radians is given by

$$\tau = \frac{T_1 T_2}{T_2 - T_1} \tag{16}$$

2.5 DESCRIPTION OF INTERFEROMETER SYSTEM

The compound rotating-lobe interferometer system used in this work was designed and constructed at the Defence Research

Telecommunications Establishment (now the Communications Research Centre) at Shirley Bay, near Ottawa. It was built for the express purpose of metric solar radio astronomy and operated at a frequency of 51.7 MHz . With an antenna separation of the order of 50λ the angular resolution of each interferometer was ±2 minutes of arc or better. A detailed technical description of the interferometer system has already been given by Winacott (1963) and will not be repeated here.

Fig. 8 shows the relative location of the antennas of the compound solar interferometer used for the measurements. The antennas were linearly polarized five element yagis and were mounted to accept signals of vertical polarization. The amplitude of the non-terrestrial incoming radio waves and their phase differences at two pairs out of a possible six pairs of antennas were recorded. In some cases the phase difference between the radio waves arriving at Y_0 and Y_3 and between Y_0 and Y_2 were recorded; in other cases, the phases between Y_0 and Y_2 and between Y_0 and Y_1 were recorded. Antenna Y_0 and a receiving channel were common to all measurements. The phase differences were converted to angles-of-arrival Θ_{SN} of the incoming waves with respect to the interferometer base-line and the center of the source. The notations for and separations of the various antenna pairs are as follows:

Y_0, Y_2 = wide E-W interferometer (49.361λ)

Y_0, Y_1 = narrow E-W interferometer (16.571λ)

Y_0, Y_3 = N-S interferometer (54.289λ)

The angle-of-arrival measurements presented here will be identified by these symbols.

2.6 MEASUREMENT OF ANGLE-OF-ARRIVAL FROM TWO SOURCES

Cassiopeia A and Cygnus A, two of the strongest radio stars in the celestial sphere were used as the independent sources for the two-source measurements described in this section. The flux density radiated by each at a frequency of 50 MHz is 3.5×10^{-22} $\omega m^{-2} Hz^{-1}$ and 2.0×10^{-22} $\omega m^{-2} Hz^{-1}$ respectively (Wild, 1955). Values of the right ascension α and declination δ used here for Cassiopeia A and Cygnus A are $\alpha = 23^h 22^m 00.6^s$, $\delta = +58° 38.7'$ and $\alpha = 19^h 58^m 25^s$, $\delta = +40° 39.2'$ respectively.

The geometry pertinent to the measurements is given in Fig. 9 which shows the intersection of the earth with a plane containing the meridian through London, Ontario. An idealized radiation pattern of a yagi antenna is indicated in position to track the radio sun. Its side and back lobes are not shown but are expected to be 20 dB down from the main beam. The lines-of-sight to the sun, Cygnus A and Cassiopeia A for various designated times of interest are indicated. Rotation of the earth causes them to trace out concentric cones whose axis consists of the London-North Pole line. During this diurnal motion Cygnus A reaches its upper culmination position $3^h 22^m 52.5^s$ before Cassiopeia A. For these measurements the yagi antennas of the wide and narrow E-W interferometers were used and rotated upwards until they pointed approximately at the position in space occupied by Cassiopeia A when at its upper culmination position. The measurements were made when both Cassiopeia A and Cygnus A were near their upper culmination positions and since the angle between their lines-of-sight is only 35 51' both were within the radiation patterns of the antennas.

Fig. 10 gives the measured angle-of-arrival of Casseopeia A [illegible] 1969 with the time-axis correct for the

4 February data. The two sets of observations were aligned by matching the time that Cassiopeia A was at its upper culmination position on these two days which was $19^h48^m23.7^s$ and $20^h00^m11.3^s$ UT on 4 and 1 February 1969 respectively. It should be noticed that the agreement between the two measurements, even at these low levels of flux density, confirms for the most part, the previously mentioned resolution (±2' of arc) of the interferometer. The poorer agreement before 1530 UT can be attributed to scintillations of the signal from Cassiopeia A caused by oblique propagation through the ionosphere.

The period of a stellar source is defined to be the time taken for the phase of the signals received at the two antennas of an interferometer to change by 2π radians due to the effective motion of the source. The periods of Cassiopeia A and Cygnus A derived from Eq. 36 for the wide E-W interferometer obervations on 4 February 1969 are given as a function of time by the solid curves in Fig. 11. The dashed curve gives the period of the perturbations caused by Cygnus A to the angle-of-arrival measurements of Cassiopeia A using Eq. 16 and the periods of the two stars.

Now it will be shown that the repeatable scintillations in the angle-of-arrival measurements of Cassiopeia A are due to interference from Cygnus A. The data points plotted in Fig. 11 were obtained from measurements of the time between peaks of the scintillations in Fig. 10. Excellent agreement occurs between the theoretical curve and the data over the complete measurement interval except for the short segment between 1510 and 1550 UT. This generally good agreement strongly suggests that the scintillations, for the most part, were due to interference

between the signals from Cassiopeia A and Cygnus A. During the interval 1510 and 1550 UT there is good agreement between the data points and the period of Cassiopeia A. This occurs because of the very low flux density levels prevalent at this time due to oblique propagation. The phase meter was in error because of the low s/n ratio over a portion of the time taken for the phase difference of the signals to go from 0 to 360 electrical degrees or, to go through a phase ramp which is approximately given by the period of Cassiopeia A. This error was preserved from phase ramp to phase ramp and appears as a scintillation with a period equal to the period of the phase ramps or of Cassiopeia A.

The amplitude of the signal received from Cassiopeia A and Cygnus A is given in Fig. 12 with a well defined fading pattern readily apparent. Good agreement exists between the periods of the angle-of-arrival scintillation shown in the insert with the amplitude scintillations. The ratio of the peak to minimum amplitude is of the order of 1.3/0.7 = 1.86, which when substituted into Eq. 15 gives $n = 0.3$, whereas n given by the ratio of the flux densities radiated by Cassiopeia A and Cygnus A is 0.57. The lower value of n obtained here results from the antenna radiation patterns being more favourably directed towards Cassiopeia A. For the value of n observed, Fig. 6 indicates that the maximum phase deviation to be expected is ±18 electrical degrees which according to Eq. 1 corresponds to ±3.6' of arc or a total variation of 7.2 minutes of arc, which is in fact what is observed in Fig. 12. Further agreement with theory is demonstrated by the minima in amplitude in Fig. 12 corresponding to null deviations in the angle-of-arrival, in agreement with $\delta\phi$ being equal to zero in Fig. 6 and c in Fig. 7 passing through

an extremum when $(\Delta' - \phi')$ equals 180°. Furthermore Fig. 13 shows good agreement between a portion of the amplitude record of Fig. 12 with a theoretical curve whose period was obtained from the curve for τ in Fig. 11 and whose shape for each indicated cycle of the curve was obtained from the curve in Fig. 7 with $n = 0.3$. This comparison was not performed over the complete time interval of Fig. 12 because the point is adequately demonstrated with the segment shown in Fig. 13.

Angle-of-arrival data for the narrow E-W interferometer are given in Fig. 14 with the solid curve referring to 4 February 1969 data and the dashed one to 6 February 1969 data. Once again the two curves were superimposed by matching the times of upper culmination on Cassiopeia A on these two days with the time scale shown being correct for the 4 February 1969 data. Scintillations in the angle-of-arrival are discernible between 1430 and 1730 UT with peak to peak magnitudes between 20 and 40 minutes of arc. One would expect the peak to peak angle-of-arrival variations for the narrow interferometer to be three times as great as that for the wide interferometer or 22 minutes of arc. This agrees with the observed variations if one considers that the resolution of this interferometer, because of its shorter base-line, is ±10 minutes of arc or so. It should also be observed that the period of the scintillations is three times as great as that predicted for the wide interferometer in Fig. 11. Thus the period and amplitude of the scintillations produced by Cassiopeia A and Cygnus A are observed to be approximately three times as great for the narrow interferometer as for the wide one. This is to be expected because the ratio of their base-lines is approximately 1:3.

The long term stability of the wide E-W interferometer is demonstrated in Fig. 15 where the phase between the signals arriving at the two interferometer antennas from Cassiopeia A and Cygnus A, when Cassiopeia A was at its upper culmination position, is given for a number of days between 17 September 1968 and March 1969. During the 30 day period between 17 September 1968 and 18 October 1968 the phase varied by some 18 electrical degrees or the angle-of-arrival varied by some 3.6 minutes of arc. The variation in measured phase is somewhat greater near the beginning of February 1969 and represents a total variation of ~ 8' of arc in the angle-of-arrival. For these measurements Cassiopeia A was at its upper culmination position during the day time. Therefore the increased phase variation may be due to enhanced ionospheric scintillations or background radio emission from the sun.

2.7 LABORATORY SIMULATION OF INTERFEROMETER AND TWO SOURCES

As a final test of the two source interferometer theory a simulation of an interferometer monitoring two sources was performed in the laboratory. A block diagram is given in Fig. 52 showing the system used and signals at various pertinent points along the signal paths.

The signal sources consisted of either two signal generators S1 and S2 whose frequencies were arbitrarily set at 15 MHz or one signal generator at the same frequency but whose output was divided into two by a power divider. The RF signals were mixed in balanced mixers with signals from an audio generator which also was arbitrarily set at a frequency of 100 Hz. A phase shifter was used to shift the phase

of one of the audio signals between -10 and +190 degrees in 10 degree increments. As shown in Fig. 52 the output of each balanced mixer was a modulated RF signal of the form given by one of the terms of Eq. 9. There was a phase shift between the modulation on the two RF signals whose magnitude was proportional to the phase shift imparted on the 100 Hz audio signal by the phase shifter.

A third output of the audio generator was doubled in frequency and transformed into a square wave in the full wave rectifier and schmitt trigger. This signal provided the reference for the phase measurements.

The two modulated RF signals were combined in the adder; the output of which is given by Eq. 10. This signal was passed through a detector (Eq. 11) and a band-pass filter centered on 200 Hz. The output of the band-pass filter is, according to the theory of Section 2.4 given by Eq. 12. The phase and amplitude of this signal was measured as a function of the phase shift imparted to the 100 Hz audio signal in the phase shifter. The phase shifter in shifting the phase of the audio signal performed the same function on the relative phases of the modulation on the two RF signals as would differential rotation of two sources in the case of a real interferometer. A variation of 0 to 180 degrees in the phase shifter produces a variation of 0 to 360 degrees in the function $\Delta - \phi$ defined in section 2.4. A RF attenuator was used to vary the amplitude of one of the modulated RF signals. This allowed for measurement of phase and amplitude perturbations between signals with various amplitude ratios.

The results of the measurements are given in Figs. 53 and 54. In the first case the two sources were incoherent since S_1 and S_2

were independent oscillators. In the second case the sources were coherent with the two RF outputs being derived from one signal generator. The agreement between the curves obtained experimentally and the theoretical ones of Fig. 6 and Fig. 7 is so striking as to leave no doubt as to the validity of the two-source theory derived in Section 2.4.

2.8 SUMMARY AND DISCUSSION

In conclusion, there is excellent agreement between the experimental results of this section and the theoretical development of Section 2.4. This strongly suggests that Eq. 12 correctly describes the operation of the swept-lobe interferometer observing two independent sources. Additionally, the following points which will be referred to in Chapter IV have been demonstrated;

(a) The period of the scintillations is given by Eq. 16 and is the time taken for $(\Delta' - \phi')$ to change by 2π radians due to the differential motion of the two sources. This period is inversely proportional to the interferometer antenna separation.

(b) The magnitude of the phase and amplitude scintillations is given by Fig. 6 and 7, respectively, and is a function of η, the ratio of the signal strengths of the two sources. It was shown in Fig. 12 that small angle-of-arrival scintillations were accompanied by large amplitude scintillations and that if the magnitude of the angle-of-arrival scintillations were measured the theory developed in Section 2.4 allowed for the calculation of the magnitude of the corresponding amplitude scintillations. The magnitude of the angle-of-arrival scintillations was shown to be proportional to the interferometer spacing.

(c) The long term stability of the interferometer was demonstrated to be within the accuracy claimed (±2'arc) except during one period which occurred in February 1969 and which was probably due to external causes.

CHAPTER III

CHARACTERISTICS OF ANGLE-OF-ARRIVAL SCINTILLATIONS PRODUCED BY TIDs

3.1 INTRODUCTION

TIDs, because of their associated horizontal electron-density gradients perturb the linear propagation of radio waves through the ionosphere. They manifest themselves to an observer on the ground as scintillations in the angle-of-arrival and amplitude of trans-ionospheric radio signals. Equations are developed here which relate the magnitude of these scintillations to both the electron-density gradients and certain characteristics of the interferometers. The apparent motion of the sun is shown to produce variations in the magnitude and period of the angle-of-arrival scintillations. This motion and the variations induced by it are described in detail; furthermore, it is shown that the line-of-travel and speed of the TIDs can be deduced from the observed variations. A two-dimensional projection of the interferometers three-dimensional constant-phase surfaces is developed to aid in visualizing their behavior as TID sensing instruments. Finally, equations are developed relating the magnitudes of the amplitude and angle-of-arrival scintillations of radio waves by TIDs.

3.2 MOTION OF THE SOLAR LINE OF SIGHT

The loci of the intersection of the solar line-of-sight with various levels in the ionosphere may be determined with the aid

of Fig. 16. In particular Fig. 16a, which shows a plane containing the solar line-of-sight, the observer O and the center of the earth C. The intersection of the solar line-of-sight with an ionospheric layer whose heignt above the earth is D is given by R. The zenith angle of the sun is z; B is the distance OR and δ is the angle RCO. It can be shown (HARROWER, 1963) that B is given by the following:

$$B = [(r + D)^2 - r^2 \sin^2 z]^{1/2} - [r^2 - r^2 \sin^2 z]^{1/2} \qquad (17)$$

and δ by the expression:

$$\delta = \cos^{-1} \frac{r^2 + (r + D)^2 - B^2}{2r(r + D)} \qquad (18)$$

where:

r = radius of the earth

The observer's celestial hemisphere is shown in Fig. 16b with the observer at O, the north celestial pole at P, and the zenith at Z. The intersection of the extension of CR in Fig. 16a with the observer's celestial sphere is given by R' and the co-latitude PZ and hour angle ZPR' of R' are given by S and t respectively.

The altitude of the sun denoted by h in Fig. 16a is given by (SMART, 1944).

$$h = \sin^{-1}[\sin(LAT)\sin(DEC) + \cos(LAT)\cos(DEC)\cos(HA)] \qquad (19)$$

where:

DEC = declination of the sun

HA = hour angle of the sun.

The zenith angle z of the sun is given by

$$z = \frac{\pi}{2} - h \qquad (20)$$

and the azimuthal angle A_z by:

$$A_z = \sin^{-1}\left[\cos(DEC)\,\frac{\sin(HA)}{\cos(h)}\right] \tag{21}$$

From the spherical triangle PZR' in Fig. 16b it follows that

$$S = \cos^{-1}\left[\cos\delta\cos\left(\frac{\pi}{2} - LAT\right) + \sin\delta\sin\left(\frac{\pi}{2} - LAT\right)\cos(2\pi - A_z)\right] \tag{22}$$

and,

$$t = \sin^{-1}\left[\frac{\sin\delta\sin(2\pi - A_z)}{\sin S}\right]. \tag{23}$$

The latitude and longitude of R or R' are given respectively by

$$LAT(R) = \frac{\pi}{2} - S \tag{24}$$

$$LONG(R) = LONG(O) + t \tag{25}$$

where:

LONG(O) = longitude of the observer.

Curves tracing out the loci of the intersection of the solar line-of-sight with various levels in the ionosphere, as a function of time, are given in Fig. 17. The paths shown were derived for values of D equal to 150, 300 and 450 km using solar parameters correct for November 12, 1969 and Eqs. 22 to 27. The intersection of the dashed lines with the curves defines the position of the intersection points, R at the indicated times: positions at other times can be obtained by extrapolation. The co-ordinate axes shown in the insert define positive values of the velocity components Vx and Vy of the intersection point R; with positive Vx directed towards the west and positive Vy directed towards the north. These two velocity components are given by

$$Vx = (r + d)\cos[LAT(R)] \times \frac{d}{dt}(LONG(R)] \tag{26}$$

$$Vy = (r + d)\frac{d}{dt}[LAT(R)]. \tag{27}$$

Curves for November 12, 1969 derived from Eqs. 26 and 27 giving Vx and Vy as a function of time for the altitude 150, 300 and 450 km are given in Fig. 18. The component Vx, although positive throughout the interval between 1330 and 2030 UT, is seen to vary considerably and in a manner characterized by high values in the morning, relatively low ones at local noon, and high ones again in the afternoon. On the other hand, Vy, whose absolute value is less than Vx throughout this interval, begins with positive values, becomes zero at local noon, and assumes increasingly negative values in the afternoon.

Since the intersection point R moves through the ionosphere, it is to be expected that the period of the scintillations in angle-of-arrival of the solar line-of-sight, caused by TIDs, will be an apparent period. The apparent period will differ from the actual TID wave period by a quantity which is a function of the component of the velocity of the solar line of sight through the ionosphere parallel to the horizontal velocity of the TIDs. In the insert accompanying Fig. 17, let $\underline{U}$ represent the velocity of the TID and $\underline{V}$ the velocity of the intersection point R. The azimuthal angles of these vectors with respect to the negative Y axis are α_U and α_V respectively. They are both defined to be positive in the counter-clock-wise direction. Their values are given by

$$\alpha_U = \tan^{-1}\frac{Ux}{Uy} \tag{28}$$

and

$$\alpha_V = \tan^{-1}\frac{Vx}{Vy} \tag{29}$$

The apparent period T' of the scintillations as a function of U is given by

$$\frac{1}{T'} = \frac{U}{\lambda_t} - \frac{V}{\lambda_t}\cos(\alpha_V - \alpha_U) \tag{30}$$

where λ_t = TID wavelength.

3.3 REFRACTION OF THE SOLAR LINE-OF-SIGHT

At VHF the refractive index, μ, of a radio wave propagating through the ionosphere is given to good approximation by

$$\mu = 1 - \frac{b}{\omega^2} N \tag{31}$$

where

$b = e^2/\varepsilon_o m = 1.6 \times 10^3$ (mks)

N = local number density of free electrons

e = charge of an electron

m = mass of an electron

ε_o = permittivity of free space

ω = angular radio frequency

Eq. 31 is approximate because it neglects the effects of the earth's magnetic field and of absorption.

Since the refractive index is nearly equal to unity, the departure from linearity of radio rays traversing the ionosphere may be considered to be small. The angular deflection $d\tau$ of the ray from a linear trajectory is given by the following;

$$d\tau = \left[\frac{d}{du}\delta\mu\right] d\ell \tag{32}$$

where, ℓ is measured along the undeflected trajectory, u is measured

along a normal to ℓ, and $\delta\mu$ is the deviation of the refractive index from its mean value (CHANDRASEKHAR, 1952). The latter is defined more specifically by

$$\delta\mu = \mu - \mu_o \tag{33}$$

where, μ is the instantaneous value of the refractive index and μ_o is the mean value. It follows from Eq. 33 that Eq. 32 may be written as

$$d\tau = \frac{d\mu}{du}\, d\ell \tag{34}$$

The total angular deflection τ of the ray from its average position given by Eq. 35 is obtained by substituting Eq. 31 into Eq. 34 and integrating over the total ionospheric path length s.

$$\tau = -\frac{b}{\omega^2}\,\frac{d}{du}\int_o^s N\, d\ell \tag{35}$$

Turnbull and Forsyth (1965), and Lawrence et al (1964) have derived an expression identical to Eq. 35 by equating τ to the gradient of the effective phase path.

3.4 MAGNITUDE OF ANGLE-OF-ARRIVAL SCINTILLATIONS

Equations are now derived giving the variations, as a function of time, of the magnitude of TID induced scintillations in the solar angle-of-arrival measured by the E-W and N-S interferometers. Consider Fig. 19 with the observer at O where:

SO = solar line of sight

OP = projection of the solar line of sight on the observer's horizon plane

h = altitude of the sun

$\underline{U}$ = projection of the TIDs horizontal velocity vector onto the horizon plane

TS = azimuth of OP with respect to the OX axis

α_u = azimuth of $\underline{U}$ with respect to the OX' axis.

In the derivations which follow it is assumed that:

a) the TIDs' direction-of-travel defined by α_u remains constant

b) the refraction of the solar line-of-sight from its average position is due, for the most part, to TID-induced horizontal electron-number-density gradients

c) the horizontal gradients are parallel to the TIDs' horizontal velocity.

It will be shown that since TS in Fig. 19, which is the azimuth of the sun with respect to the OX axis, changes from positive values in the morning to negative values in the afternoon in a regular and defined fashion due to apparent motion of the solar ray S, the magnitude of the solar scintillations will vary in a unique manner determined by the TIDs' direction of travel.

It follows from the spherical triangle, ABC, in Fig. 2 that

$$\cos\theta = \cosh\cos A_z' \tag{36}$$

where:

$A_z' = Az - \frac{\pi}{2}$, for the E-W interferometers and, $A_z' = \pi - Az - 0.3098$, for the N-S interferometer.

The magnitude of the phase variations measured by the interferometers due to changes in h and TS caused by refraction of the solar line-of-sight may be obtained by finding the differential of Eq. 36 and substituting in the appropriate value for A_z'. It follows from a comparison of Figs. 8 and 19 that A_z' is equal to $\frac{\pi}{2}$ - TS and TS - 0.3098 radians respectively for the E-W and N-S interferometers.

The equations resulting from the substitution of A_z' into the differential of Eq. 36 are:

$$\Delta\phi_1 = -\beta_1 \sin(h)\sin(TS)\Delta h + \beta_1\cos(h)\cos(TS)\Delta TS \quad (37)$$

$$\Delta\phi_2 = -\beta_2 \sin(h)\sin(TS)\Delta h + \beta_2\cos(h)\cos(TS)\Delta TS \quad (38)$$

$$\Delta\phi_3 = -\beta_3 \sin(h)\cos(TS - 0.3098)\Delta h - \beta_3\cos(h)\sin(TS - 0.3098)\Delta TS \quad (39)$$

where:

$$\beta_1 = 2\pi\ (49.361)$$

$$\beta_2 = 2\pi\ (16.571)$$

$$\beta_3 = 2\pi\ (54.289)$$

In the above, Eqs. 37 and 38 give the magnitude of the phase scintillations $\Delta\phi_1$ and $\Delta\phi_2$ measured by the wide and narrow E-W interferometers respectively and Eq. 39 gives the magnitude of the phase scintillations $\Delta\phi_3$ measured by the N-S interferometer. The variations in the interferometer angle θ which are also equal to the variations in the angle-of-arrival as defined in Eq. 2 may be obtained by equating the differential of Eq. 1 to Eqs. 29, 38 and 39 in turn

$$\Delta\theta_{1,2} = \frac{\sin(h)\sin(TS)\Delta h}{\sin\theta} - \frac{\cos(h)\cos(TS)}{\sin\theta}\Delta TS \quad (40)$$

$$\Delta\theta_3 = \frac{\sin(h)\cos(TS - 0.3098)\Delta h}{\sin\theta} + \frac{\cos(h)\sin(TS - 0.3098)}{\sin\theta}\Delta TS \quad (41)$$

where:

$\Delta\theta_{1,2}$ = perturbation of angle θ for the wide and narrow E-W interferometers due to refraction of the solar ray

$\Delta\theta_3$ = perturbation of angle θ for the N-S interferometer due to refraction of the solar ray.

An expression, giving the variation of, $\Delta\theta_{1,2}$ and $\Delta\theta_3$ as a function of TS or local time may be obtained from a consideration of Fig. 19. The point C denotes the intersection of the solar ray with a

layer in the ionosphere. The average horizontal electron number density gradient $\underline{\xi}$ is indicated and shown to be parallel to OA. Close inspection of Fig. 19 reveals that the component of $\underline{\xi}$ perpendicular to the solar line-of-sight ξ_1 is contained in the plane defined by OS and OA. Thus the refracted solar ray whose angular deflection τ is given by Eq. 35 will be contained within this plane.

If a ray undergoes a deflection of τ it follows from the geometry in Fig. 19 that

$$\Delta h = \tau \sin\gamma \cos(TS - \alpha_U) \tag{42}$$

where

$$\gamma = \tan^{-1}\left[\frac{\tan(h)}{\sin(TS - \alpha_U)}\right] \tag{43}$$

$$\Delta TS = \tau \frac{\cos\gamma}{\cos(h)} \tag{44}$$

Substitution of Eq. 42 and 43 into 40 and 41 and dividing by τ to normalize the equations, allows one to write the following:

$$F_{1,2} = \frac{\Delta\theta_{1,2}}{\tau} = \frac{\sin(h)\sin(TS)\ \sin\gamma\ \cos(TS-\alpha_U)}{\sin\theta} - \frac{\cos(h)\ \cos(TS)\ \cos\gamma}{\sin\theta\ \cos(h)} \tag{45}$$

and

$$F_3 = \frac{\Delta\theta_3}{\tau} = \frac{\sin(h)\cos(TS - 0.3098)\ \sin\gamma\ \cos(TS-\alpha_U)}{\sin\theta} + \frac{\cos(h)\sin(TS - 0.3098)\cos\gamma}{\sin\theta\ \cos(h)} \tag{46}$$

where it is assumed that τ is constant with time.

The functions $F_{1,2}$ and F_3 are called the 'response' of the E-W and N-S interferometers respectively. They give the efficiency of the interferometers in measuring angular deflections in the solar line-of-sight as a function of time and geometry. The response given by Eq. 45 of the E-W interferometers as a function of time is plotted in Fig. 20 with α_U in degrees indicated on the curves. It is seen that the shape of the curves is a function of the parameter α_U; in particular, the local time at which, $F_{1,2}$ becomes zero is a function of α_U. This suggests that the line along which TIDs travel may be determined by the modulation imposed by the interferometers on the observed magnitude of the solar angle-of-arrival scintillations. In Fig. 21 the corresponding response F_3 of the N-S interferometer is plotted as a function of time for various values of α_U.

3.5 TWO DIMENSIONAL PROJECTIONS OF THE INTERFEROMETER CONSTANT PHASE SURFACES

The simplest three-dimensional surfaces which can be generated as an aid to visualizing the operation of an interferometer are obtained by setting θ in Eq. 1 equal to certain constant values. The surfaces thus defined are cones whose axes are coincident with the interferometer's base line. A two-dimensional projection of these surfaces is developed as an aid to visualizing the response of the interferometers to angle-of-arrival variations. Specifically, equations are derived giving the loci of the intersection of these cones with a plane perpendicular to the north-south direction. In Fig. 19 imagine a plane parallel to the plane containing OY and OZ and intersecting the OX axis at a distance C south of O. Let,

$$Y_N = \frac{Y}{C} \quad \text{and} \quad Z_N = \frac{Z}{C}$$

The loci of the intersection of the E-W interferometer surfaces of constant θ with this plane is given by

$$Z_N^2 = (Y_N^2 \tan^2\theta - 1)^{\frac{1}{2}} \qquad (47)$$

and the loci of the intersection of the solar line of sight with the same plane is given by

$$Y_N = \tan(TS) \qquad (48)$$

and

$$Z_N = \tan(h)/\cos(TS) \qquad (49)$$

Equation 47 describes a family of hyperbolas which are plotted in Fig. 22 for indicated values of θ. The 'paths' of the solar line-of-sight, defined to be the loci of the intersection of the solar line-of-sight with the defining plane, are given by the dashed curves for various times in the year. The numbers shown give the universal time of the solar ray at the indicated positions. With the aid of Fig. 22 one may readily check the general shape of the curves plotted in Fig. 20. In the case where $\alpha_u = 0^o$, for example, the solar ray, when refracted by the ionosphere, remains in the plane described previously, which in Fig. 19 contains the X-axis and a line joining the origin and the sun. The intersection of this plane with the one defined to obtain Fig. 22 would be represented in Fig. 22 by a straight line joining the origin with the position of the sun. Since the interferometer is sensitive only to angular deflections transverse to the curves of constant θ and the magnitude of this component varies with time throughout the daily period of observation the sensitivity of the interferometer varies with time in a similar manner. Between October and February the early

morning magnitude of the component of angular deflection transverse to the curves of constant θ is relatively large because of the large angle between the above line and the curves of constant θ. The magnitude of this angle decreases as the sun progresses towards its local noon position and correspondingly the response of the interferometer, which is proportional to the magnitude of the component of the angular deflection observed, decreases as shown in Fig. 20. The 0^{o} curve in Fig. 20 is anti-symmetrical about the local noon position because of the symmetry of Fig. 22. A similar procedure may be employed to verify the shape of the other curves in Fig. 20. For each value of α_u considered, the line to be drawn on Fig. 22 representing the plane of the refracted ray is defined by the 'position of the sun' and the point

$$Z_N = 0$$

$$Y_N = \tan(\alpha_u)$$

The shift of the latter point from the origin is responsible for the increasing loss of symmetry in Fig. 20 as α_u increases in magnitude from 0^{o} to 90^{o}. There is a small distortion present in Fig. 22 which becomes apparent for large values of α_u. If one follows through with the argument used above for $\alpha_u = 90^{o}$, for example, one finds that the response of the interferometer would appear to increase monotonically in magnitude as the sun progressed from its early morning position to its local noon position, at which time it would be equal to unity, and then would decrease with time. However, as indicated in Fig. 20 the response is equal to unity throughout the interval 1900 to 2100 UT because the plane containing the refracted ray also contains the

interferometer's base-line. This small discrepancy is due to the use of a plane to generate Fig. 22 instead of a cylinder whose axis coincident with the interferometer's base-line.

It is worth noting that the angle-of-arrival as defined by Eq. 2 may change slowly during the period of observation, even though the localized source of emission on the sun's disk is stationary with respect to its center and the solar line-of-sight is not bent by the earth's ionosphere. This can be seen by referring to Fig. 22 once again. Let us assume that the path of the sun is given by the curve for November 12, 1969. The localized noise source, if not at the center of the sun, will have a declination and hour angle which will differ from that of the center of the sun. For purposes of illustration assume that its path is given by the curve for October 20, 1968. The angle of arrival θ_{SN} gives the angular displacement of the noise source with respect to the center of the sun transverse to the surfaces of constant θ. In this case θ_{SN} is positive at 1300 UT, becomes zero at local noon and assumes increasingly negative values thereafter. These inherent long-term variations will not be significant for the results reported here since the scintillations of interest have periods of thirty minutes or less.

The loci of the intersection of the N-S interferometer's surfaces of constant θ with the plane described above and used to generate Fig. 22 is given by

$$Z_N = [(\cos^2 e \tan^2\theta - \sin^2 e) + 2Y_N \sin e \cos e (\tan^2\theta + 1) + Y_N^2 (\sin^2 e \tan^2\theta - \cos^2 e)]^{1/2} \quad (50)$$

where, $e = 0.3098$.

A small correction term resulting from the somewhat greater height of the south antenna with respect to the north one is neglected in Eq. 50. The curves described by Eq. 50 are ellipses and not circles as would be the case for a north-south interferometer because the interferometer's base-line is inclined to the north-south direction. The family of ellipses defined by Eq. 50 are plotted in Fig. 23; also the 'paths of the sun' for various times of the year are drawn in once again with dashed lines. The response of the N-S interferometer to scintillations can be determined using Fig. 23 in a similar manner as the response of the E-W interferometer was determined using Fig. 22.

3.6 FOCUSING AND DEFOCUSING EFFECTS OF TIDs

Closely following Turnbull and Forsyth (1965) focusing and defocusing of the radio-wave energy by TIDs is now considered. Only the simplest case dealing with relatively small deviation angles or irregularities at low altitudes is considered. In this case the only effect on the ground is slight focusing and defocusing of the radio-wave energy as the solar line-of-sight encounters TIDs. The more complex case where rays from two or more widely separated points in the TID reach the observer, while rays from intervening regions do not, is not considered because the deep amplitude fading which would result from this type of mechanism was not experimentally observed.

The geometry is illustrated in Fig. 24 where the plane of the diagram is assumed to be the plane containing the solar line-of-sight and the TIDs' line of travel. The refracted solar line of sight will also be in this plane. Since only variations within this plane are of interest, it is convenient to consider energy densities as for

a system of cylindrical symmetry. Two solar rays SPB and S'QE are shown meeting the ground at B and E. They intersect the ionosphere MN at P and Q and undergo angular deflection θ and $\theta + d\theta$ respectively. The undeflected rays make an angle e with the ground. The distance r between the observer and the ionospheric intersection point of the solar ray is given by:

$$r = H/\cos(h) \tag{51}$$

where:

H = height of the intersection point

h = altitude of the sun

Energy falling on the element of the irregularity ds would, in the absence of the irregularity, fall on the ground spread over an element dp and in the presence of the irregularity spread over an element dx.

Since: $dq = r d\theta/\sin(e)$

$dp = ds$

then $$dx = ds + \frac{r d\theta}{\sin(e)} \tag{52}$$

If the energy density at MN is E_o then the energy density at point x on the ground is given by

$$E_o ds = E(x) dx \tag{53}$$

By combining Eqs. 48, 52 and 53 one may write

$$\frac{d\theta}{ds} = \frac{\sin(e)\cos(h)}{H} \left[\frac{E_o}{E(x)} - 1 \right] \tag{54}$$

This distance of separation ds of the rays may be written as

$$ds = U' dt \tag{55}$$

where:

$U' = U - \underline{U}.\underline{V}/U$

$\underline{U}$ = TID velocity

$\underline{V}$ = velocity of the point of intersection of the solar line of sight with the ionosphere.

Eqs. 54 and 55 are combined to give

$$U' = H/K \tag{56}$$

where:

$$K = \frac{\sin(e)\cos(h)}{d\theta/dt}\left[\frac{E_o}{E(x)} - 1\right] \tag{57}$$

Since $\underline{V}$ is known as a function of height and the direction of travel of the TIDs can be determined from Fig. 20, the apparent speed U of the TIDs can be obtained as a function of height from Eq. 56.

CHAPTER IV

EXPERIMENTAL AND ANALYTICAL RESULTS

4.1 INTRODUCTION

Interferometer measurements of amplitude and angle-of-arrival of 51.7 MHz solar radio waves are now presented and described. They were made on those days between 16 October 1968 and 2 March 1970 when the sun was radiating metric wavelength radio waves at an enhanced level during most of the time that it was visible. Scintillations in the angle-of-arrival were observed on at least eighteen days. It will be shown that these can be interpreted as being due to TIDs and that pertinent TID parameters can be deduced from the observation.

The measurements reported here can be divided into two categories according to which set of three antennas in Fig. 8 was employed to make two phase measurements:

(a) measurement of the phase differences between radio signals arriving at antennas Y_0 and Y_1 and antennas Y_0 and Y_2.

(b) measurement of the phase differences between radio signals arriving at antennas Y_0 and Y_2 and antennas Y_0 and Y_3.

It is to be noted that in each case antenna Y_0 and the associated electronic receiving channel was common to the two phase measurements. The measured phase differences were converted to angle-of-arrival θ_{SN} of the solar ray with respect to the interferometer base-line and the centre of the sun. The amplitude of the solar radio signal was also recorded. These

records were converted to flux density by means of calibration curves.

4.2 CALIBRATION CURVES FOR AMPLITUDE RECORDS

The calibration curves for the interferometer amplitude records were obtained by recording the signal radiated by an antenna fed by an external test oscillator. Its output was reduced with an attenuator by known amounts until the amplitude of the recorded signal was equal to or less than that recorded by the interferometer when monitoring Cassiopeia A. The known flux density emitted by Cassiopeia A was then used as a reference to calibrate the amplitude records in terms of flux density. Calibration curves obtained on 22 November 1968, a day during which the sun was particularly quiet with respect to metric wave emissions, are given in Fig. 25. An internal test oscillator was used by check the sensitivity of the interferometers from day to day. It follows from Fig. 25 that for signals with amplitudes greater than one unit the relationship between the flux density P and the recorded amplitude x is of the form

$$P = e^{b}e^{ax}$$

where a is the slope of that portion of the calibration curve with, $x > 1$; and

b is the y-axis intercept of the projection of the above curve. The factor e^{b} may be as much as 70% in error because of changes in the sensitivity of the interferometer and inaccuracies in establishing the reference calibration level; therefore the absolute values of flux densities reported herein may be this much in error. On the other hand, the error in the ratio of flux densities recorded at two

separate times, for time duration of up to an hour or so, is only of the order of 15% because the factor e^b does contribute to its magnitude.

4.3 EXPERIMENTAL RESULTS

4.3.1 Angle-of-Arrival for 28 October 1968

The angle-of-arrival versus time measured with the wide E-W interferometer on 28 October 1968 is given in Fig. 26. The curve is fairly steady between 1330 and 2030 UT: although it does show some evidence of quasi-periodic scintillation with peak-to-peak (p-p) amplitude of 10' arc. This is the type of result one would expect for the case of relatively undisturbed ionosphere; one in which TIDs, for example, if present possessed small amplitudes.

4.3.2 Angle-of-Arrival for 12 November 1969

The angle-of-arrival versus time measured with N-S interfometer on 12 November 1969 is shown in Fig. 27. In this case the curve shows well-defined quasi-periodic scintillation between 1430 and 2000 UT, or so, with maximum p-p amplitude of 45' arc. The slow decrease and then increase of angle-of-arrival between 1300 and 2100 UT is not considered here and may be due to the solar source of the radio waves not being located at the centre of the solar disk. The quasi-periodic scintillations betwen 1430 and 2000 UT are attributed to refraction of the solar line-of-sight by TIDs. The solar flux density recorded by the N-S interferometer on 12 November 1969 is also given in Fig. 27. There are some scintillations discernible on the solar flux density; in particular, near 1515 UT. These are attributed to focussing and defocussing effects or in other words, to redistribution of the radio-

wave energy by refraction of the solar line-of-sight.

Fig. 28 shows a direct comparison of the wide E-W and N-S interferometer angle-of-arrival data recorded on 12 November 1969. The dashed curve gives the angle-of-arrival for the E-W interferometer and the solid curve gives the equivalent data for the N-S interferometer. It can be seen that there is a high degree of correlation in the occurrence of the scintillations on both sets of data. The solid vertical lines indicate the times when "peaks" or local maxima in angle-of-arrival occurred for both sets of data. In one case, namely at 1516 UT, a peak in the E-W curve corresponds to an inflection in the curve. The dashed vertical lines suggest possible coincidences in the peaks but are not used in the analysis since the coincidences are not well defined.

4.3.3 Angle-of-Arrival for 27 October 1968

The angle-of-arrival for 27 October 1968 is shown in Fig. 29. The solid curve gives the data recorded by the wide E-W interferometer and the dashed curve gives the data recorded by the narrow E-W interferometer. Quasi-periodic scintillations are present between 1340 and 1830 UT. The agreement between the two sets of data is excellent except between 1330 and 1420 UT; during which time the narrow E-W interferometer appears to have undergone a slow phase drift; although the agreement between the small scale structure is good. The scintillations that appear on both sets of data are attributed to refraction by TIDs. Fig. 30 shows the magnitude of the solar flux density on 27 October 1968. For purposes of comparison the angle-of-arrival for 27 October 1968 is shown once again. A comparison of the 27 October 1968 wide E-W interferometer

angle-of-arrival data with two sinusoids; one with a period of 21 minutes and the other with a period of 13 minutes, is given in Fig. 31. Local noon is indicated by the dashed line at 1709 UT. The period of the scintillations is approximately 21 minutes between 1340 and 1630 UT and again between 1750 and 1840 UT. The 21 minute scintillations in the first interval are in phase with the sinusoid; whereas, the 21 minute scintillations in the last interval are approximately 180° out of phase with the sinusoid. The period of the scintillations in the interval 1645 to 1740 UT is approximately 13 minutes.

The angle-of-arrival and solar flux density measured with the wide E-W interferometer on 29 October 1968 are given in Fig. 32. Scintillations in the angle-of-arrival are present between 1330 and 1700 UT. The solar radio-wave emissions on this day were sufficiently constant in amplitude to show scintillations in the measured flux density between 1330 and 1700 UT. The scintillation in flux density at 1600 UT is especially well defined and approximately 90° out of phase with the corresponding angle-of-arrival scintillations. The scintillations in angle-of-arrival are due to refraction of the solar line of the sight by TIDs. The scintillations in solar flux density are attributed to focussing and defocussing associated with refraction of the solar line of sight.

4.3.4 Angle-of-Arrival for 16, 18, 25 October 1968; 10, 11 November 1969 and 2 March 1970

Angle-of-arrival results for 16 October 1968 are given in Figs. 33 and 34. In the first figure the dashed curve gives the angle-of-arrival recorded by the wide E-W interferometer and the solid curves give the product of the sum of three sine waves with periods 21, 30 and 60 minutes with a function which decreases monotonically towards local

noon. A comparison of the angle-of-arrival measured with the narrow and wide E-W interferometers is given in Fig. 34. The agreement between the two sets of data is good except for the short interval between 1337 and 1350 UT. The magnitude of the recorded solar flux density between 1330 and 1510 UT and 1510 to 1800 UT was approximately 2.5×10^{-22} and $7.5 \times 10^{-22} wm^{-2} Hz^{-1}$, respectively. The scintillations appearing on both sets of data in Fig. 34 are attributed to refraction of the solar line of sight by TIDs.

Figs. 35 and 36 give angle-of-arrival results for 25 October 1968. A comparison of the wide and narrow E-W interferometer data in Fig. 35 shows good agreement between 1410 and 1540 UT. The scintillations appearing in the interval of high correlation are attributed to TIDs. Fig. 36 shows that the period of the scintillations is 21 minutes. The magnitude of the solar flux density for the time of the solar angle-of-arrival data was about $8 \times 10^{-23} wm^{-2} Hz^{-1}$.

The 18 October 1968 results are given in Figs. 37 and 38. A comparison of the wide E-W interferometer angle-of-arrival data and flux density received is given in Fig. 37. There does not appear to be a correlation between the two; therefore the scintillations in angle-of-arrival appearing between 1530 and 1630 UT are attributed to TIDs. Fig. 38 indicates that the period of the scintillations is again 21 minutes.

The results for 10 November 1969 are shown in Fig. 39. A comparison between the wide E-W and N-S interferometer angle-of-arrival data is given, with good correlation occurring between the scintillations on the two sets of data, although the scintillations are larger on the N-S data. If one does a mental Fourier transform on the data one finds

a dominant period of 20 minutes.

A comparison between the N-S and wide E-W interferometer angle-of-arrival data for 11 November 1969 is given in Fig. 40. Once again the scintillations are larger on the N-S interferometer data but the correlation between the two sets of data is in general good. The dominated periods of the scintillations in the time intervals 1330 to 1730 and 1730 to 2015 UT are 32.1 and 15.9 minutes respectively.

The angle-of-arrival data for 2 March 1970 given in Fig. 41 shows a remarkable large angle-of-arrival scintillation between 1530 and 1556 UT with peak-to-peak amplitude of 100 minutes of arc. Correlation between the N-S and wide E-W angle-of-arrival scintillations is good for the time interval 1400 to 2100 UT shown in Fig. 40. The amplitude of the N-S scintillations is again greater than that of the wide E-W scintillations. The solar flux density recorded by the interferometer is also shown in Fig. 41 and gives a well defined minimum at 1541 UT which coincides with the time at which the large scintillation has progressed through 180 degrees of phase, has zero deflection and is undergoing its maximum rate of change of angle-of-arrival. The dominant period of the scintillations in the time interval 1415 and 1830 UT is 21 minutes.

4.4 ANALYTICAL RESULTS

4.4.1 Properties of East-West Moving TIDs

The magnitude of the angle-of-arrival scintillations observed by the wide E-W interferometer on 12 November 1969 is given in Fig. 44. The average amplitude throughout the interval is approximately 6' of arc. According to Fig. 20 the line of travel of the responsible TIDs is in the east-west direction with a possible deviation of $\pm 35^{\circ}$. Only for

angles between 55° and 90° and -55° and-90° is the response of the E-W interferometer sufficiently constant to account for the observed constant average amplitude.

The apparent period of the scintillations on 12 November 1969 is given in Fig. 46. These values were obtained by measuring the distance between the vertical lines in Fig. 28. A scintillation is defined for this measurement as a local maximum in the angle-of-arrival that occurs on both the E-W and N-S interferometers simultaneously. The scintillations defined by the dashed lines do not meet this requirement and therefore are not used in the analysis. They are mentioned here because there is some indication that a scintillation may have occurred at these times. The peaks of the scintillations have been used but the troughs could have been used equally well. There is a monotonic decrease of the period of the scintillations with time before local noon (1709 UT) and a monotonic increase with time after local noon. Since the east-west component of velocity of the intersection of the solar line-of-sight and the ionosphere varies in the same manner, this behavior is consistent with the direction of travel deduced above; namely the east-west direction. Futhermore, the variation of the period of the scintillations, namely, the decrease towards local noon and increase afterwards, rather than the reverse, suggests that the TIDs move towards the west. From the degree of symmetry of the pattern produced by the systematic variation of the period in Fig. 46 about local noon, and Eq. 30, one can estimate that the deviation of the line of travel from the E-W direction is at most ±15°. Finally, it is to be noted that the average period of the scintillations between 1600 and 1830 UT, when the apparent speed of the

sun reaches its lowest value, is approximately 13 minutes. It follows that because of the motion of the solar line of sight the true TID period is somewhat less than 13 minutes.

A plot of the inverse of the apparent period of the scintillations observed on November 12, 1969 versus the E-W component of the velocity of the solar line of sight through the ionosphere is given in Fig. 47. The altitude of the intersection point used is 200 km. The dashed line was obtained from a least squares fit of the data. The dashed curve shown in Fig. 46 was derived from the straight dashed line in Fig. 47 and is appropriate for an intersection altitude of 200 km. Similar analyses at other values of altitude would produce curves which were indistinguishable from the one shown in Fig. 46. The dashed curve in Fig. 46 appears to explain the systematic variation of the period of scintillations. The questionable data point at 1940 appears to be in agreement with the curve and the one at 1430 UT does not. Further evidence that the point at 1940 UT may be real is given by the fact that there appears to be a scintillation in the flux density at 1940 UT in Fig. 27 which correlate well with the angle-of-arrival scintillation. At 1420 UT, on the other hand, it is difficult to tell whether or not there is a corresponding scintillation in the flux density.

It follows from Eq. 32 that if, $\alpha_U = 270^0$, as is the case here, the slope of the straight line in Fig. 47 is equal to $1/60\lambda$, and the intercept with the vertical axis at, $V_x = 0$, is, $1/T$; where T is the true TID wave period in minutes. Thus, one is able to solve for the period, wavelength, and velocity of the TIDs. The only unknown is the altitude, so that the analysis must be repeated for a number of altitudes between 100 km and 500 km, or so. The velocity of the TIDs as a function

of height is indicated by the solid curve in Fig. 48; the period in minutes is indicated by the numbers beside the data points. The standard deviation of the period is ± 4 minutes. The period decreases with increasing height. The wavelength as a function of height is shown in Fig. 49.

The dashed curve in Fig. 48 was obtained by correlating the scintillations in angle-of-arrival and flux density in Fig. 27 between 1445 and 1505 UT. From the ratio of maximum flux density the apparent velocity, U', given by Eq. 56 can be solved for as a function of height. Since one knows the velocity of the solar line-of-sight through the ionosphere as a function of height, the 'true' TID velocity can be solved for as a function of height, and is given by the dashed curve in Fig. 48. There is agreement between the two curves in the lower ionosphere. The curves appear to diverge above 300 km, or so, suggesting that the centroid of the TIDs was contained between 100 and 300 km.

The magnitude of the angle-of-arrival scintillations recorded by the N-S interferometer on November 12, 1969 is given in Fig. 45. Fig. 21 indicates that the response of the N-S interferometer to TIDs whose line of travel is inclined by +75 to +90° or -75 to -90° with the X-axis in Fig. 17 goes to zero between 1530 and 1600 UT. Therefore the magnitude of the scintillations in Fig. 45 should go to zero in this interval, since, according to the E-W interferometer data, these TIDs have an east-west line of travel. The magnitude of the scintillations does in fact approach zero in Fig. 45 at 1600 UT, but since the period of scintillations is perturbed from the dashed curve in Fig. 46 at this time, this is likely due to the TID motion being perturbed at this time.

One might guess that the unperturbed value would be 7' arc to make it consistent with the magnitude of the scintillations immediately before and after the interval 1600 to 1625 UT. Since the amplitude of the scintillations does not go to zero at this time there exists an inconsistancy between the data and the theoretical curves of Fig. 21. Furthermore, at 1640 UT, for example, the magnitude of the scintillations in Fig. 45 is about 7' arc, whereas the E-W interferometer recorded a scintillation amplitude of about 6' arc (Figure 44). According to Figs. 20 and 21 the response of the N-S interferometer at this time is between 0.3 and 0.55 of the E-W interferometer, therefore the scintillation amplitude recorded by the N-S interferometer should only be between 2' and 3.5' arc. In summary, the amplitude of the N-S interferometer is roughly 5 to 3.5' arc greater than one would expect.

The above discrepancy can be explained in the following way. One can see by referring to Fig. 22 that the E-W interferometer measures angular deflection of the solar line-of-sight produced by horizontal gradients, for TIDs moving in the east-west direction, but does not measure angular deflections produced by vertical gradients. The deflections caused by the latter are parallel to the constant interferometer phase surfaces and therefore are not detected whereas the former are at right angles to them and are detected. At 1640 UT, on the other hand, the N-S interferometer registers one half or so of the amplitude of any horizontal angular deflection of the solar line-of-sight as shown by Fig. 21; but, as can be seen from Fig. 23, it also measures or is sensitive to, vertical deflections of the solar line-of-sight. Actually, it measures the component of the vertical deflection transverse to the constant interferometer phase surfaces which in this case is somewhat

smaller than the vertical angular deflection. The above is true only if a vertical deflection upwards is accompanied by a horizontal deflection to the west or a vertical deflection downwards is accompanied by a horizontal deflection to the east. If the reverse were to happen, the resultant angular deflection would take place parallel to a constant interferometer phase surface and would not be detected by the interferometer. This argument indicates that the TIDs constant phase surfaces are titled forward in the direction of TID motion. In other words, the angular deflection of the solar line of sight has both a vertical and horizontal component, and of the correct polarity as outlined above to be detected by the N-S interferometer. The angle of forward tilt, from the vertical, is very roughly given by the following equation, which is the ratio of the horizontal component of the angular deflection divided by the vertical component. The horizontal component is equal to the deflection measured by the E-W interferometer; whereas, the vertical component is deduced from the total deflection measured by the N-S interferometer, the geometry of Fig. 23 and the value of the horizontal component from the E-W interferometer.

$$\tan \theta_f \approx \frac{6' \text{ arc}}{4.7' \text{ arc}} = 1.28$$

$$\theta_f \approx 50^{\circ} \ (\pm 20^{\circ})$$

where: θ_f is the angle of forward tilt,

There is evidence that the motion of the TIDs responsible for the scintillation on November 12, 1969 was perturbed by a disturbance with a relatively long period. Evidence of this is seen in Fig. 45 where the amplitude of the scintillations recorded by the N-S interferometer

deviates significantly from a likely average value of 8' arc at 1500, 1610 and 1730 UT. Furthermore, the apparent period in Fig. 46 departs from the dashed curve at 1540, 1610 and 1720 UT. Finally, in Fig. 27 one can discern an enhancement in flux density at 1430, 1520, 1630 and 1730 UT. The good agreement that exists between the times at which these parameters were perturbed suggests the presence of a perturbation with a period of approximately one hour.

4.4.2 Properties of North-South TIDs

The magnitude of the 21-minute scintillations measured by the E-W interferometers on October 27, 1968 is given in Fig. 50. It can readily be seen that after 1520 UT the amplitude decreases toward local noon and increases after local noon. In addition, as mentioned above, the phase of the 21-minute scintillations occuring after local noon is approximately 180° out of phase with those occuring before local noon. One can see by referring to the 0° curve in Fig. 20 that the above characteristics are just what one would expect for scintillations recorded by an east-west interferometer caused by TIDs moving along a north-south line of travel. There is a two-fold ambiguity in that one does not know whether the motion is towards the north or towards the south along this line of travel. The maximum deviation of the line of travel from the N-S direction is ($\pm 8^{\circ}$). The increase in magnitude of the scintillations before 1520 UT in Fig. 47 is not inconsistent with the above interpretation. In all likelihood the observed TIDs consists of wave-packets, so that the increase in magnitude corresponds to the increase in magnitude one would expect at the beginning of a realistic wave-packet.

Close inspection of Fig. 31 shows no discernible systematic change in the period of the 21-minute scintillations between 1345 and 1630 UT. The speed of the responsible TIDs is therefore greater than 870km/hr assuming that the centroid of the TIDs was contained between 200 and 500 km, since the north-south component of the velocity of the solar line-of-sight changed by about 135 km/hr in this interval. The TID wavelength is greater than 300 km because the wave-period, to a good approximation, is 21 minutes.

Since the 13 minute scintillations are discernible at local noon the responsible TIDs are travelling in a predominantly E-W direction. Their magnitude is smaller and they are only discernible when the response of the E-W interferometers is low or non-existent to the larger scintillations produced by the N-S TIDs. These scintillations are similar to those produced by the E-W TIDs observed on November 12, 1969. They have similar apparent periods, amplitude, and constancy of amplitude about local noon.

The direction of travel of the TIDs which produced the scintillations shown in Fig. 32 is not readily discernible from the characteristics of the scintillations. The period of the scintillations between 1515 and 1610 UT being 21 minutes suggests that the responsible TIDs may have travelled north-south because the scintillations in Fig. 32, caused by north-south travelling TIDs also had a period of 21 minutes. The scintillations in flux density are again attributed to focusing and defocusing of the radio-wave energy by TIDs. If one makes no assumption concerning the direction of travel of the TID, assumes only that its height was approximately 300 km and then correlates the angles-of-arrival and amplitude scintillations between 1540 and 1610 UT, as before, one can deduce the speed of the TIDs responsible for bending the solar ray as

being greater than 300 km/hr. The upper limit of the speed is a function of the line of travel; for a north-south line of travel, for example, it is roughly 1500 km/hr and for an east-west line of travel it is roughly 700 km/hr.

The maximum observed TID induced angular deflection was roughly ±20 minutes of arc, indicating, according to Eq. 35, a maximum gradient in columnar electron content for the TID of 3.5×10^{14} el/m^2km. If one assumes that the TID which generated the scintillation was contained between 250 and 350 km the above columnar electron gradient corresponds to an electron number density perturbation of only 1 percent, or so.

The magnitudes of the angle-of-arrival scintillations observed on October 16, 1968 (Fig. 33), October 25, 1968 (Fig. 35) and October 18, 1968 (Fig. 38) are all observed to decrease with time approaching local noon. These scintillations are attributed to TIDs travelling along a line orientated predominantly in a north-south direction with a maximum deviation of $\pm 10^{o}$. The average period of the scintillations in each case is approximately 21 minutes. A scintillation 'peak' appears to be absent in Fig, 33 at 1450 UT. This may be due, as suggested by the solid curve in Fig. 33, to interference between three waves with periods of 21, 30 and 61 minutes.

4.5 DISCUSSION OF THE TID INTERPRETATION

4.5.1 Alternate Mechanisms

A number of phenomena other than TIDs can be put forward to explain the scintillations observed in the solar angle of arrival. Some seven are now listed and shown in Section 4.5.2 to be incapable of explaining the observations. The alternate mechanisms to be

considered are as follows:

(a) transverse quasi-sinusoidal motion of the source with respect to the center of the solar disk

(b) refraction of the radio waves by irregularities in the corona of the sun or irregularities in the intervening space between the sun and the earth

(c) instrumentally produced phase variations

(d) interference between the direct ray from the sun and a second ray originating from -

(i) a reflected ray

(ii) Cassiopeia A or Cygnus A

(iii) splitting of the original ray into two modes ordinary and extraordinary

(iv) a ground based transmitter

(e) interference between multiple sources

(f) interference between two sources on the solar disk varying sinusoidally in amplitude

(g) periodicities introduced by the 'phase ramps'

4.5.2 Discussion of Alternate Mechanisms

The mechanisms listed in Section 4.5.1 are now discussed and shown to be invalid.

(a) Quasi-periodic motion of the source would be a most remarkable phenomenon because of the magnitude of the motion requiring velocities as large as 4.5×10^3 km/sec transverse to the solar disk. Moving type IV solar bursts have been observed with speeds of the order of 1.0×10^3 km/sec but they have been observed to move radially and away from the sun (Wild et al, 1963). These bursts only last

typically for a few minutes, although on occasion durations of up to two hours have been observed. In addition, they are characterized by a very large source (>10' arc) with low directivity, which suggests that the angle of arrival measurements would vary in a random manner over an angle $\geq \pm 5'$ arc. The angle of arrival measurements in Figs. 27-41 are quite well defined and the width of the curves, for the most part, is considerably less than ±5' arc.

On the other hand the long lived continuum storms, which may persist for a day or more and which were employed as radio sources for this work, have been observed to be stationary. They lie close to the plasma level in the solar corona appropriate to the frequency of emission which in the case of 50 MHz is one solar radius above the photosphere. The sources have a small diameter of the order of 3' to 5' arc and the cone of emission is narrow, since they are rarely observed when the source is near the solar limb. The radiation is strongly circularly polarized, indicating that the magnetic fields of sunspot influence its generation or propagation (Wild, 1955).

(b) It will be shown that if irregularities in the corona of the sun or irregularities in the intervening space between the sun and the earth were responsible for the observed scintillations the observer must have been in their near field pattern. In other words, rays from two widely separated points on the irregularity did not reach the

observer and interfere with each other. If interference between two rays had caused the scintillations in angle-of-arrival shown in Fig. 27 or 30 the recorded solar flux density would have, according to the development of section 2.4, undergone deep fading which is not present in either of the amplitude records.

For example, the amplitude of the smaller scintillations in Fig. 27 is of the order of ±6' arc. It follows from the differential of Eq. 1 that this corresponds to a phase perturbation of $\pm 34^{o}$. The value of n in Fig. 6 corresponding to this phase perturbation is 0.57; therefore Aop/Aom from Eq. 15 or Fig. 7 is 3.6. This suggests amplitude fading with maximum and minimum values of solar flux density in the ratio 13:1. For angle-of-arrival scintillations in Fig. 27 with the largest amplitude this ratio becomes greater than 800:1. Since the ratios of maximum to minimum solar flux density in Fig. 27 are less than 2:1, the angle-of-arrival scintillations shown there are not due to interference effects.

In a similar manner, interference effects cannot account for the angle-of-arrival scintillations shown in Fig. 30. In order to do so that magnitude of the ratios in flux density would be greater than 400:1 and 7:1 for the scintillations with largest and smallest amplitudes respectively; whereas, if there is any evidence of flux density fading in Fig. 30, the ratio of maximum to minimum flux density is clearly less than 3:1.

There is well defined fading, on the other hand, in the solar flux density shown in Fig. 32 which is also roughly 90^{o} out of the phase with the corresponding scintillations in angle-of-arrival; characteristics of scintillations caused by either interference or refraction effects. Once again the fading cannot be due to interference because the ratio of the flux density magnitudes is much less than the value 80:1 which would be the case if they were caused by interference.

Further evidence against interpretation of the angle-of-arrival scintillations as being due to interference effects is given by the following factors;

(i) the period of the scintillations measured by two interferometers whose base-lines have different geometries is the same (Fig. 28, 29, 34, 35, 39, 40, 41).

(ii) the amplitude of the scintillations measured by two interferometers with different antenna separation is the same (Fig. 29, 34, 35).

(iii) the amplitude of the scintillations measured by two interferometers with similar antenna separations is different (Fig. 28, 39, 40, 41).

It has been shown that if the bending of the solar ray was caused by irregularities in the solar corona the observer was located in the near field. Now it will be shown that because of the large scale sizes implied by the observations it is most unlikely that the irregularities were in the solar

corona. The minimum spatial extent of the irregularities transverse to the solar line of sight is related to the distance from the observer by the following expression;

$$S = 2\tau r$$

where

S, is the minimum extend of the irregularities (km)

τ, is the amplitude of the scintillations expressed in radians

r, is the distance from the earth to the irregularities (km)

For the large scintillations with τ = 20' arc the minimum scale size increases with distance from the earth and would be of the order of 2 solar radii if the refraction was caused by irregularities near the sun. Further evidence that makes this hypothesis untenable is the large degree of order required of the irregularities to account for the quasi-periodic nature of the scintillations and also the large gradients in electron density required by the irregularities, because of their immense size if they are near the sun, to bend the solar ray sufficiently to intercept the earth.

(c) The phase stability of the E-W interferometer was demonstrated in Fig. 10 where good agreement was shown between angle-of-arrival measurements made with Cassiopeia A and Cygnus A on two separate days. Its long-term stability showing phase variations of only 20 degrees, or so, was demonstrated in Fig. 15. The good agreement shown between scintillation appearing on measurements made with interferometers

having different geometries suggests that the scintillations were not produced within the instruments themselves.

It might be argued, on the other hand, that the receiving channel common to the two interferometers in use at any particular time may have produced temporal phase variations in its signal which would affect the angle-of-arrival measurements made by both interferometers. In the case of the wide and narrow E-W interferometers it follows from the differential of Eq. 1 that phase variations produced by the common element could produce scintillations in the narrow E-W interferometer's angle-of-arrival measurements which were about three times as large as those of the wide E-W interferometer because their base-lines are approximately in the ratio 1:3. Since the observations show that the amplitudes of the scintillations measured by these two interferometers are the same their origin cannot be instrumental.

A careful look is required at the agreement shown in Fig. 28 between the wide E-W and the N-S_0 interferometers measurements with regards to the possibility of temporal phase variations in the common channel. A plot of the ratio of the magnitudes of the scintillations measured by these two interferometers is given in Fig. 42. The dashed curve gives the theoretical ratios that would be observed if phase variations did occur in the common channel. There are some cases where there is disagreement between the data and this curve. The hypothesis of the common channel causing

the scintillations may be discarded on grounds that the measurements are not consistent with it at all times, which must be the case for it to be valid. In addition this mechanism cannot account for the scintillation in flux density in Fig. 27 associated with the large angle-of-arrival scintillations. Finally, the stability of the wide E-W interferometer discounts the possibility of a phase instability in one of its channels.

(d) The supposition of a second signal interfering with the direct signal from the sun may be discounted on the following two grounds;

(i) it is unlikely that a second signal of sufficient amplitude was present

(ii) the observed scintillations have properties which are not consistent with this hypothesis. The reply to item (b) is directly applicable here and will not be dealt with further.

It can be shown that the second ray did not consist of a ray reflected from the ground. The coefficient of reflection for 50 MHz vertically polarized radio waves varies from 0.42 for an elevation angle of 30^{0} to 0.28 for an elevation angle of 20^{0} (Beckmann and Spizzichino, 1963). The radiation pattern of the antennas would further reduce the amplitude of the reflected signal relative to the direct ray. Therefore the effective reflection coefficients are approximately 0.04 and 0.12 respectively. It follows from

Fig. 6 that for the latter value phase scintillations whose magnitude was ±8 degrees could be generated by the reflected signal. This corresponds to variations in angle-of-arrival of only ±2, ±6 and ±3 minutes of arc for the narrow E-W, wide E-W and N-S interferometers respectively, which, in each case, is much smaller than the variations measured. Also according to Eq. 16 the period of the scintillation would approach infinity because the period of the sun and its image are essentially the same. Therefore, for the above reasons, the reflected ray could not have been the source of the second ray.

The contention which attributes the solar scintillations to interference between the ordinary and extraordinary components of the solar signal is invalid for the following reasons;

(i) since the characteristic modes for quasi-longitudinal propagation through the ionosphere are left or right circularly polarized and the radiation emitted from 'continuum storm' is strongly circularly polarized, most of the solar radiation will, as a result, propagate through the ionosphere in one or the other mode.

(ii) Since the disturbed sun is a noise source the solar radio waves will only have phase coherence over short intervals of time and therefore Faraday rotation effects will not be observed.

(iii) Interference between the O and X modes will manifest itself as Faraday fading in the amplitude of the received radiation and would only affect the angle-of-arrival

measurements if the amplitude of the incoming radiation is reduced to such an extent that phase measurements made with the interferometer are in error because of the low signal-to-noise ratio.

Palmer et al. (1970) observed variations, due to Faraday rotation, of $\pm 20^{\circ}$, or less; in the measured phase between two signals from a satellite. They measured fading in signal power with a maximum to minimum ratio of 25:1, which is much greater than any flux density fading observed for the solar measurements reported in this thesis. Therefore any phase scintillations generated by Faraday rotation of the solar signal would be less than that reported by Palmer et al. and thus too small to explain the solar angle-of-arrival scintillation.

Further evidence for discounting Faraday rotation effects is derived from a consideration of the rate of Faraday rotation due to the apparent motion of the sun. Bowhill (1958) has shown that the rate of Faraday rotation of a plane-polarized wave transmitted by a satellite is proportional to the component of the earth's magnetic field resolved along the satellite's path. This proportionality must also apply to emissions from the sun since, the electrons below, say, 1000 km are the only ones which are effective in producing Faraday rotation (Lawrence et al., 1964). For purposes of this discussion therefore the sun can be considered to behave as a satellite because it has an effective height of 1000 km.

The variation of the rate of Faraday rotation of a solar signal can be obtained by considering the above proportionality and Fig. 17. Let us assume that the effective magnetic field along the solar line-of-sight is its value at the F-region peak. The dip angle and declination of the magnetic field at the mid-point of the path is 70° and roughly 30° respectively. Now consider the 300 km path in Fig. 17. The component of the earth's magnetic field along the path between 1310 and 1510 UT and along the path between 1910 and 2110 UT is greater than the component along the path between 1510 and 1910 UT. It goes to zero shortly after local noon. Therefore the period of any Faraday rotation of the solar signal should be a monotonically increasing function before local noon and a monotonically decreasing function shortly after local noon. The scintillations in Fig. 28 and 29 have just the reverse behaviour.

(e) It follows from the development in Section 24 that the simplest first order expression for the multiple source case consists of a term for each source similar to those shown in Eq. 12. The resulting signal, being a vector sum of those signals, would be complex with respect to phase and amplitude and in the case of many signals would be "noise-like". In addition some deep fading of the recorded flux density would be associated with the angle-of-arrival scintillation. Also, both the period and magnitude of the scintillation would be a function of the interferometer's antenna separation and geometry. Since the solar scintillations are relatively

simple, good agreement exists between measurements made with interferometers having different geometries and deep fading is not present in the recorded solar flux density, it follows that they were not generated by interference between multiple sources.

(f) Two sources on the solar disk emitting radio waves whose amplitude remains constant with time cannot generate short term angle-of-arrival scintillations such as those observed on the solar measurements. They move together and thus both have essentially the same period, which according to Eq. 16 means that the period of any scintillations caused by interference effects would be very large. On the other hand, if the amplitude of emission of one or the other of the sources were to fluctuate in a quasi-periodic manner, angle-of-arrival scintillations would be measured by the interferometer. The scintillation in angle-of-arrival produced by this mechanism would be proportional to the interferometer antenna separation and in addition the angle-of-arrival and flux density scintillations would be 0 or 180 degrees out of phase with one another. The scintillation shown in Figs. 29, 34 and 35 could not have been generated by this mechanism since the magnitude of the scintillation measured with the wide and narrow E-W interferometers is the same; whereas, if they were generated by this mechanism the magnitude of the scintillation would be in the ratio 1:3, respectively. Since for the most part the angle-of-arrival scintillations shown in Figs. 27 and 32 are approximately 90 degrees out of phase with respect to the solar flux density [illegible] not generated by the

two solar source mechanism. Enchanced radio emissions from the sun have an amplitude which is random with time except for ionospheric scintillation effects, so that it is somewhat far-fetched to imagine two sources on the sun emitting radio waves with amplitudes which are quasi-periodic with time.

(g) The phase measured by the interferometers and recorded on chart paper appears, for the most part, in the form of ramps, which for obvious reasons are called 'phase ramps'. Distance along the chart paper is proportional to time and distance transverse to the chart paper is proportional to the phase between the signals at the antennas. As a result, each time the phase between these signals changes monotonically with time by 360^{o} a complete phase ramp is recorded. If the interferometer is in error over part of the 360-degree phase range, scintillations in the angle-of-arrival can be generated with a periodicity given by that of the phase ramps. The periods of the phase ramps of the wide E-W interferometer for October 27, 1968 and November 12, 1969 are shown in Fig. 43. The period of the phase ramps of the N-S interferometer on November 12, 1969 are also shown. In each case the period is the time taken for the interferometer to execute a phase ramp or the phase of the signals at the antennas to change by 360 degrees.

The period of the narrow E-W interferometer's phase ramps are approximately three times as great as those shown for the wide E-W interferometer, and additionally, the period of the wide E-W interferometer's phase ramps do not

agree with the period of the scintillation in Figs. 29, 34 and 35, therefore this type of mechanism cannot account for the scintillation shown in these figures. The period of the phase ramps is different for the N-S and wide E-W interferometers except at 1950 UT and the periods of the phase ramps disagrees for the most part with the periods of the scintillation shown in Fig. 28, therefore this mechanism does not explain the scintillations shown in Fig. 28. A similar argument can be made for the scintillations shown in Figs. 39, 40 and 41 since in general the periods of the phase ramps differ for the N-S and E-W interferometers by a significant amount.

4.6 SUMMARY AND DISCUSSION

TIDs were observed as quasi-periodic scintillations in the angle-of-arrival of radio waves emitted by localized disturbed regions on the solar disk. A summary of the observations is given in Table I. Speed, line of travel, period and wavelength of the TIDs were deduced from the manner in which the period and magnitude of the observed scintillations varied with time. The speed of the TIDs as a function of height was also determined by correlating the degree of amplitude fading due to defocussing and focussing effects with the maximum observed rate of change of angle-of-arrival. The observations reported here show good evidence for TID wave trains consisting of 15 to 20 wave cycles. The angular deflections of the solar line-of-sight at 51.7 MHz were measured to be ±6 to ±28 minutes of arc (in one case it was a remarkable ±50 minutes of arc) and corresponding electron number density

perturbations are calculated to be of the order of 1 to 2 percent. The forward tilt to the TIDs observed on 12 November 1969 was measured to be 50^{0} ($\pm 20^{\circ}$). Amplitude variations corresponding to the larger angle-of-arrival scintillations were about 5dB. The TIDs were of two types; one with a period of approximately 6 minutes, the other with a period of 21 minutes. The former travelled with a speed of about 200 km/hr and a corresponding wavelength of 20 km. The speed of the latter was between 800 and 2000 km/hr and the corresponding wavelength between 300 and 700 km. These also had a preferred line of travel which was orientated north-south.

A lengthy digression was made to show that the measured quasi-periodic scintillations were not produced by a mechanism other than TIDs. In a large measure the repudiation of alternate mechanisms was based on the two source theory developed in Chapter II.

TABLE I

SUMMARY OF SCINTILLATION RESULTS

DATE	PERIOD (minutes)	MAXIMUM MAGNITUDE (minutes of arc)	DURATION (cycles)	SPEED (km/hr)	LINE OF TRAVEL	AMPLITUDE FADING (dB)	FLUX DENSITY ($X10^{-22} wm^{-2} H_z^{-1}$)
16 OCT 68	22(21,30,60)	±20	5	800-2000†	N-S	-	2.5 - 7.5
18 OCT 68	21	±14	2½	800-2000†	N-S	0	3
25 OCT 68		±28	5	800-2000†	N-S	-	0.8
	14.2*	±7	3	200††	E-W	-	0.8
27 OCT 68	21	±22	14	800-2000	N-S	0	8-44
	13*	±5	6	200††	E-W	0	8-44
28 OCT 68	30(?)	±5	9(?)	-	-	-	-
29 OCT 68**	18.1	±19	9	800-2000†	N-S(?)	5	120-400
10 NOV 69	20.1	±12	16	>500†††	-	-	-
11 NOV 69	24*	±22	20	200††	W-10^0 -S*** (towards SW)	-	-
12 NOV 69	6	±24	19	200	E-W (towards west)	5	2.25
2 MAR 70	21.1	±60	17	>500†††	-	3	5-40

TABLE I (Cont'd)

DATE	PERIOD (minutes)	MAXIMUM MAGNITUDE (minutes of arc)	DURATION (cycles)	SPEED (km/hr)	LINE OF TRAVEL	AMPLITUDE FADING (dB)	FLUX DENSITY ($X10^{-22}$ wm^{-2} H_z^{-1})
15 OCT 68 (Fig.55)	13.2*	±6	7	-	-	-	-
	28.6*	±15	3	-	-	-	-
	64.5*	±6	2	-	-	-	-
17 OCT 68. (Fig.55)	31.2	±18	10	>500+++	-	-	-
19 OCT 68 (Fig.55)	13.1*	±10	7	-	-	-	-
20 OCT 68 (Fig.55)	29.2	±10	8	>500+++	-	-	-
21 OCT 68 (Fig.55)	17.3	±30	8	800-2000+	N-S	-	-
	38.5*	±5	4	-	-	-	-
22 OCT 68	19.8	±20	7	800-2000+	N-S	-	-
23 OCT 68 (Fig.56)	-	-	-	-	-	-	-
24 OCT 68 (Fig.56)	18.4	±15	14	7500+++	E-W (predominantly)	-	-
30 OCT 68 (Fig. 56)	21.2	±6	10	>500+++	E-W (predominantly)	-	-
1 NOV 68 (Fig.57)	-	-	-	-	-	-	-
2 NOV 68 (Fig.57)	9.72	±17	19	>500+++	N-S	-	-

* APPARENT VALUE

** SCINTILLATIONS EXTREMELY WELL DEFINED BECAUSE OF HIGH FLUX DENSITY

*** SYSTEMATIC VARIATION IN PERIOD SIMILAR TO 12 NOV 69 DELAYED IN TIME BY 1.5 HRS.

\+ PROBABLE VALUE BECAUSE PERIOD SIMILAR TO THAT OF 27 OCT 68

++ PROBABLE VALUE BECAUSE PERIOD SIMILAR TO THAT OF 12 NOV 69

+++ NO SYSTEMATIC VARIATION IN PERIOD

CHAPTER V

CONCLUSIONS

5.1 INTRODUCTION

In the first part of this chapter a comparison is made between the measurements made herein with those made by other workers. Secondly, a comparison is made between the observed TID parameters and parameters of gravity waves derived theoretically by various workers. Finally, the results of this work will be summarized.

5.2 COMPARISON WITH OTHER MEASUREMENTS

Wild et al. (1959) observed quasi-periodic scintillations in the angle-of-arrival of a solar source on 23 August 58 and 13 July 58. They reported that the period was about 22 minutes. This agrees with the period of the scintillations, reported here, caused by the north-south moving TIDs. Their measurements were made near Sydney, Australia (150^{o}E) at radio-wave frequencies of 45, 50, 55 and 60 MHz. The interferometer antenna separation at 50 MHz was about 167 λ. They observed angular deviations of up to ±20 minutes of arc. The measurements of 23 August 58 (their Fig. 6) show the scintillations occurring in a wave train with five, or so, wave periods during the interval from 0000 UT and 0200 UT. The amplitude of the scintillations begins to decay at about 0100 UT and continues to do so until the time of local noon at about 0200 UT. This suggests that the line of travel of the responsible TIDs is in the north-south direction. Since the amplitude of the observed scintillations was

proportional to f^{-2}, Wild et al., concluded that they were due to large-scale irregulatities in the ionosphere. They concluded that the scale size was about 25 km by assuming that the irregularities were at a height of 200 km and were stationary with respect to the ionosphere.

If in fact the irregularities were stationary the period of the observed scintillations would have increased or decreased towards local noon because of the variation in velocity of the solar line-of-sight through the ionosphere. Clearly their results show a fairly constant period throughout, and thus their assumption that the irregularities were stationary is incorrect.

The response of E-W interferometers to scintillations produced by TIDs moving in a north-south direction as a function of the time of year for an observer at 42° N latitude is given in Fig. 51. It can be seen that the response of the interferometers in the morning and the afternoon increases as the declination of the sun becomes more negative. The response for a northern observer is a maximum when the declination of the sun reaches its most negative value on 21 December and becomes a minimum when the declination reaches its maximum positive value on 21 June. Since the response of E-W interferometers on 21 June is low, any scintillations in angle-of-arrival of a solar source induced by north-south moving TIDs, would probably not be discernable. The dates given in brackets in Fig. 51 refer to an observer in the southern hemisphere at 42° S latitude. Sydney, Australia is located at about 34°S latitude, and therefore the response of an E-W interferometer located there would be somewhat lower than shown in Fig. 51. Bearing this in mind one can see that the measurements made in Australia and Canada were made at times of the year when the responses of the

respective E-W interferometers to north-south moving TIDs were roughly comparable and when the response had a sufficient magnitude to allow for their detection. Actually the response of an E-W interferometer at Sydney will be about 19 percent lower than at London. In the case of the Canadian observations the observer was about 18° of latitude south of the auroral zone over northern Canada. The Australian observer was about 22° north of the auroral zone which is located south of Australia. In either case the observers were removed by approximately equal distances from their respective auroral zones.

Lawrence and Jesperson (1961) measured the angle-of-arrival of radio waves from the radio star Cygnus-A using radio interferometers on east-west base lines operating at frequencies of 53 and 108 MHz. The antenna separation of the former was 84 λ and of the latter 171 λ. Slow variations in angle-of-arrival with a period of the order of 5 to 20 minutes were observed. Since the variations showed a high correlation between records taken simultaneously at the two frequencies and the ratio of the average excursion at 53 MHz to that at 108 MHz was approximately 4:1, as demanded by Eq. 35 they attributed the deviations to refraction by the ionosphere. On one occassion the amplitude of the scintillations at 108 MHz was about 30 min. of arc. Typically the amplitude of the scintillations at 53 MHz was 15 minutes of arc. They had evidence that the ionospheric irregularities responsible for the scintillations were most common in the hours immediately after sunrise and tended to disappear steadily throughout the day. This observation is in close agreement with the observed occurrence of the north-south TIDs at London. Furthermore, Lawrence and Jespersen found that the irregularities were uncommon at night, but occurred on about one-third of all days.

They found that the amplitude of the scintillations decreased as the elevation angle h of Cygnus-A increased. When h was 5 degrees the amplitude at 108 MHz was about 7.7 minutes of arc, whereas when h was 40 degrees the amplitude was only about 4.2 minutes of arc. Their explanation was based on a particular model of the irregularities which assumed that they were "thin prisms". They attempted to explain the observed elevation-angle dependence in terms of the anisotropic properties of these irregularities. Alternately, the elevation angle dependence may also be explained in terms of the response of east-west interferometers, if one assumes the irregularities to be predominantly due to TIDs moving in a north-south direction. The response of these interferometers when h is 5 degrees is 0.94 and the response when h is 40 degrees is 0.52. The ratio of the amplitudes of the scintillations when h equals 40 degrees to that when h equals 5 degrees is 0.55. Since the ratio of the responses of the interferometers at the corresponding values of h is 0.56, the observed elevation-angle dependence of the amplitude of the scintillations may be explained by the elevation-angle dependence of the response of the interferometers.

Lawrence and Jespersen concluded that the refraction effects that they observed were due to large ionospheric irregularities whose electron content per unit vertical column varied by a few percent from the mean value. They assumed that the irregularities were stationary and thereby deduced that the scale size was of the order of 200 km.

Vitkevich (1958b) observed refraction effects on radio waves from powerful local sources on the sun. On occassion the scintillations had a "repetition, close to periodic character". The scintillations were observed on frequencies between 15 and 490 MHz, or so, and since

2 2

OF/DE

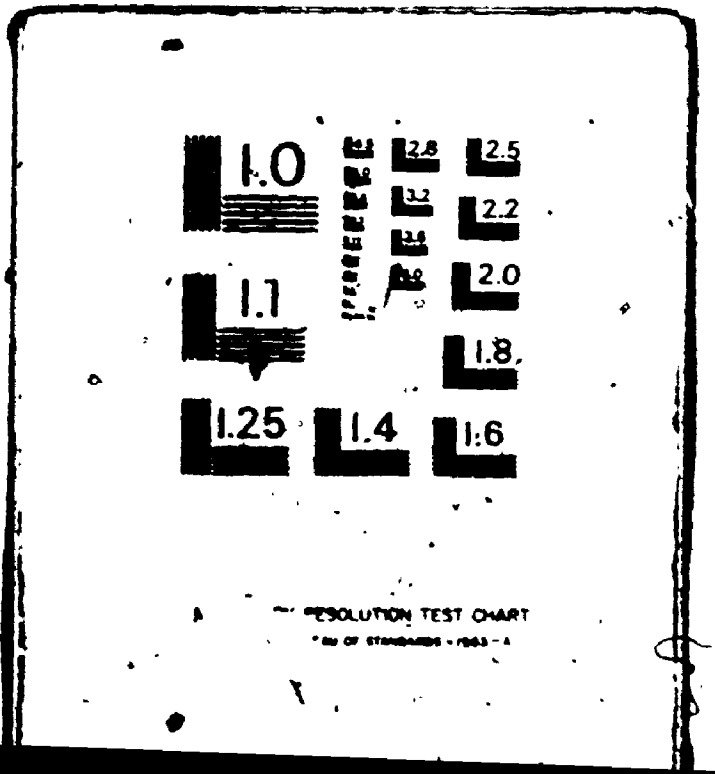

their amplitudes varied approximately as the wavelength squared they were attributed to ionospheric irregularities. He assumed that the irregularities were stationary and deduced that their scale sizes were of the order of 250 to 400 km.

Georges (1968) observed TIDs with a network of CW Doppler sounders. The centrally located receiving station was located at Little Rock, Arkansas (35^{o}N, 92^{o}W). His observations suggested two distinct types of TIDs to which he gave the prefixes, 'very large' and 'medium scale'. The former were usually observed to follow mangetic storms, possess quasi-periods from about 20 minutes to about 2 hours, consist of two or three nearly sinusoidal cycles, possess speeds in the range 720 to 1450 km/hr., and have wavelengths of the order of 1000 km. For the most part they were observed to travel southward. The latter type appeared on Doppler records as a single cycle or, more often, as a train of quasi-periodic oscillations with periods between about 10 and 30 minutes. In addition they had speeds mostly in the range 360 to 720 km/hr, wavefront tilts from the vertical in the range 30^{o} to 60^{o}, and wavelengths of a few hundred km. In addition, on one occassion he observed the passage of a TID on the records from four spaced bottomside virtual height sounders. The virtual height versus time contours at Springfield, Missouri (39^{o}N, 93^{o}W), for example, showed quasi-periodic variations whose average period was about 34 minutes. There were about four discernible wave periods present.

Bramley (1953) made TID observations at Slough, England. He measured the direction of arrival of pulse signals reflected from the ionosphere, either at vertical incidence or over an oblique path, on various frequencies in the range 2 to 15 MHz. The TIDs had wavelengths

of 50 to 400 km and speeds of 144 to 1300 km/hr. The direction of motion tended to be more often towards the east or west than towards the north or south.

Tveten (1961) observed TIDs at Sterling Virginia (39°N, 77.4°W) with a backscatter sounder operating at a frequency of 13.7 MHz. The observations were obtained principally during the daylight hours of December 1952. Most of the observed speeds are included in the interval 80 to 1000 km/hr with a median speed of the order of 580 km/hr. The overall direction of motion of the TIDs was towards the southeast. The horizontal wavelengths fell between 40 km and 700 km, for the most part, with most frequency value at 180 km. His Fig. 16 shows the speed for very large-scale travelling disturbances. Most of the indicated results have speeds between 800 and 2300 km/hr, or so. The motion is directed towards the south-south-east with most of the results falling between azimuthal angles of 140 and 200 degrees east of north. Tveten indicates that his results are consistent with those of a large number of experimenters, obtained prior to the time of his results.

The large nuclear detonation low in the atmosphere over Novaya Zemlya on 30 October, 1961 caused TIDs which were observed widely on ground based radio-frequency radio sounders (Stoffregen, 1962). They were observed as variations in the critical penetration frequency f_0F_2 at a number of stations: the most distant one being some 4,400 km. from the point of explosion. The amplitude of the perturbations in f_0F_2 varied from 1 MHz about an ambient value of 5 MHz at Kiruna some 1300 km from Novaya Zemlya to 2 MHz about an ambient value of 9 MHz at Athens some 4,400 km away. The period of the disturbance increased with distance from 30 minutes at Kiruna to 3 hours or so at Athens. Hines

(1967) has indicated that the horizontal group velocity of the TIDs was 700 - 1400 km/hr. He interpreted the observations in terms of oblique propagation of long-period gravity waves. This interpretation suggests that the nuclear detonation introduced, into the neutral atmosphere, a local time dependent disturbance, the low-frequency components of which travelled out from the source region as gravity-wave trains which then produced TIDs as they passed through the ionosphere. The observed increase of TID period with distance was explained in terms of a certain characteristic of gravity wave propagation; namely, the larger the wave frequency of a wave train the larger the angle of ascent into which its energy at a given period is beamed.

The maximum angular deflection observed by the author was of the order of ±20 minutes of arc, indicating a maximum gradient in columnar electron content of 3.5×10^{14} el/m^2km. If one assumes that the TID was contained between 250 km and 350 km this corresponds to electron density perturbations of only 1%, or so. The corresponding variation in a f_0F_2 whose average ambient value was 6 MHz would be of the order of 0.3 MHz, approximately 1/9 that produced by the disturbance with period 30 minutes travelling over Kiruna as a result of the nuclear explosion over Novaya Zemlya.

Newton et al. (1969) measured local variations in the atmospheric density with density gages aboard the Explorer 32 satellite. They were consistent with waves propagating in the neutral atmosphere. These variations were observed in the northern hemisphere over the altitude range from 286 km (satellite perigee) to at least 510 km. They were observed to be most prevalent at the higher latitudes near the auroral

zone and were observed most frequently in the late evening and early morning hours, but were not limited to these latitudes and times. The most commonly observed wave density perturbations had half-amplitudes which were 10-20% of the smoothed density profiles. These waves were interpreted to be free internal gravity waves propagating predominantly north-south or south-north, with maximum horizontal wavelengths between 130 and 520 km.

Dryson et al. (1970) reported that a comparison between in situ measurements of neutral particles and electron densities with the Explorer 32 satellite has provided direct evidence that neutral-wave structure in the thermosphere is associated with wave-like structure in the F-region electron density. The observed ionospheric electron-density-wave-structure amplitude and spatial extent were consistent with TID characteristics. They also reported that their results are consistent with Hooke (1968), who showed that neutral density variations of about 10% can cause electron density perturbations of 20%.

Davies and Jones (1971, 1972) reported observations of ionospheric waves detected at F-region heights whose power had peaks at periods near 3.5 and 4.5 minutes and occasionally between 7 and 10 minutes. The waves were detected as quasi-periodic disturbances in the Doppler shift of high frequency radio waves reflected by the ionosphere. They showed events lasting up to two hours consisting of 12 or more consecutive wave cycles and indicated that they are likely due to acoustic waves generated by mechanical motion of tropospheric thunderstorms. In addition they observed an increase of power for periods greater than about 10 minutes due to background gravity waves which were reported to be nearly always present.

5.3 COMPARISON WITH GRAVITY WAVE PARAMETERS

The properties of TIDs deduced from the solar angle-of-arrival measurements are compared with certain properties of gravity waves and the effects of these waves on the ionosphere. This is pursued because the most successful explanation of TIDs has been in terms of the effects of these neutral waves on the ionosphere. Hooke, (1968) stated that, "this interpretation is consistent with TID observations in so many respects as to leave little doubt as to its basic correctness". Following Chimonas and Hines, (1970) it is taken, as established by previous workers, that TIDs are a manifestation of gravity waves in the ionosphere.

Hooke, (1968) has derived theoretically the effect of atmospheric gravity waves on the ionosphere. His Fig. 6 is relevant to the north-south TIDs observed at London. It shows an ionospheric disturbance (TID) produced by the passage of a gravity wave with a period of 24 minutes at a latitude where the magnetic dip angle I is 60°. Although the measurements at London were made at a latitude where I is equal to 70°, this difference will have little effect on the present discussion. The TID calculated by Hooke resulting from this gravity wave has a wavelength of 400 km, period of 24 minutes, and a gradient in total electron content, transverse to a line inclined at 30° with the horizontal, of 3×10^{14} el/m^{2}km. These values are consistent with those of corresponding parameters deduced for the north-south TIDs. The isoionic contours deduced by Hooke have an inclination of the order of 9° with the horizontal. Since the angle between the horizon plane and the plane containing the solar line-of-sight and the east-west interferometer axis is of the order of 30°, the angle-of-arrival measurements would not be sensitive to the tilt of the isoionic contours and thereby of the surfaces of constant phase of the gravity wave in this case. Thus one could

not, for example, necessarily determine whether the TID was moving towards the north or towards the south.

Chimonas and Hines, (1970) have made model calculations of gravity waves launched by auroral currents. According to these authors the driving force arises from the Lorentz force and/or Joule heating caused by the auroral currents in the atmosphere. Thus they introduce a local time-dependent disturbance, the low frequency components of which, travel out as a gravity wave train. Their Fig. 5a shows the Lorentz generated fractional pressure perturbation at a point 1000 km equatorwards of the auroral current and at an altitude of 216 km, or so. The wave packet consists of a sharp head with a quasi-periodic train whose local period approaches a limiting value which is a function of the altitude of the field point with respect to the source point and of the distance of the field point from the source point. In the above case the wave train has a period of the order of 28 minutes. It contains four or five wave periods, but the slow decay of the wave train indicates that it could consist of many more wave periods than the number indicated. They state, though, that in a calculation that took account of viscosity and thermal conduction, the long-enduring tail would be suppressed. The results contained herein indicate that on a number of occasions the long enduring wave train did in fact exist. They state that the Lorentz mechanism will readily give rise to TIDs of observable magnitudes.

Chimonas (1970) has considered the equatorial electrojet as a possible source of low frequency TIDs. His fig. 4 shows wave forms of fractional pressure perturbation received 1000 km horizontally away from the source region and 300 km above the current center. The wave forms are for all practical purposes identical with those launched by auroral

currents, except the amplitudes are only one tenth, or so, as large. In this case the wave packet contains about seven wave periods and the period is of the order of 20 minutes. Chimonas states that the TIDs launched by the equatorial electrojet are likely to be much weaker than those launched by the auroral electrojet.

In an ideal isothermal non-dissipating atmosphere the amplitude of gravity waves (air parcel velocity or perturbation pressure) increases with height Z as exp (Z/2H). This property is a consequence of the conservation of energy flux with height, since the ambient air density off as exp (-Z/H), (Midley and Liemohn, 1966). Wave dissipation by viscosity and thermal conduction causes the waves to reach a maximum amplitude at some altitude. This occurs because the damping processes, which increase with height, eventually overcome the normally increasing wave amplitude with height. These authors show, that a gravity wave whose period is 10 minutes and horizontal wavelength is 20 km attains its maximum amplitude at an altitude of 120 km, or so. It is likely that the centroid of a TID generated by this gravity wave will also be approximately at this altitude; actually it is likely to be at a somewhat greater altitude, because the ambient electron density increases with altitude. Thus although the perturbation due to the gravity wave decreases above 120 km, since the ambient electron density increases, the electron density perturbation is likely to reach a maximum at a greater altitude. They also show that the vertical wavelength of the 10 minute wave at the maximum altitude is of the order of 15 km. The tilt of the wave fronts with the horizontal is given by arctan (λ_z/λ_x), and therefore is of the order of 37 degrees, or stated in other words, the forward tilt of the constant phase fronts is 53 degrees. Furthermore, it follows from the gravity wave theory that the period of a gravity wave propagating

in the atmosphere must be greater than the local Brunt-Vaisala period. Since the Brunt-Vaisala period becomes greater than 10 minutes at an altitude of about 180 km, waves with periods less than 10 minutes are restricted to altitudes less than 180 km (Georges, 1967, Fig. 3-12). It is readily seen that the parameters of the 10-minute gravity wave described above are consistent with the parameters of the east-west TIDs deduced from the measurements at London.

5.4 STATEMENT OF RESULTS AND DISCUSSION

5.4.1. The Theory of a swept-lobe interferometer observing two sources was developed.

The theory of a swept-lobe interferometer and one source was discussed and a more general description than has appeared elsewhere was given. The theory of a swept-lobe interferometer monitoring two sources was developed and described. Experimental results were given using Cassiopeia A and Cygnus A on the one hand and two signal generators in a laboratory simulation on the other. These results were shown to be in close agreement with the theory. In addition the accuracy of the interferometers was demonstrated to be ±2 minutes of arc.

It was shown that if two sources illuminate an interferometer they can interfere with one another and produce scintillations in the measured angle-of-arrival, which is a function of the ratio of the signals and the antenna separation. Each time the phase difference between the signals at the antennas from one source changes by 2π radians with respect to the phase between signals at the antennas from the other source the measured angle-of-arrival varies through one complete scintillation cycle. It was shown that the period and amplitude of these scintillations was a function of the antenna separation and that the interference produced deep fading in the recorded amplitude.

The reason for investigating these properties, whose description is generally relevant to other radio-wave applications, such as direction finding or over-the-horizon radar systems, is the following much more specific one. An explanation of the observed scintillations of solar sources in terms of interference between two independent sources is the most serious objection to their interpretation in terms of TIDs in the ionosphere. Once these properties are understood and the objection refuted the interferometer can then be used as a very effective tool for observing TIDs.

5.4.2 The solar interferometer was shown to be an effective instrument for observing TIDs.

Theoretical development work was performed in a number of areas, to allow for the effective use of the interferometer as a TID-sensing instrument. The paths and velocities of the intersection of the solar lines-of-sight with the ionosphere were determined since their motions affect the periods of TIDs and thereby provide a means by which the disturbance velocities may be determined. The response of the interferometers was defined and developed because the modulation that it causes in the amplitude of the scintillations is a function of their line-of-travel. A two dimensional projection of the interferometers constant-phase surfaces was developed as an aid to visualizing the interferometers as TID-sensing devices. Finally, some focussing and defocussing theory was modified to make it relevant to TID observations.

It was shown that TIDs can be detected as quasi-periodic scintillations in the angle-of-arrival of radio waves emitted by enhanced localized sources on the solar disk. The direction-of-travel of the TIDs was shown to be determinable from the modulation of the amplitude of the

observed scintillations. The modulation was imposed by the changing angle, during the period of observation, of the solar line-of-sight with respect to the interferometer axis. The speed of the TIDs was shown to be determinable from the variation in the period of the scintillations produced by the motion of the solar line-of-sight through the ionosphere. In the case where no variation was discernible then, at least, a lower limit to the speed could be deduced. The speed was also determined by correlating the degree of fading in amplitude due to focusing and defocusing effects with the maximum observed rate of change of angle-of-arrival. It was also shown that with a particular compound interferometer the tilt of east-west TIDs could be determined. The compound interferometer consisted of a base line on an east-west direction and one on a predominantly north-south direction. The tilt was obtained by finding the ratio, shortly before local noon, of the amplitude of the scintillations observed on the east-west interferometer to that observed on the north-south interferometer the latter corrected for deflections in azimuth. At this time the east-west interferometer is most sensitive to angular deflections in azimuth and the north-south interferometer is most sensitive to deflections in elevation.

The sun, when emitting rf energy at an enhanced level, is an effective source for observing TIDs. In effect it tends to select times, for the observer, when there is a good likelihood of TIDs being present in the ionosphere. TIDs tend to be present when the ionosphere is disturbed and the ionosphere tends to be disturbed when the sun is disturbed. Furthermore, the sun radiates at an enhanced level only at times when it is in a disturbed state. On the other hand it is not an effective source for obtaining synoptic measurements because they are possible only on those infrequent

occassions when the sun is radiating at an enhanced level. A transmitter located on the moon radiating a VHF circularly polarized radio signal would be a very effective source. It would combine the advantages of using the sun, when it is radiating, for TID observations and the capability of making synoptic measurements.

5.4.3 Long-lasting Quasi-periodic TIDs

The main new result of this work is the observation of long-lasting TID wave trains. The wave trains observed on 27 October 1968 and 12 November 1969 are probably the longest, in terms of number of wave periods, that have been reported to date. They are of the order of four to six times longer than those normally observed. Their parameters were determined and shown to be consistent with values from previous observations and with calculated parameters of gravity waves, which are usually taken to be responsible for producing TIDs as they propagate through the ionosphere

The TID observations are summarized in Table I. TIDs were observed on about 18 out of the 21 days that the sun emitted metric radiation in the 1.5 year period between 15 October 68 to 2 March 70. A total of 24 distinct TID wave trains were observed in that period of time. Two types of TIDs were observed at London. One type tended to travel in a north-south direction and the other type tended to travel in an east-west direction. The magnitude of the wave period in the wave trains was observed to be approximately constant throughout the duration of the wave train, after a correction was applied for the motion of the sun, suggesting the presence of one main spectral component. Fig. 56 shows that three perdominant wave periods were observed; i.e. (a) 5 and 10 minutes, (b) 20 and 25 minutes, and (c) 60 and 65 minutes.

5.4.3 A. Properties of the north-south travelling TIDs

These TIDs were found to travel along a north-south direction to within ($\pm 10^{o}$). They were observed on a number of days, and the nominal value of their period was 21 minutes. Their speed was between 400 and 2000 km/hr and consequently their wavelength was between 140 and 700 km. On the 27 October 1968 the lateral extent of the TID wave train was at least 1200 km because this is the distance that the solar line of sight travelled through the ionosphere during the period of observation. The north-south TIDs were observed at London between 15 October 1968 and 1 November 1968; a period of time during which the sun emitted meter wavelength radio waves at an enhanced level almost every day. This is most remarkable because it is unusual for the sun to radiate at an enhanced level even for one complete day. Since the sun was disturbed during this time it is likely that the ionosphere was also disturbed. At the end of this time period a polar cap absorption event took place. In particular, enhanced auroral zone heating is likely to have occurred during this interval.

It appears likely, because of the period of these TIDs and line of travel that they were in fact generated in the auroral zone and travelled equatorwards. Other workers who have observed TIDs travelling along a north-south direction have found them to be travelling equatorwards in, at least, the overwhelming majority of the cases. The TIDs observed in Australia by Wild et al., also had a period slightly greater than 20 minutes, which suggests that their observation point was a similar distance from the source point as for the observer at London, provided the period is a function of the distance from the source point. The distance of the point of their observations from the southern auroral is similar to the distance of the point of the present observations from the northern auroral zone. If

the gravity waves responsible for the TIDs observed at London were generated in the equatorial region, a possibility which should be investigated, their period would be of the order of 120 minutes (Chimonas, 1970), unless they were ducted in the earth's atmosphere. Furthermore, the probability of the equatorial zone acting as a source is small because it is a much weaker and distant source than the auroral zone. It follows from Chimonas and Hines (1970), that the distance of the gravity wave source responsible for the 21 minute TIDs, provided that the gravity waves propagated freely in the earth's atmosphere, was less than 1000 km from the point of observation. It is assumed here that the gravity wave source was located at an altitude of 116 km, or so, and the TIDs were detected at an altitude of 316 km. Since the TIDs were observed at a latitude of 35^{o}N, this suggests that the gravity wave source was situated at 45^{o}N, which is unlikely even though the auroral zone moves southwards of its nominal latitude of 60^{o}N during times of magnetic storms. It appears likely that at least partial ducting of the gravity waves took place in the earth's atmosphere and that the angle-of-arrival technique either happens to be sensitive to TIDs with period of 21 minutes or the average period of the gravity waves was 21 minutes due to filtering of the gravity wave spectrum by the earth's atmosphere.

Friedman (1966) has shown, using the gravity wave theory and a model of the earth's atmosphere, the existence of propagation modes which are strongly ducted by the atmosphere. His mode S1 which is strongly ducted in the mesosphere may be an appropriate one to consider for purposes of this discussion. The horizontal phase and group velocities of this mode are 1100 km/hr. This is consistent with the TID observations, although it was only the phase velocity which was measured. On the other hand, since

the gravity waves were probably generated at a height of 116 km, or so, his mode W2, for example, may be more pertinent since it is ducted by the E-region. Its group and phase velocities are of the order of 835 km/hr, which is a phase velocity consistent with the velocity of the observed TIDs. He shows in his Fig. 15 that a gravity wave with a period of 52 minutes propagating according to modes W5 or S5 is ducted up to 3000 km. in the E-region. The velocities of these modes are about 645 km/hr.

5.4.3 B. Properties of the East-West travelling TIDs

TIDs with a nominal period of 6 minutes were observed on six occasions. They were observed to travel in an predominantly east-west direction, and on one of these occasions; namely, 12 November 1969, they moved towards the west. On two days their direction of travel was unknown. These TIDs had a horizontal velocity and wavelength of about 200 km/hr and 20 km respectively. They were detected at an altitude greater than 100 km and probably less than 300 km. It is likely that they are an E-region phenomena. Since the maximum observed angular deflections were of the order of 8' arc the maximum horizontal gradients in total columnar electron content were about 1.5×10^{14} el/m^2km. If one assumes that the TIDs were contained in the height range between 125 and 175 km and that the average total columnar electron gradient was 0.7×10^{14} el/m^2km, then, since the ambient electron density is about 2×10^{11} el/m^2, the magnitude of this perturbation in electron density due to the TID was about 1 percent. Thus it is readily seen here that the angle-of-arrival technique is sensitive to small electron density perturbations; to a large extent, because it in effect integrates throughout the vertical extent of the perturbation. It was shown that the surfaces of constant phase of these TIDs were tilted forward in the direction

of motion, which is consistent with other observations of TIDs. It was also shown that the magnitude of the tilt is consistent with the gravity wave theory.

If one looks closely at the solar flux density in Fig. 27 one may just be able to discern a structure with a quasi-period of one hour. The solar flux density appears to have local maxima at 1430, 1530, 1630 and 1730 UT. The N-S angle-of-arrival appears to have maximum amplitudes at two of these times; namely, 1530 and 1730 UT, and possibly at a third, 1630 UT. These observations suggest that there may, in fact, have been a gravity wave present in the E-region with a period of one hour, perturbing the motion of the TIDs whose period was 6 minutes. The long period gravity wave may not have been directly detectable as a TID because it may not have manifested itself as such until it passed through the F-region (Hooke, 1968). Further examples of TIDs with a period of one hour occurred on 15 and 16 October 1968. Since long period waves have been observed to travel predominantly equatorwards (Georges, 1968) the line of travel of these probably is also equator-wards. This conclusion is consistent with the period of the east-west moving TID trains being perturbed, as it was, by a disturbance with an one-hour periodicity. Since the horizontal distance travelled by a 60-minute gravity wave generated in the auroral zone prior to reaching F-region heights is of the order of 2000 km (Hines, 1967) it is possible that freely propagating gravity waves from a disturbed auroral region at 55°N could explain the F-region observations. The E-region observations cannot be explained in this manner and ducted gravity waves must again be resorted to.

It is interesting to note that Heisler and Whitehead, (1962) reported certain properties of mid-latitude sporadic-E reflections. These

properties included an oscillatory variation of the critical and blanketing frequencies, with a quasi-period of 60 minutes and a secondary one with a period of 10 minutes. In addition the Sporadic-E clouds of ionization were observed to travel with a velocity of the order of 240 km/hr. Hines (1963) attributed these effects to the formation of Sporadic-E by wind shears due to gravity waves. He indicates that small-scale irregularities in the E region could be due to gravity waves with periods lying in the range 5-30 minutes. It should also be pointed out that Gossard (1962) has shown that the strongest efflux of energy from the troposphere in the form of internal gravity waves occurs at periods of 10-30 minutes. The above agreement between Sporadic-E and East-West TID observations suggests that there may be some correlation between the two and should be investigated further. Furthermore, it is possible that the source of these TIDs lies in the troposphere. Therefore their correlation with possible sources, such as jet streams or intense localized meteorological thunderstorms also warrants further investigation.

5.4.4 FINAL REMARKS

A comprehensive listing of TID parameters measured by other workers is given in Fig. 2. These were obtained by a number of different experimental techniques and are given in Section 2.2. TIDs with a N-S line of travel are well documented and are usually associated with heating in the auroral zone during particle-precipitation events (Georges, 1967). The N-S TIDs reported here appear to be consistent with the other N-S TIDs shown in Fig. 2. E-W TIDs on the other hand have only been observed by one worker (Bramley, 1953). It should be emphasized that the angle of

arrival technique developed in this Thesis is capable of giving a more comprehensive description of the TIDs it detects than are other techniques. The following TID parameters may be infered from the scintillation measurements:

(a) speed

(b) line of travel

(c) period

(d) wavelength

(e) height

(f) tilt

(g) electron number density perturbation

Other techniques are usually limited to about four of the seven parameters listed above.

Another point to be emphasized is the sensitivity of the interferometers as TID detectors. The maximum resolution of other TID detectors, such as vertical incidence ionosondes, incoherent backscatter radars, doppler HF circuits, etc. to electron density perturbations is at most ±1%. The angle of arrival technique developed here will now be shown to be capable of measuring electron density perturbations which are smaller by a factor of 5 than those measured by the techniques listed in Section 1.1.

Since the angular resolution of the wide interferometers was ±2' arc or $\pm 2.33 \times 10^{-3}$ radians it follows from Eq. (35) that

$$\frac{d}{du} \int_0^S N \, dl = \pm 3.85 \times 10^{13} \text{ el/m}^2\text{km}$$

and

$$\text{average}\left(\frac{d}{du}\int_0^S N\,dl\right) = \overline{\frac{d}{du}\int_0^S N\,dl} = \pm 2.29 \times 10^{13}\ \text{el/m}^2\text{km}$$

assuming that the TID is sinusoidal.

First, let us specifically calculate the sensitivity of the interferometers to E-W TIDs. Although the horizontal wavelength of these TIDs is 10 km, the separation of their constant phase surfaces is

$$20 \sin 40^\circ = 13\ \text{km}$$

because their tilt angle was measured to be 50°. This tilt angle agrees with those Georges (1967) attributes to "medium-scale" TID events; namely 45°. Thus the change in columnar electron content from a point within the TID of zero ΔN to a point along the TID of maximum ΔN is

$$\overline{\Delta\int_0^S N\,dl} = \pm 2.29 \times 10^{13} \times \frac{13}{4} = \pm 0.744 \times 10^{13}\ \text{el/m}^2$$

If one assumes that the vertical extent of the E-W TIDs is 25 km (Georges, 1967) then the total columnar length through the TID being sampled by a solar ray is considerably greater than this because of the low elevation angle of the sun during the winter season when most of the measurements were made. Since the average elevation angle of the sun is 22° the columnar length is given by

$$\frac{25\ \text{km}}{\sin 22^\circ} = 6.6 \times 10^4\ \text{m}$$

The TID associated perturbation in electron density is given by

$$\Delta N = \frac{0.747 \times 10^{12}}{6.6 \times 10^{7}} = \pm 1.13 \times 10^{5} \text{ el m}^{3}$$

Since the ordinary penetration frequency of the ionosphere f_0F2 during the time of most of the measurements was 10.5 MHz it follows that the peak electron density was 1.4×10^{12} el/m^3. If one assumes that the TIDs where contained between the altitudes 175 and 200 km and uses a standard ionospheric electron density height profile the ambient electron density for this altitude is 6×10^{11} el/m^3. It follows that the sensitivity of the interferometer is

$$\frac{\Delta N}{N} \doteq 0.2\%$$

If one were to assume the height of these TIDs to be greater than 200 km $\frac{\Delta N}{N}$ would decrease because of the increased valde of N. At a height of 225 km for example it would become 0.11%.

Let us now consider the sensitivity of the interferometers to N-S TIDs.

The period of these TIDs was measured to be 20 minutes. Since the tilt of TIDs with this period is roughly 60° (Thome, 1967) the phase surfaces of the N-S TIDs are approximately parallel to the solar line of sight whose average zenith angle was 68°. This fortuitous circumstance enhanced the sensitivity of the angle of arrival technique to this type of TID because the solar line of sight sampled the maximum electron density gradient along the vertical extent of the TID and no phase cancelling effects could take place. It can also be argued that since

these TIDs were detected by the interferometers it follows that their forward tilt corresponded to the zenith angle of the sun and in addition they travelled towards the equator because TIDs are always observed to travel in the direction of their forward tilt.

Since the horizontal wavelength of the N-S TIDs is 400 km and their tilt is 60° the separation of their surfaces of constant phase is given by

$$d = 400 \sin 30^{\circ} = 200 \text{ km}$$

Following Thome (1964) the vertical extent of the N-S TID in the F region is chosen as 225 km. It follows that

$$\overline{\Delta \int_0^S N \, dl} = \pm 2.29 \times 10^{13} \times 50 = \pm 11.5 \times 10^{14} \text{ el/m}^2$$

and the length of a column parallel to the solar line of sight contained in the 225 km section of the ionosphere is

$$\frac{225}{\sin 22^{\circ}} = 6 \times 10^5 \text{ m}$$

therefore

$$\Delta N = \frac{11.5 \times 10^{14}}{6 \times 10^5} = \pm 1.91 \times 10^9 \text{ el/m}^3$$

The average electron density of the ionosphere between 150 and 375 km height levels is assumed to be 8.4×10^{11} el/m^3. It follows that

$$\frac{\Delta N}{N} \doteq \pm 0.2\%$$

It can be concluded from the above that the angle of arrival technique developed in this Thesis has by a factor of 5 greater sensitivity to TID electron density perturbations than the other techniques listed in Section 1.1. This may explain why the solar interferometers detected long lasting TID wave trains where other instruments have failed in the past. A geographical effect may also be in play here since these measurements were made closer to the auroral zone, which is the likely source of the N-S TIDs, than the other ones listed in Fig. 1. It should be emphasized that each technique tends to detect that regime of TIDs to which it is most sensitive and fails to detect all others. This accounts for the quasi-sinusoidal appearance of the angle of arrival scintillations measured here.

The enhanced sensitivity of the interferometers over other TID detectors is due to three main factors. These are satisfied by a certain class of TIDs, particularly in the winter months which happened to be when most of the measurements were taken. This seasonal bias was caused by the sun only behaving as an effective radio source during the winter months for the time period of interest.

(a) The measurement being one of the gradient of the total columnar electron content results in the complete vertical extent of the TID electron density perturbation being sampled.

(b) The low elevation angles of the sun:

  (i) increased the response of the E-W interferometers to N-S TIDs;

  (ii) allowed for the fortuitous agreement between the zenith angle of the sun and the forward tilt of the N-S moving

TIDs and thereby further increased the sensitivity of the angle of arrival technique to these TIDs;

(iii) allowed for an even greater integration effect because of oblique rather than vertical sampling through the TID.

(c) The F-region electron densities being greater in the winter than in the summer, TIDs which would be undetected in the summer, become of sufficient magnitude to be detected in the winter months because of the enhanced ambient electron densities.

REFERENCES

Becker, W., R. Ruster and J. Klostermeyer, J. Res. NBS, 69D, 1083 (1965).

Beckmann, P. and A. Spizzichine, "The Scattering of Electromagnetic waves from Rough Surfaces", The MacMillan Company, 220, (1963).

Beynon, W.J.G., Nature, 163, 887 (1948).

Blackman, R.B. and J.W. Tukey, "The Measurement of Power Spectra", Dover Publications, Inc., New York (1959).

Bowhill, S.A., J. Atmosph. Terr. Phys., 13, 175 (1958).

Bramley, E.N., Proc. Roy. Soc. (A), 220, 39-61 (1953).

Calvert, W. and J.M. Warnock, Proceedings of the IEEE, 57, (1969) 6.

Chan, K.L. and O.G. Villard, J. Geophys. Res., 67, 973 (1962).

Chandrasekhor, S., M.N. of the Roy. Astr. Soc., 112, 478 (1952).

Chimonas, G., and C.O. Hines, Planet Space Sci., 18, 565-581, (1970).

Chimonas, G., Planet Space Sci., 18, 583-589, (1970).

Davies, K. and J.E. Jones, NOAA Professional Paper 6,"Ionospheric Disturbances produced by Severe Thunderstorms", U.S. Department of Commerce, (1972).

Davies, K. and J.E. Jones, J. Atmosph. Sci., 28, 254, (1971).

Davies, K. "Ionospheric Radio Propagation", Dover Publications, Inc.,(1966).

Dixon, A.F., Ph. D. Thesis, University of Western Ontario, (1969).

Dryson, P.L., G.P. Newton, and L.H. Brace, J. Geophys. Res., 75, 3200, (1970), 16.

Echart, C., "Hydrodynamics of Oceans and Atmospheres", Pergamon Press Oxford, (1960).

Elkins, T.J. and F.F. Slack, J. Atmosph. Phys., 31, 421, (1969).

Friedman, J.P., J. Geophys. Res., 71, 1033, (1966).

Forsyth, P.A., Personal Communication, (1970).

Litva, J., Agard Conference Proceedings No. 115 on Effects on Atmospheric Acoustic Gravity Waves on Electromagnetic Wave Propagation, (1972).

Georges, T.M., J. Atmosph. Terr. Phys., 30, 735 (1968).

Georges, T.M., ESSA Technical Report IER 57-ITSA 54, "Ionospheric Effects of Atmospheric Waves", U.S. Dept. of Commerce, (1967).

Goddard, E.E., J. Geophys. Res., 67, 745, (1962).

Hartz, T.R., Defence Research Telecommunications Establishment Radio Physics Laboratory, Project report 23-2-1, (1955).

Hartz, T.R. and R.L. Hutchinson, Defence Research Telecommunications Establishment, Report No. 1057, (1961).

Heisler, L.H., and J.O. Whitehead, J. Atmosph. Terr. Phys., 24, 753-764, (1962).

Heisler, L.H., Aust. J. Phys., 11, 79, (1958).

Hines, C.O., J. Atmosph. Terr. Phys., 30, 845, (1968).

Hines, C.O., J. Geophys. Res., 72, 1877, (1967).

Hines, C.O., "Physics of the Earth's Upper Atmosphere", Published by Prentice-Hall Inc., pp. 134-156, (1965a).

Hines, C.O., Radio Sc. J. Res. NBS/USNC-URSI, 69D, (1965b), 3.

Hines, C.O., J. Atmosph. Terr. Phys., 25, 305-306, (1963).

Hines, C.O., Can. J. Physics, 38, 1441, (1960).

Hooke, W.H., J. Atmosph. Terr. Phys., 30, 795, (1968).

Kraus, J.D., "Radio Astronomy", McGraw-Hill Book Company, (1966).

Lawrence, R.S. and C.G. Little, Proceedings of the IEEE, 52, 4, (1964).

Lawrence, R.S. and J.L. Jespersen, Space Research II, Proc. 2d Intern. Space Sci. Symp., 277, (1961).

Little, C.G. and R.S. Lawrence, J. of Res., NBS, 64D, 335, (1960), 4.

Lindzen, R.S., J. Atmosph. Terr. Phys., 31, 449, (1969).

Maeda,K.I. and T. Sato, Proc. IRE, 47, 232, (1959).

Martyn, D.F., Proc. Roy. Soc., A201, 216, (1950).

Munro, G.H., Aust. J. Phys., 11, 91, (1958).

Newton, G.P., D.T. Pelz and H. Volland, J. Geophys. Res., 74(1), 183, (1969).

Palmer, F.H., J.W. Doan, and P.A. Forsyth, Can. J. Phys., 48, 554 (1970).

Pierce, J.A. and H.R. Mimno, Phys. Rev., 57, 95, (1940), 2.

Price, R.E., Report of the Physical Society Conference on Physics of the Ionosphere, London, 181-190, (Sept. 1954).

Stoffregen, W., FQAS-Rept. A517, Res. Inst. National Defence, Electronics Dept., Stockholm 80, Sweden, (1962).

Thomas, L., J. Atmosph. Terrest. Phys., 14, 123, (1959).

Thome, G.D., J. Geophys. Res., 73(19), 6319, (1968).

Titheridge, J.E., J. Geophys. Res., 68, 3399, (1963).

Titheridge, J.E., J. Geophys. Res., 74, 1195,(1969).

Tolstoy, I., Rev. Mod. Phys., 35, 207, (1963).

Toman, K., J. Geophys. Res., 60, 57, (1955), 1.

Turnbull, R.M. and P.A. Forsyth, Can. J. Physics, 43, 800, (1965).

Tveten, L.H., J. Res. NBS, 65D, 115, (1961).

Vasseur, G. and P. Waldteufel, J. Atmosph. Terr. Phys., 31, 885, (1969).

Vitkevich, V.V., Radiotekhnika, Electronika, 3, 478, (1958b).

Wells, H.W., J.M. Watts and D.E. George, Phys. Rev., 69, 540, (1946).

Wild, J.P., Advances in Electronics and Electron Physics, 1, 299, (1955).

Wild, J.P., S.F. Smerd and A.A. Weiss, Annual Review of Astronomy and Astrophysics, 1, 291, (1963).

Wild, J.P., K.V.Sheridan and A.A. Neylan, Aust. J. Phys., 12, 369, (1959).

Winacott, E.L., Defence Research Telecommunications Report No. 1057-2, (1961).

Winacott, E.L., Defence Research Telecommunications Report No. 1057-3, (1963).

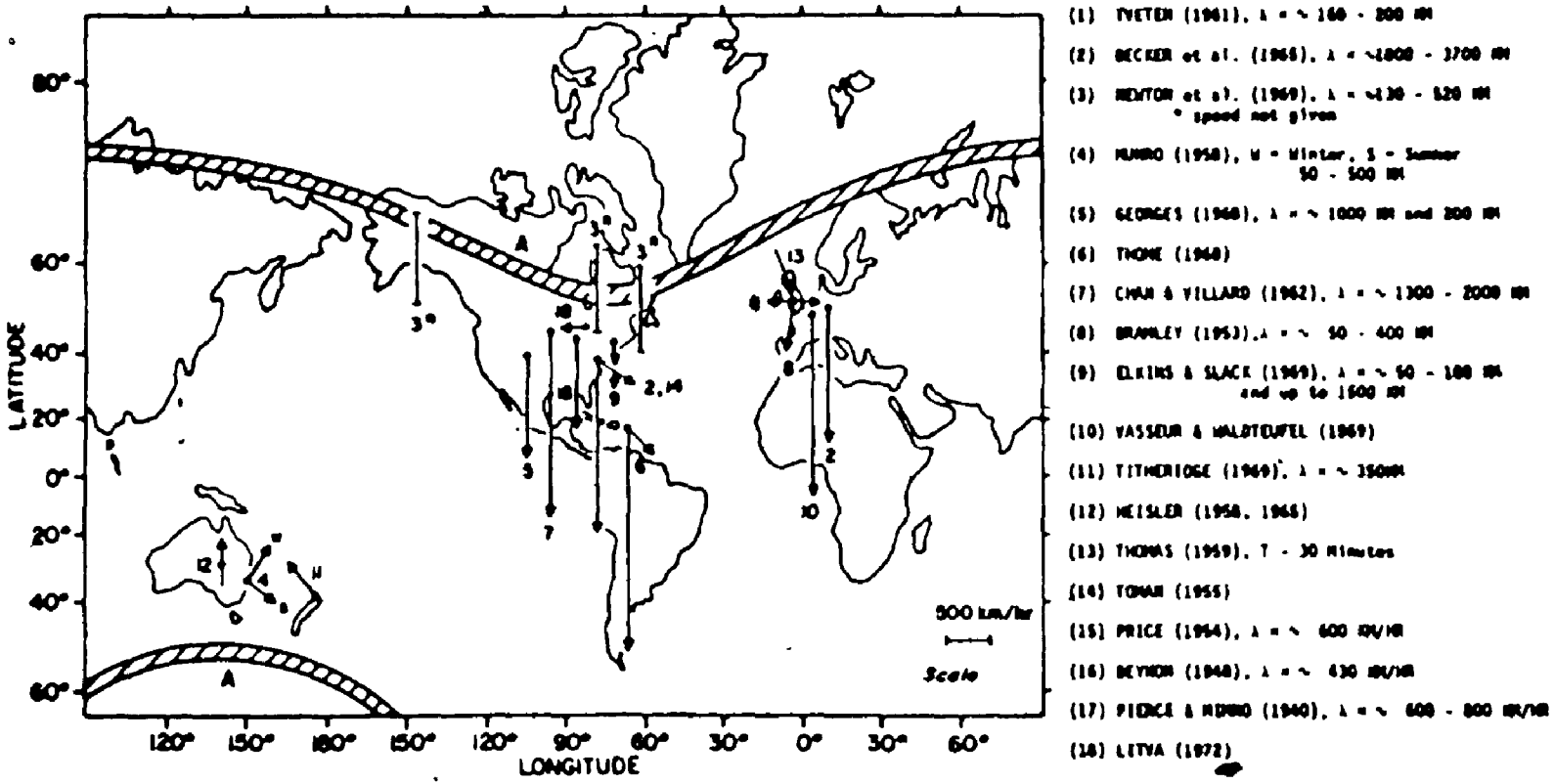

FIGURE 1: Summary of previous TID measurements. Average values published by the indicated authors are plotted.

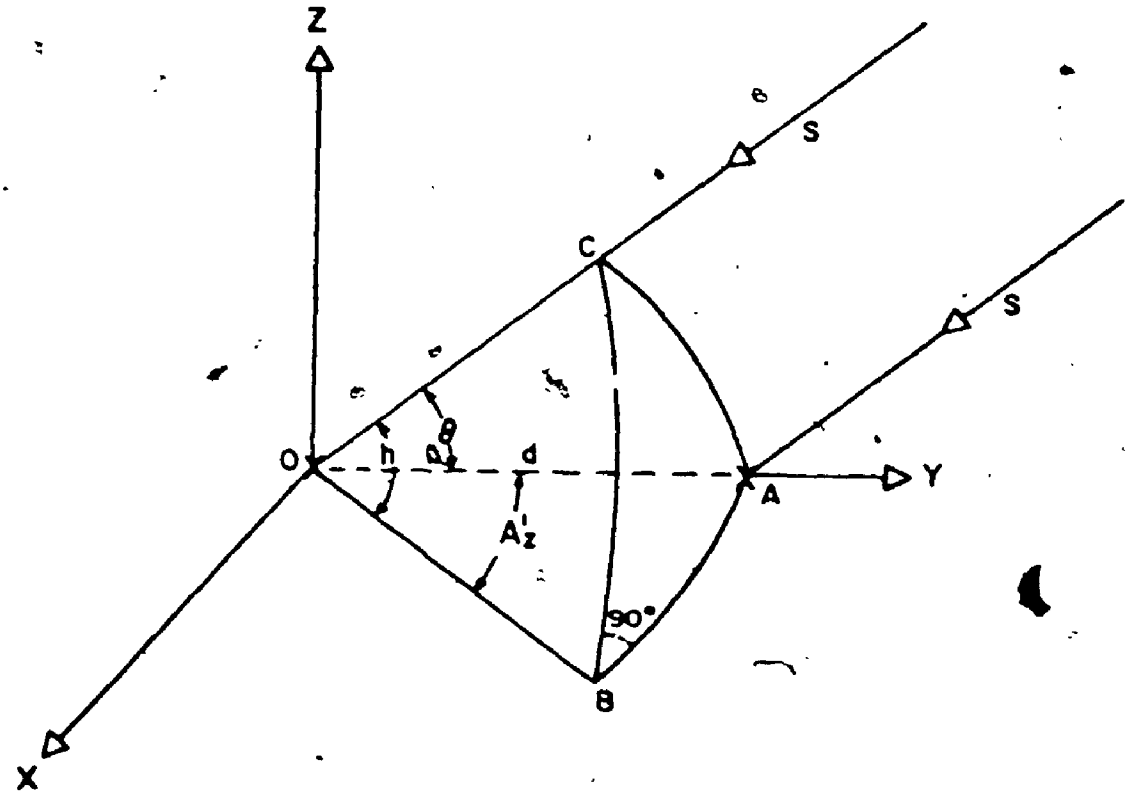

FIGURE 2: Geometry of two rays S from a radio source and an interferometer with its base-line on the OY axis. The two elements of the interferometer are located at O and A. The interferometer angle is θ; the altitude of the source is h; and the azimuth of the source with respect to OY is Az'.

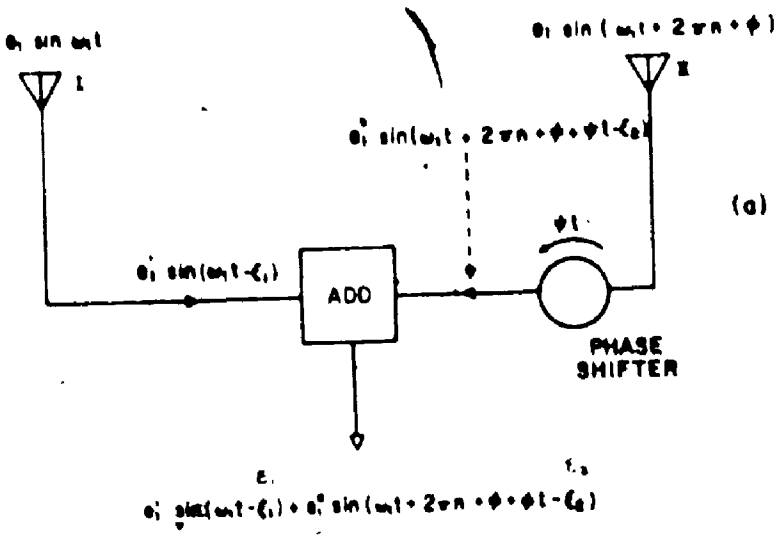

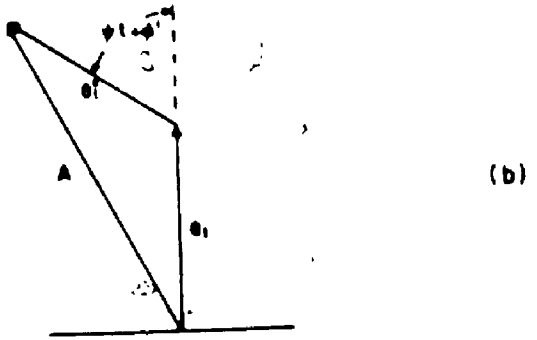

Figure 3: a) Block diagram of a basic swept-lobe interferometer. The interferometer signal for two sources is given by,

$$A_1 \cos(\omega t + \theta_1) + A_2 \cos(\omega t + \theta_2 + \beta)$$

b) Geometrical diagrams for determining the values A_1 and A_2

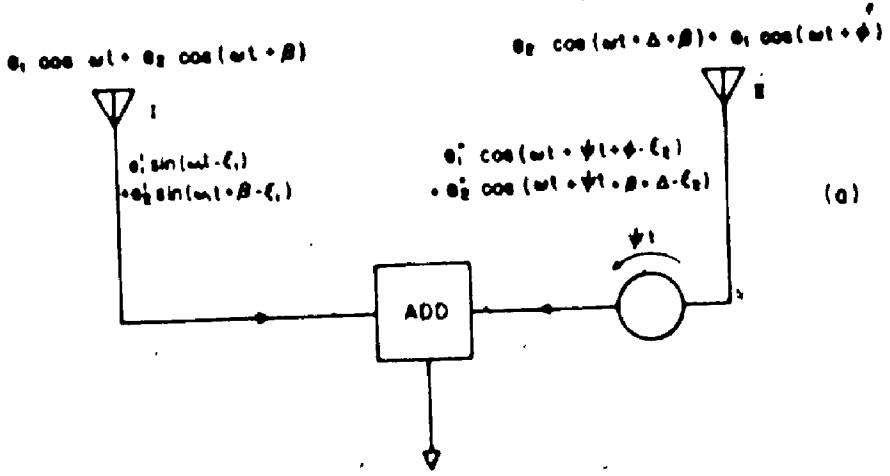

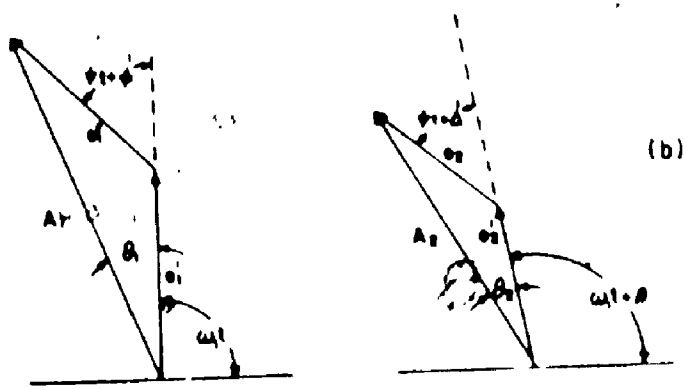

Figure 4 a) Block diagram of a basic swept-lobe interferometer (After, Winecott, 1961) The interferometer signal for one source is given by.

$$e_1' \sin(\omega t - \ell_1) + e_2' \sin(\omega t + 2\pi n + \phi + \psi t - \ell_2)$$

b) Geometrical diagram for determining the amplitude of the interferometer signal

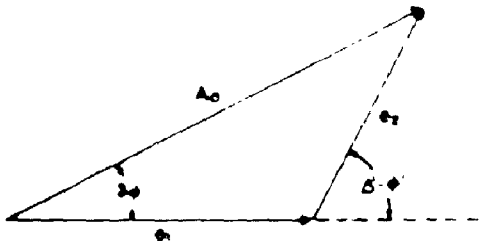

Figure 5 Geometrical diagram for determining the variation in phase and amplitude measured by a swept-lobe interferometer observing two signals with [illegible] and e2

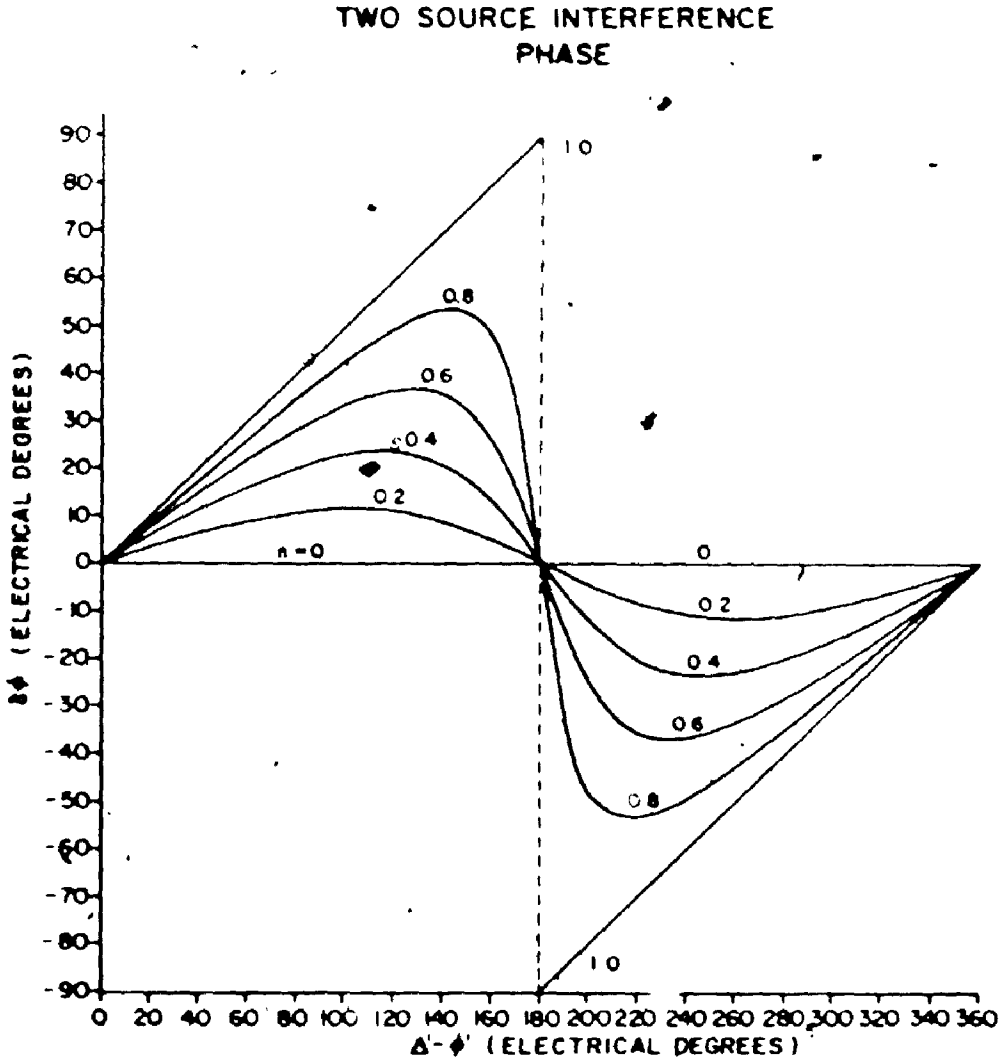

Figure 6 Variation of phase measured by a swept-lobe interferometer observing two signals with certain amplitude ratios given by [illegible] e2/e1

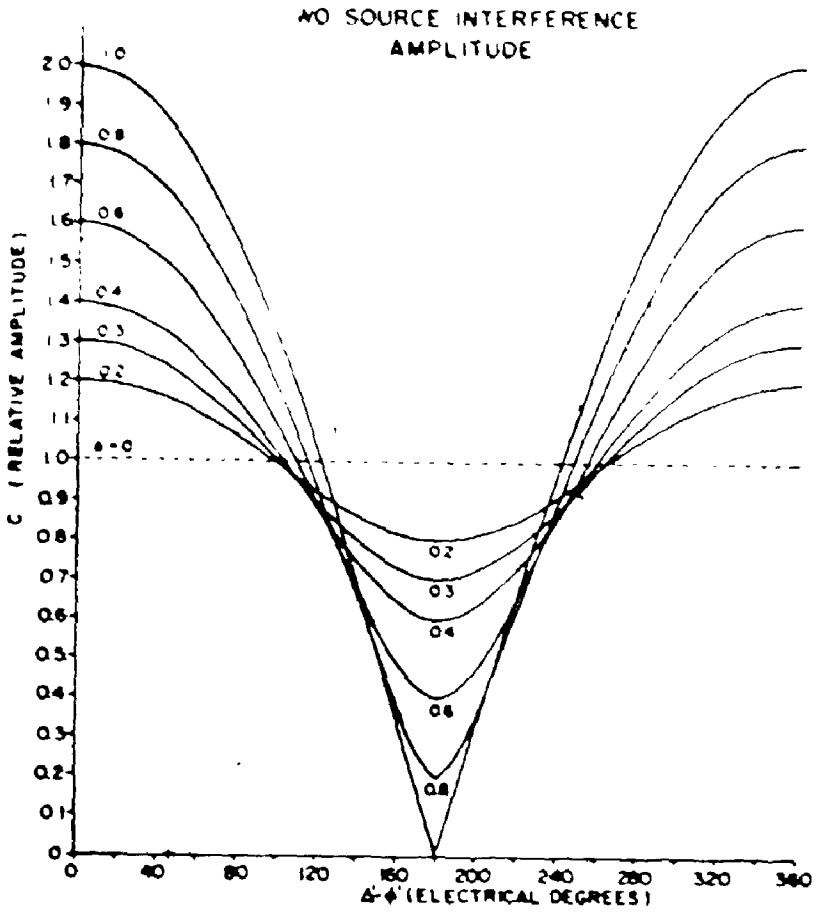

Figure 7 Variation of amplitude measured by a sweep lobe interferometer observing two signals with certain amplitude ratios.

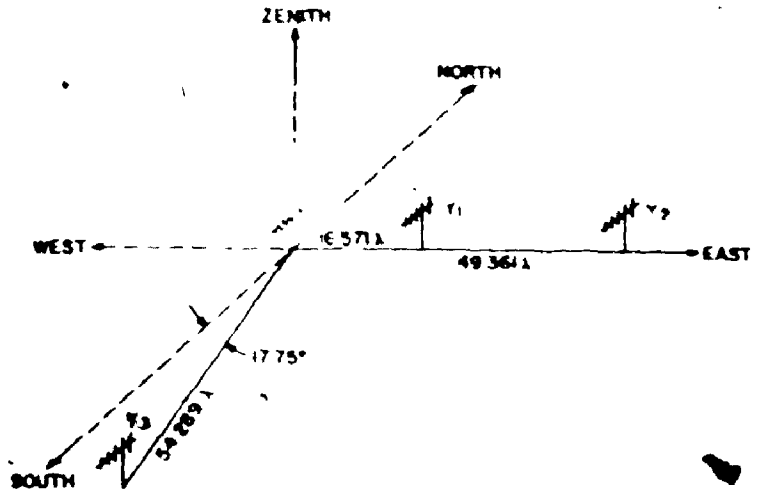

Figure 8 Geometry of the north (E, X) and east (E, Y) east-west interferometers and the north-south (E, Y') interferometers

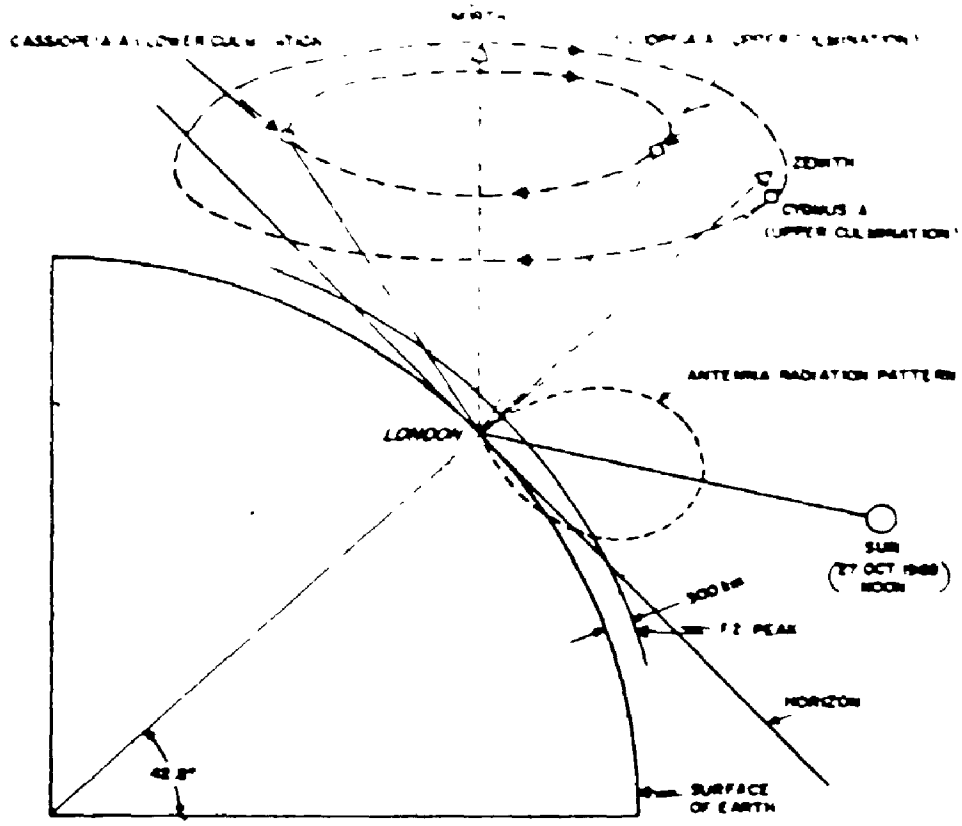

Figure 9 Plane containing center of earth, observer, and solar line of sight at local noon. An idealized radiation pattern is shown of a vertically polarized yagi antenna. The geometry and motion of both Cygnus A's and Cassiopeia A's lines of sight are shown.

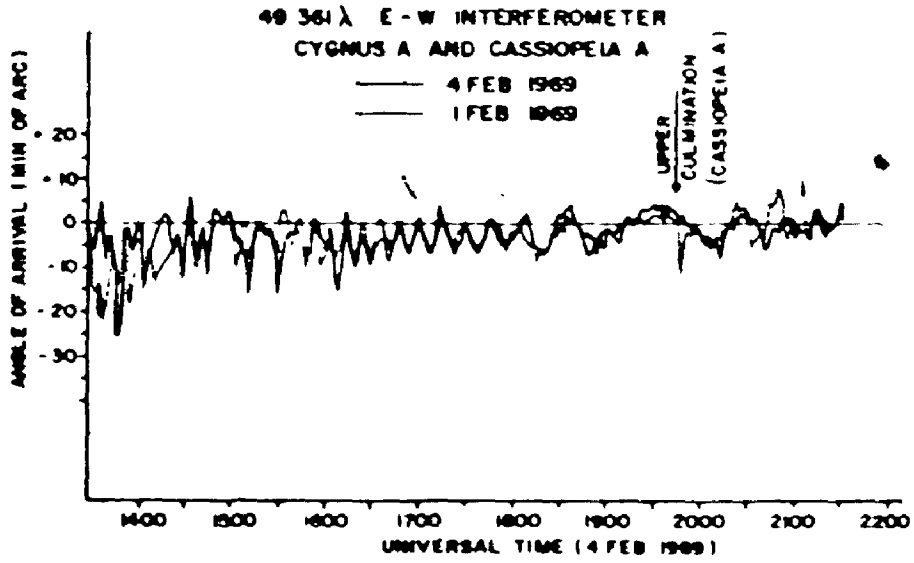

Figure 10 Angle-of-arrival of Cygnus A and Cassiopeia A observed by the wide E-W interferometer on the 4 and 5 February 1969. Abscissa is correct for 4 February 1969.

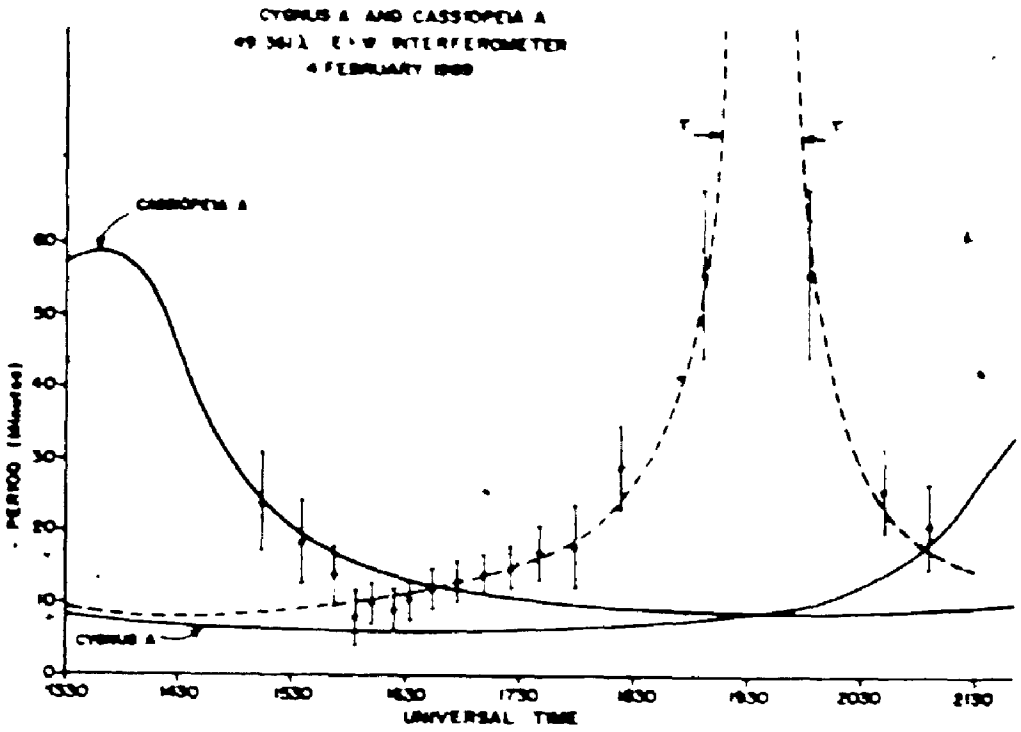

FIGURE 11 Period of scintillations observed by the wide E-W interferometer on 4 February 1969 and caused by interference between Cassiopeia A and Cygnus A. Dashed curves give theoretical values. Solid curves give the time required for the phase of the signals from Cassiopeia A and Cygnus A to increase or decrease by 2π radians when observed individually.

AMPLITUDE
1 FEBRUARY 1969
CYGNUS A AND CASSIOPEIA A
49 361 λ E-W INTERFEROMETER

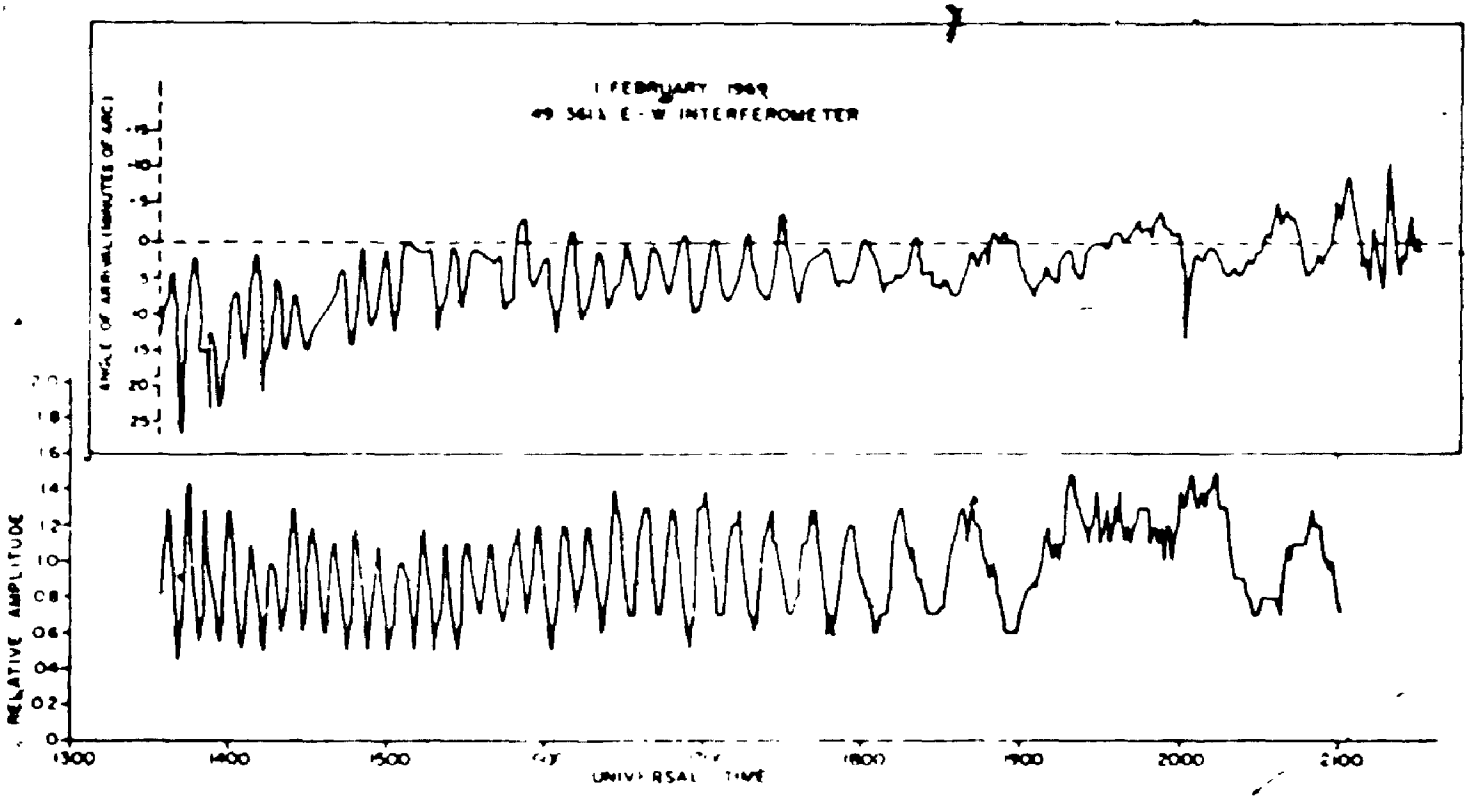

FIGURE 12 Angle of arrival and relative amplitude of the sum of the signals from Cygnus A and Cassiopeia A on 1 February 1969. Dashed lines give the corresponding angle of arrival measurements.

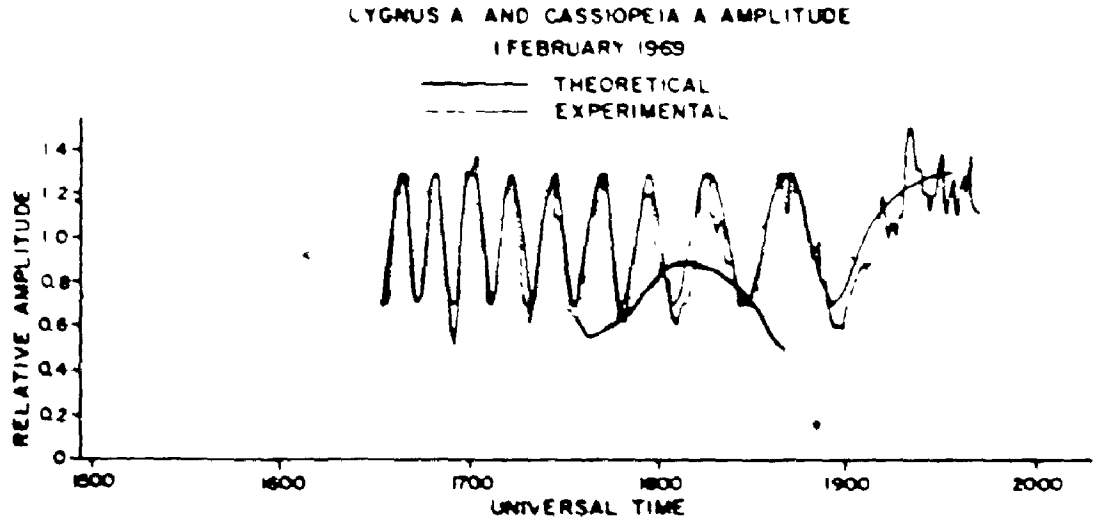

FIGURE 13 Amplitude scintillations of the sum of the signals from Cygnus A and Cassiopeia A on 1 February 1969 compared with a theoretical curve

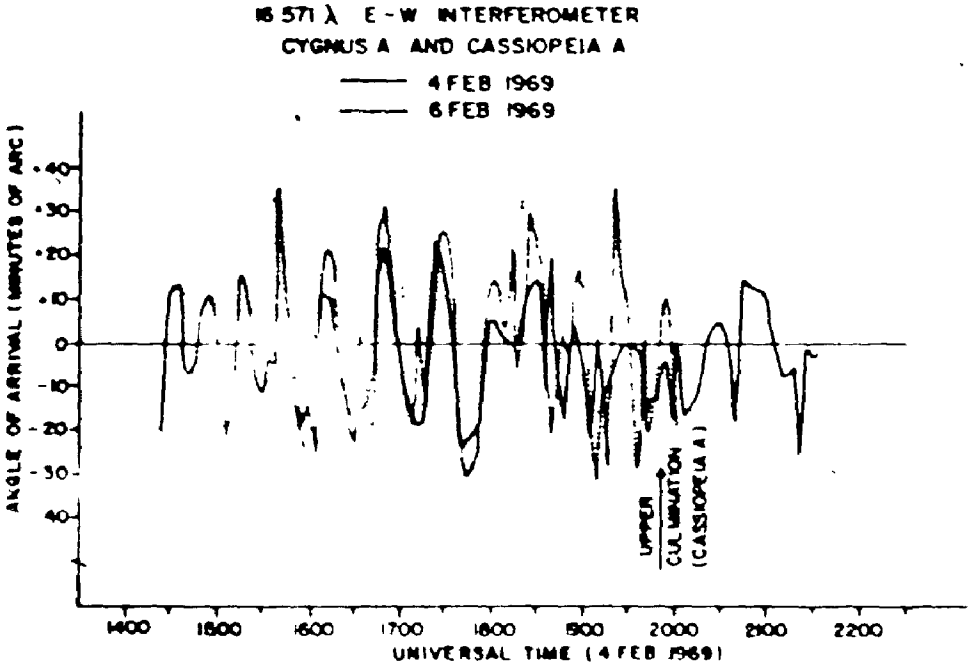

FIGURE 14 Comparison of angle-of-arrival scintillations recorded on the narrow E-W interferometer on 4 February and 6 February 1969

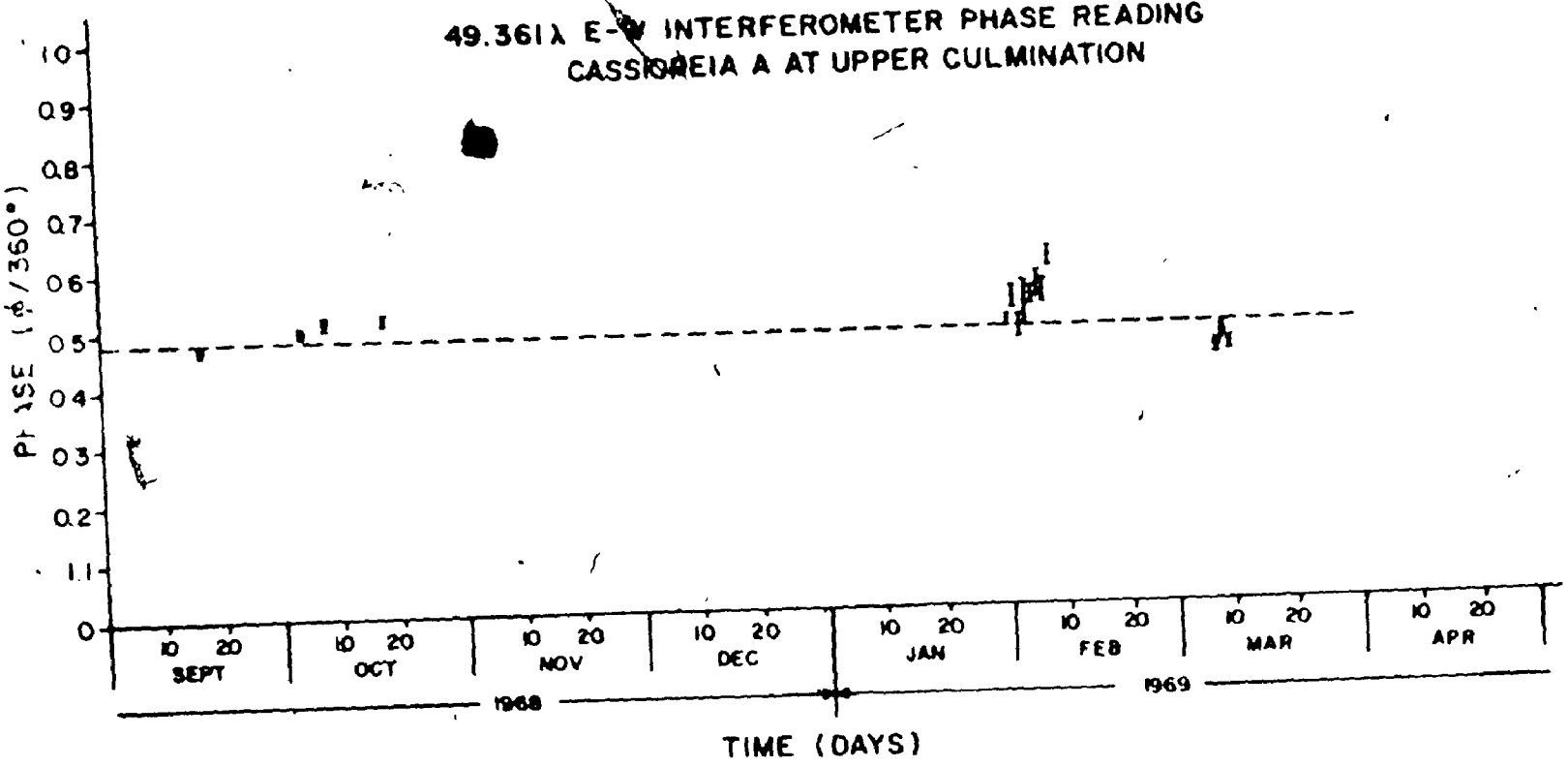

FIGURE 15: Phase measured by the wide E-W interferometer at the time of the upper culmination of Cassiopeia A for a number of days over a six month-interval. Measurements were made with the antennas roughly pointed at the upper culmination position of Cassiopeia A.

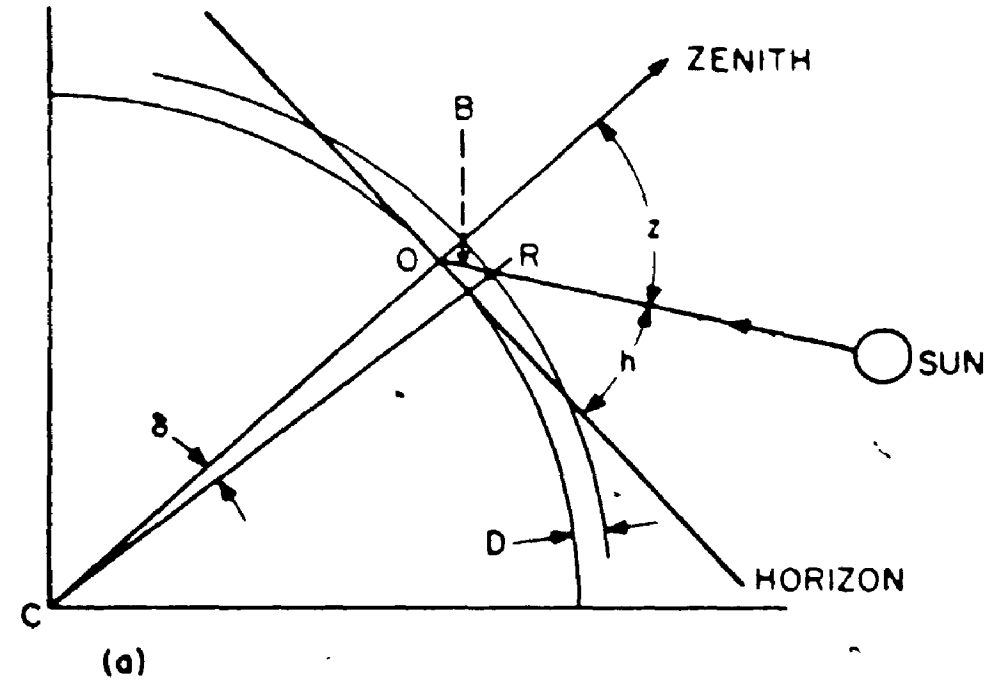

(a)

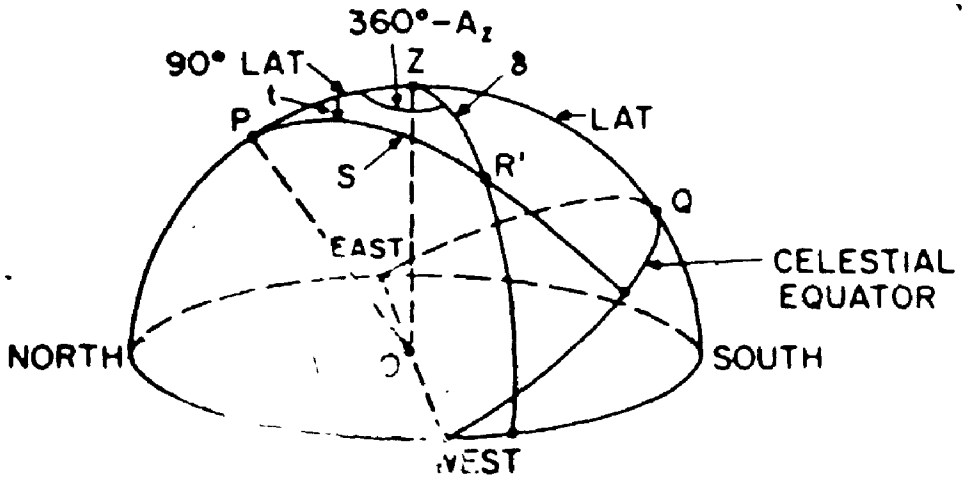

Fig. 16 a) Plane defined by observer's location, center of the earth and solar line of sight.

b) Observer's celestial hemisphere showing angles used in defining the point of intersection of the solar line of sight with the ionosphere.

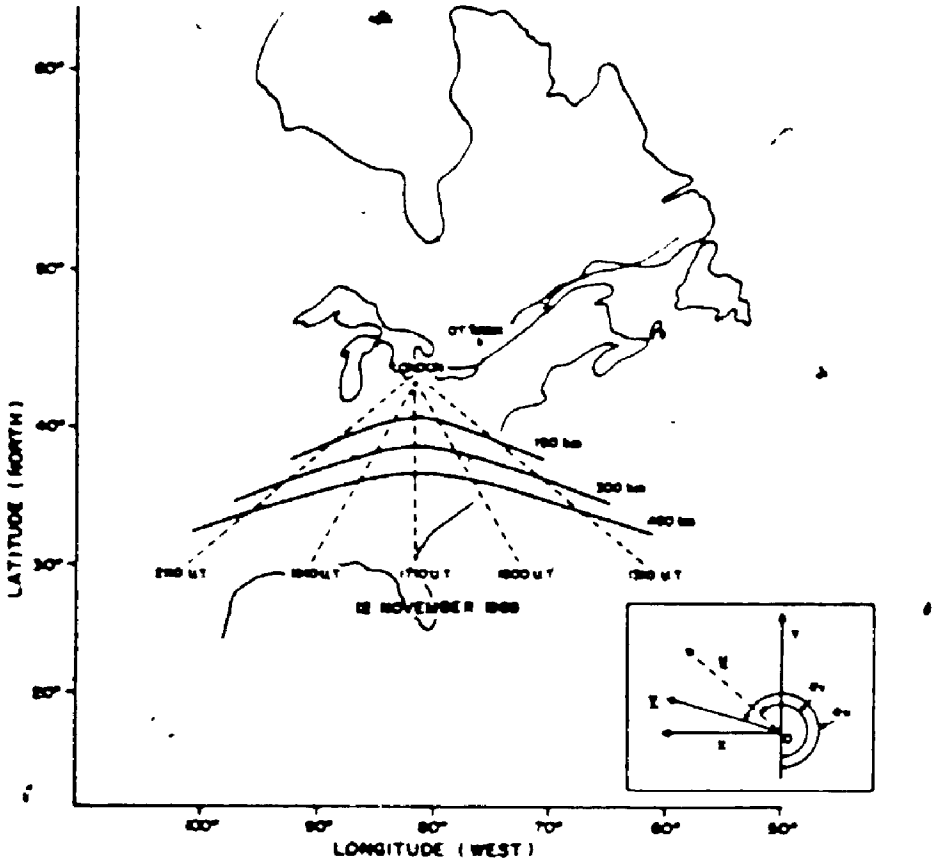

Fig. 17 The curves show the loci of the intersection of the solar line of sight with various levels in the ionosphere as a function of time. Co-ordinate axes shown in the insert define positive values for the two velocity components, V_x, and, V_y, of the sun's line of sight through the ionosphere

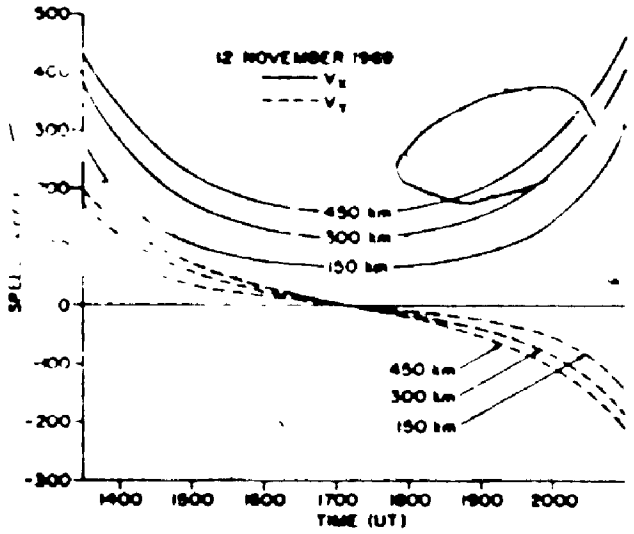

Fig. 18 Plot of November 12, 1969 values of, V_x, and, V_y, as a function of time for various heights

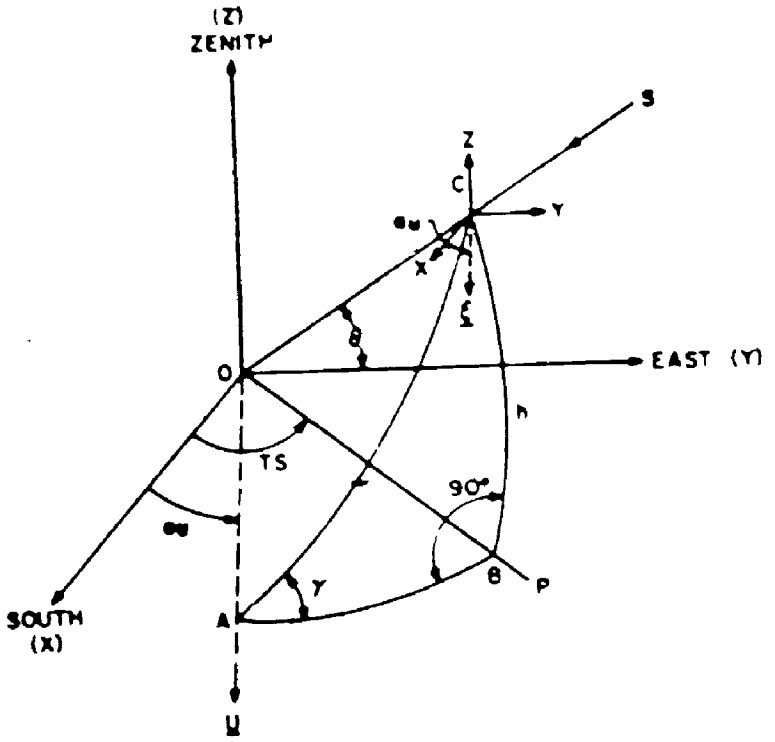

Fig 19 Solar ray - interferometer geometry showing spherical triangle, ABC, which is defined by the solar line of sight, OS, projection, OP, of the solar line of sight onto the observer's horizon plane, and the projection, $\underline{U}$, of the TIDs' horizontal vector onto the observer's horizon plane

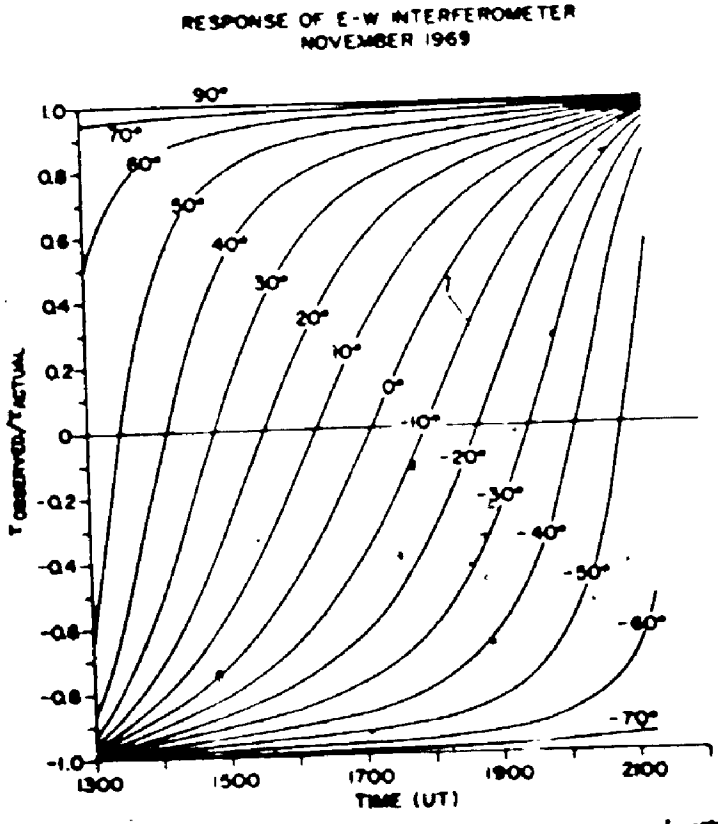

Fig. 20 Plot of response, $F_{i,t}$, of the E-W interferometers versus time, on November 12, 1969, to angular deflections of the solar line of sight due to refraction. The numbers on the curves give the TIDs' direction of travel.

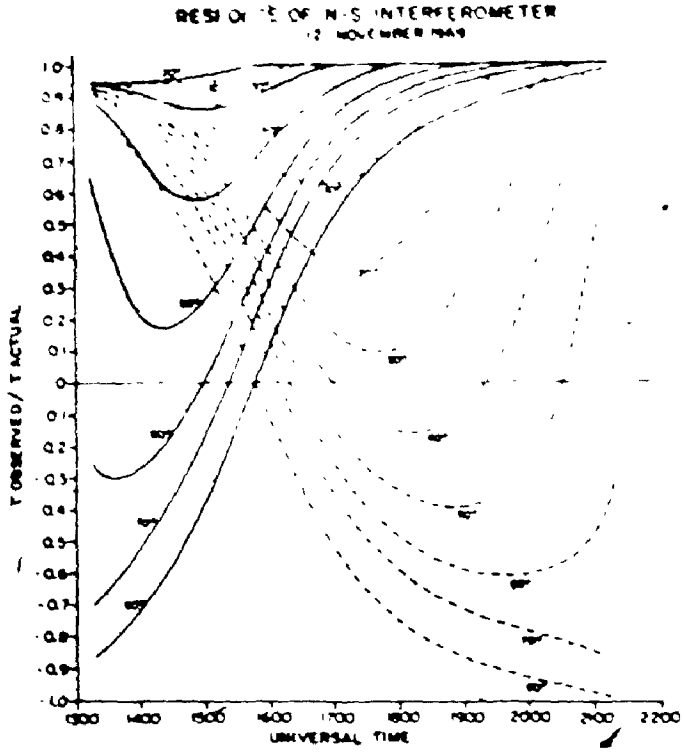

FIGURE 21 Response of the N-S interferometers on 12 November 1969 to angular deflections of the solar line of sight due to refraction by TID induced horizontal gradients in electron density within the ionosphere. The numbers on the curves give the TIDs' direction of travel

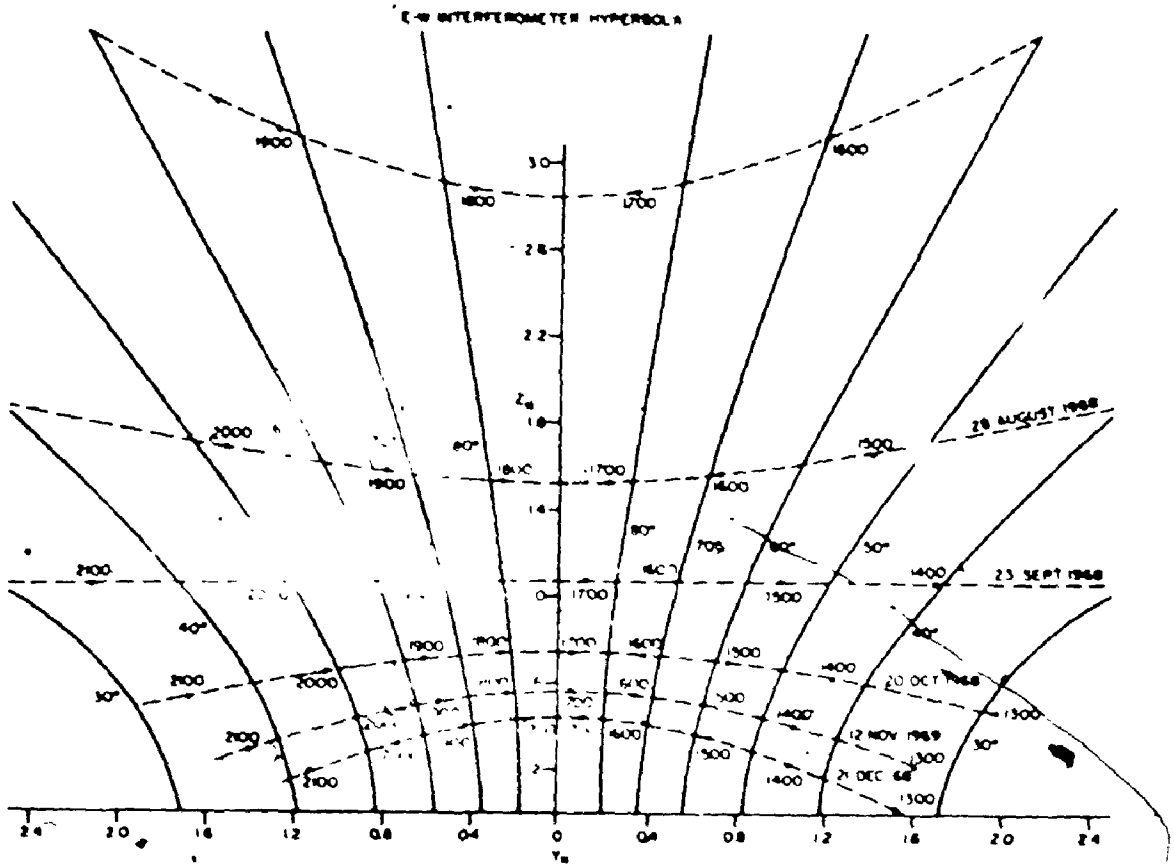

FIGURE 22 Loci of the intersection of the surfaces of constant phase for the E-W interferometer with a plane south of the observer and at right angles to the observer-south axis. Dashed curves give loci of the intersection of the solar line of sight with the above plane for various times of the year

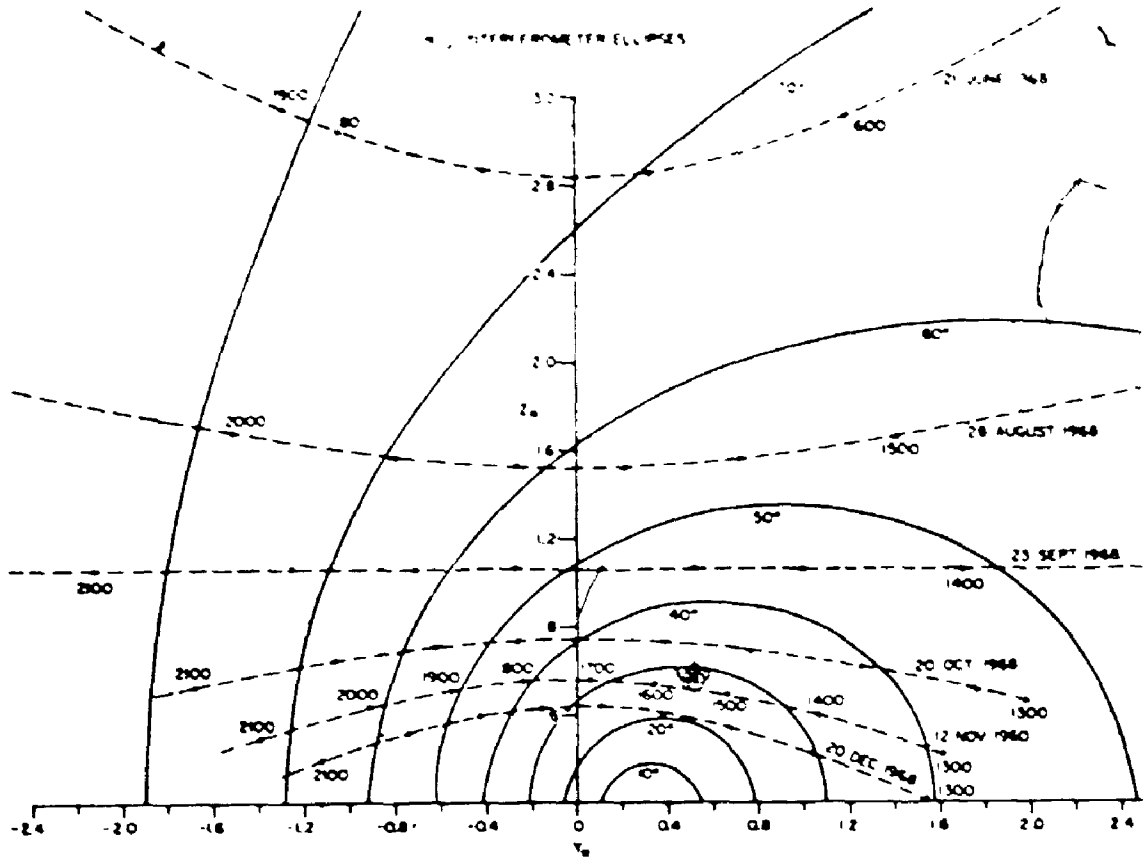

FIGURE 23 Loci of the intersection of the surfaces of constant phase for the N-S interferometer with a plane south of the observer and at right angles to the observer-south axis

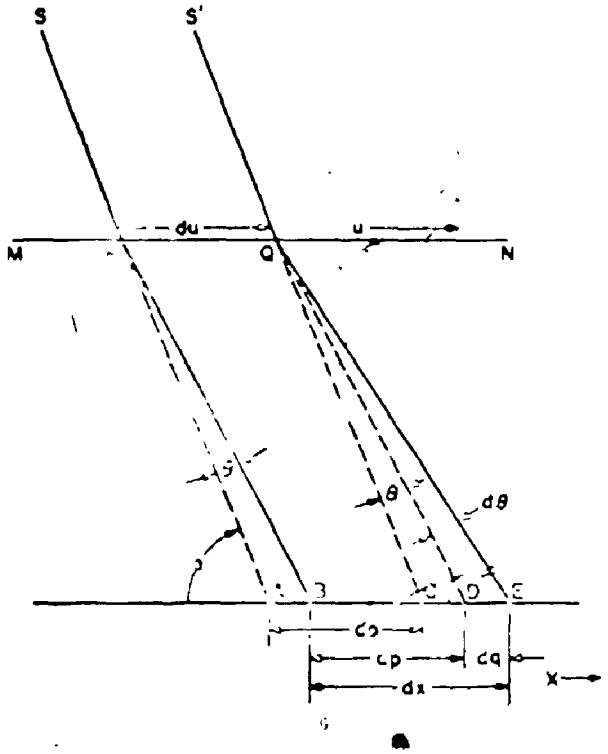

FIGURE 24 Refraction of two solar rays by a spatially varying horizontal electron density gradient in the ionosphere (After, Turnbull and Forsyth, 1965)

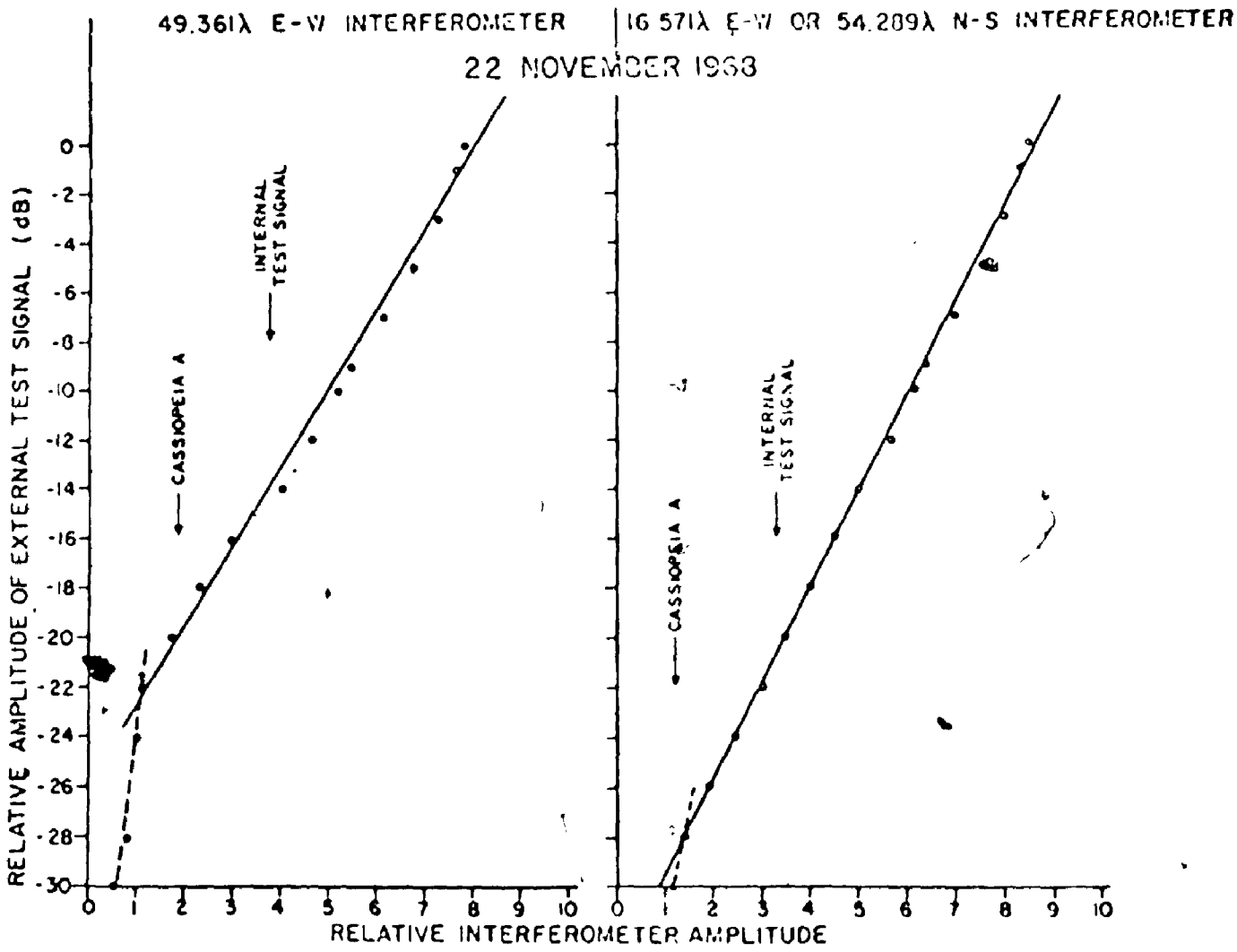

FIGURE 25: Calibration curves to convert amplitude deflection to flux density.

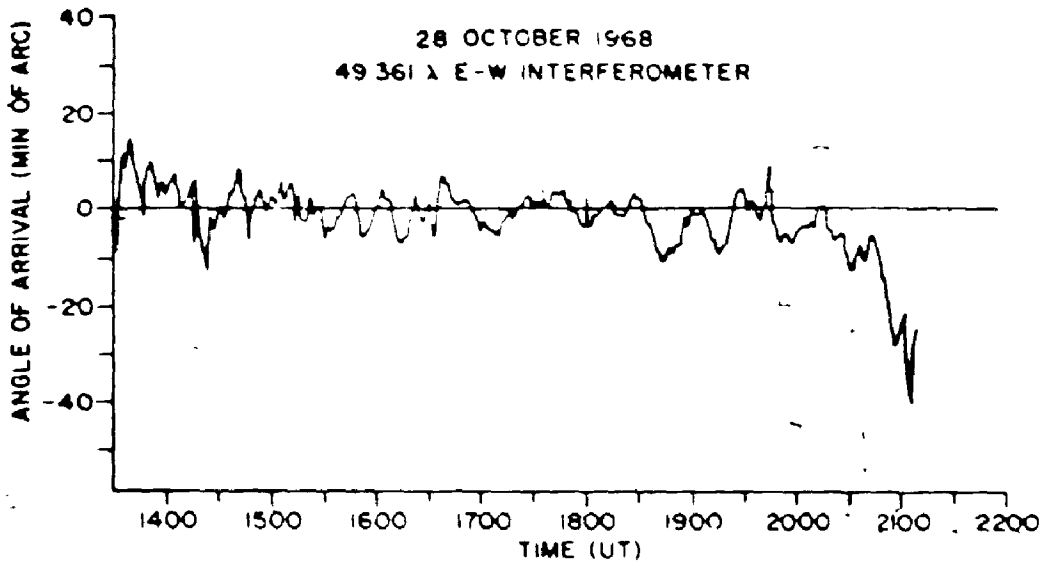

Fig. 26 Angle of arrival versus time measured by wide E-W interferometer on October 28, 1968. This result is consistent with a stationary solar source and a relatively undisturbed ionosphere.

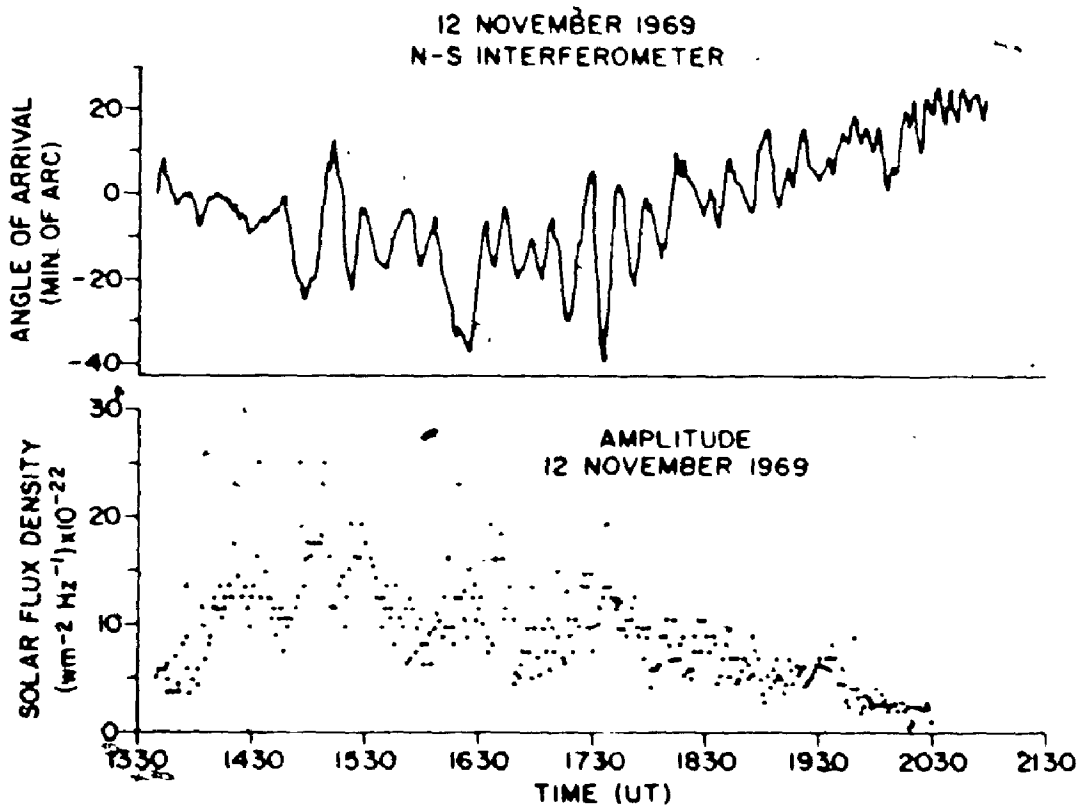

Fig. 27 Comparison of angle of arrival and solar flux density measured with the N-S interferometer on November 12, 1969

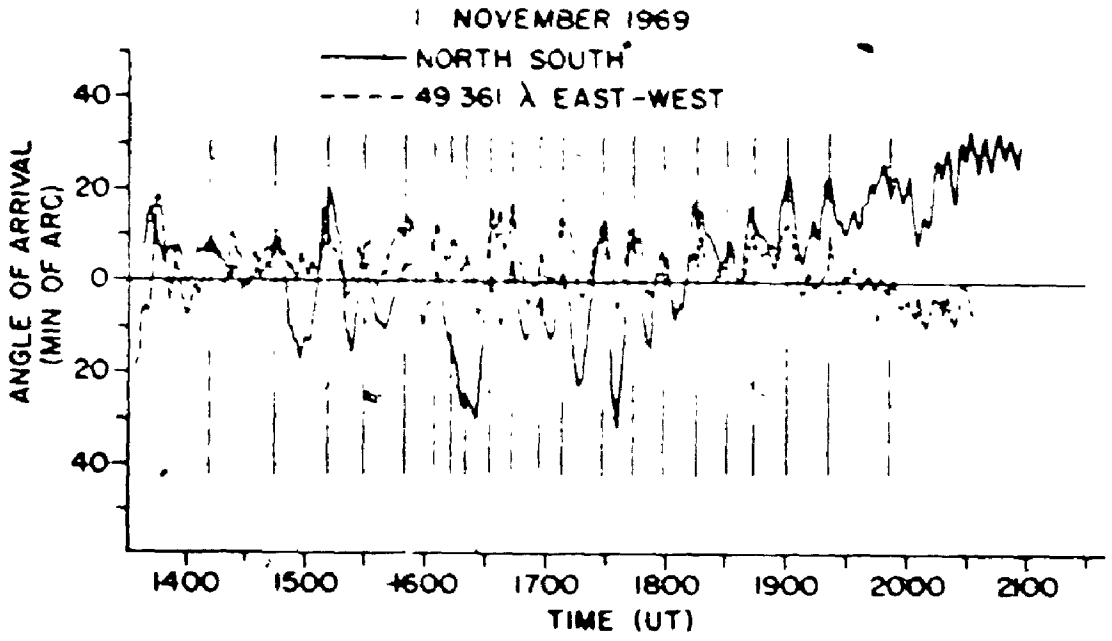

Fig. 28 Comparison of angle of arrival measured by both the wide E-W and the N-S interferometers on November 12, 1969

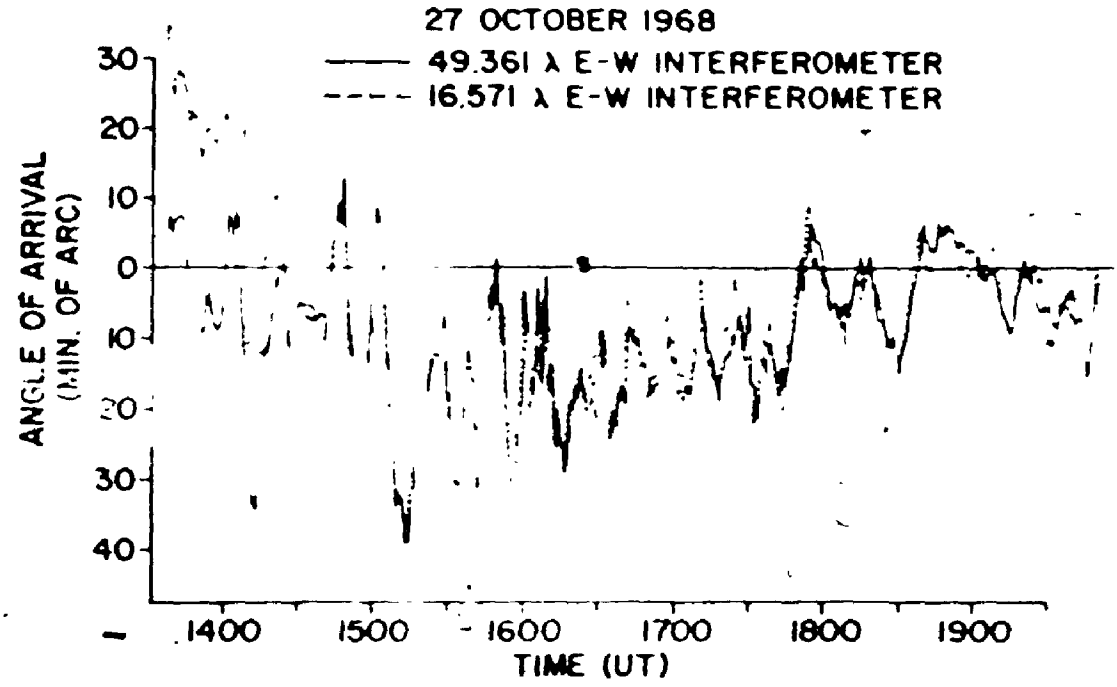

Fig. 29 Comparison of the angle of arrival versus time measured by the wide E-W and narrow E-W interferometers on October 27, 1968

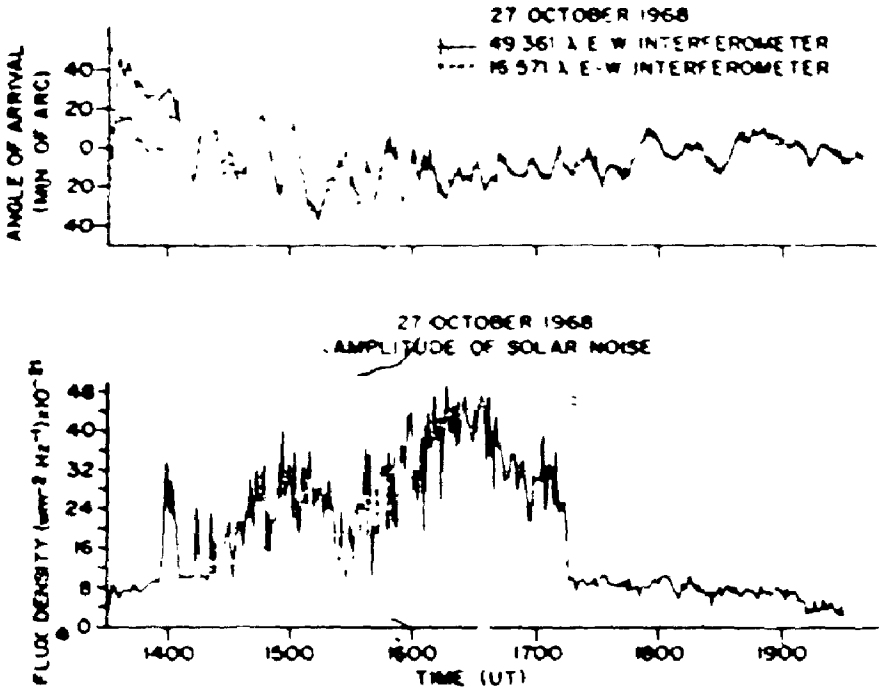

Fig 30 Comparison of angle of arrival and solar flux density measured on October 27, 1968

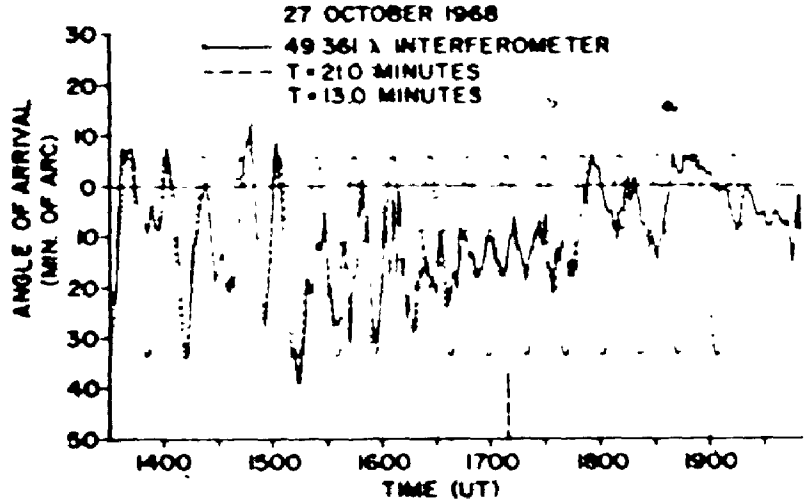

Fig 31 Comparison of the angle of arrival measured with the wide E-W interferometer on October 27, 1968 with two sinusoids one with a period of 21 minutes, the other with a period of 13 minutes

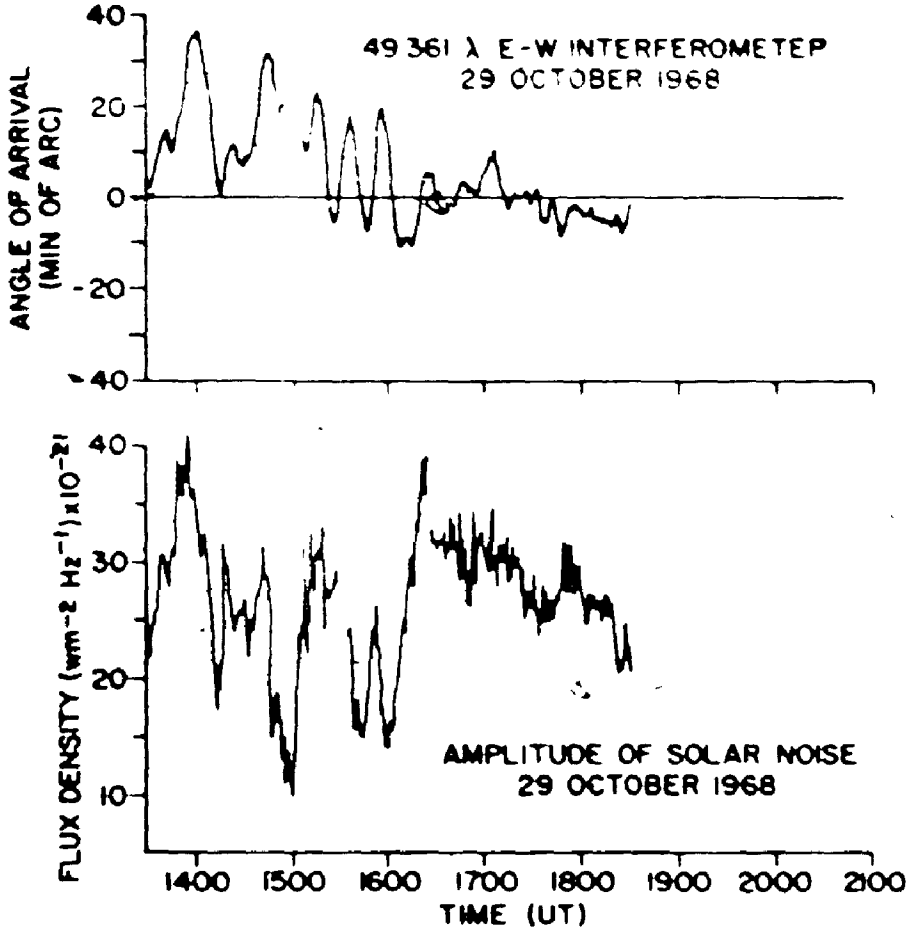

FIGURE 32: Angle-of-arrival and solar flux density measured with the wide E-W interferometer on October 29, 1968.

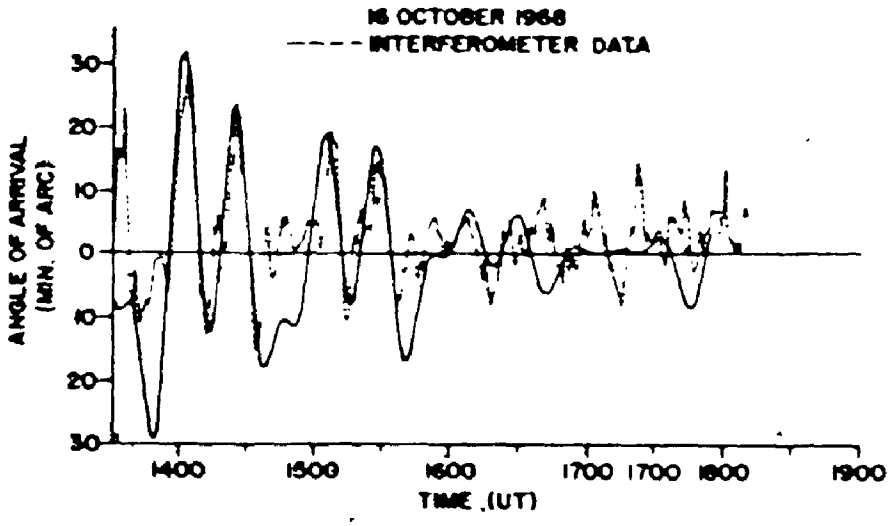

FIGURE 33: Comparison of angle-of-arrival measured by the wide E-W interferometer on 16 October 1968 with a synthesized curve.

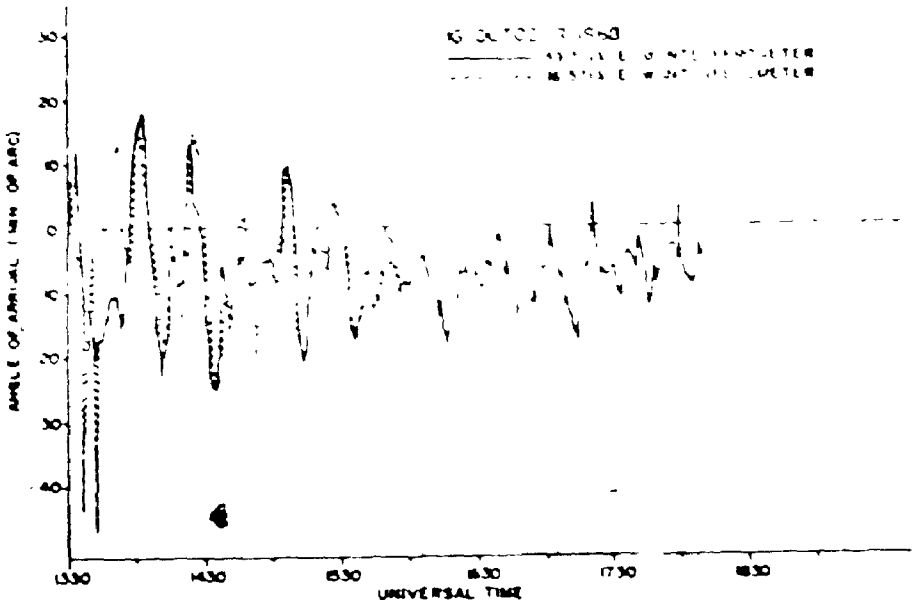

FIGURE 34 Comparison of angle-of-arrival measured by the wide and narrow E-W interferometers on 16 October 1968

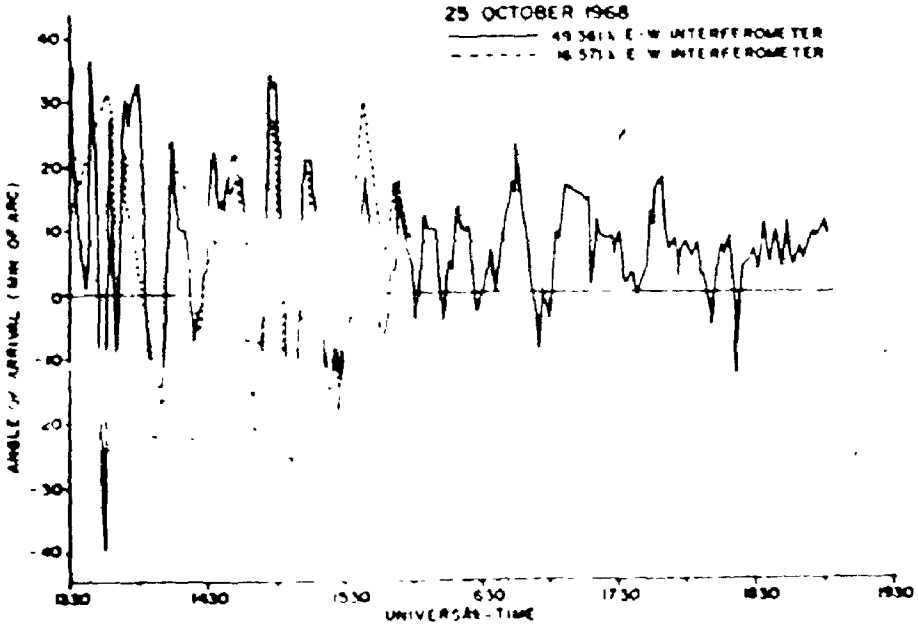

FIGURE 35 Comparison of angle-of-arrival measured by the wide and narrow interferometers on 25 October 1968

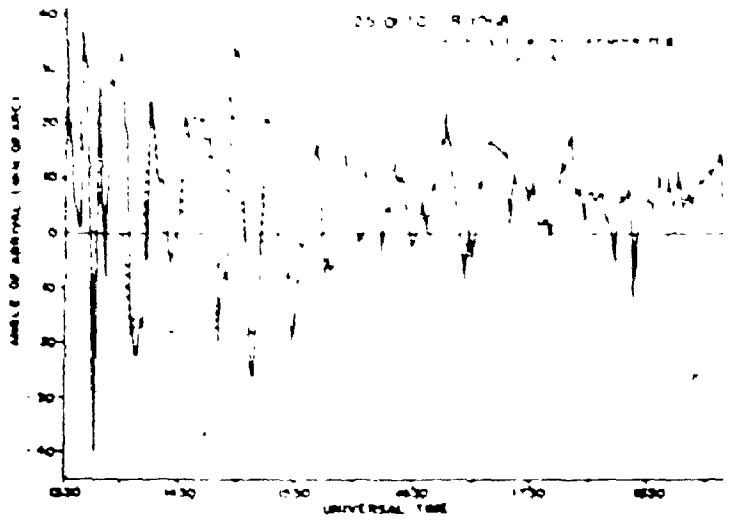

FIGURE 36

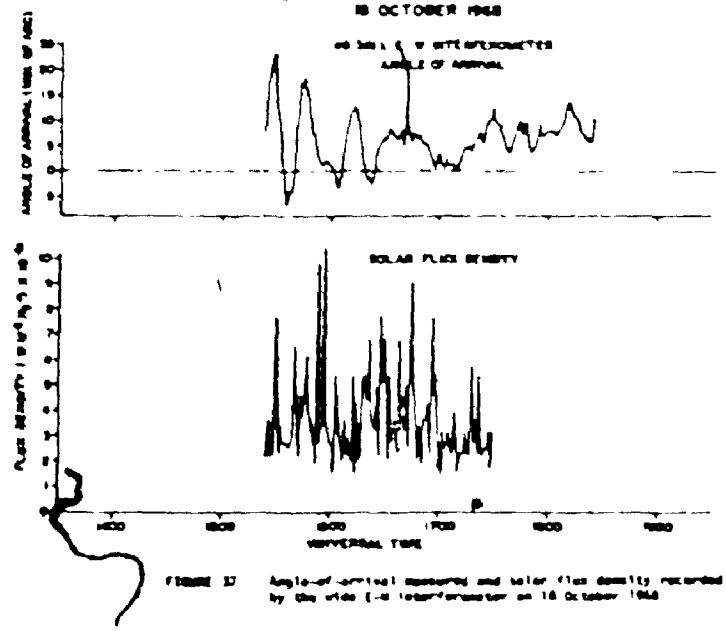

FIGURE 37

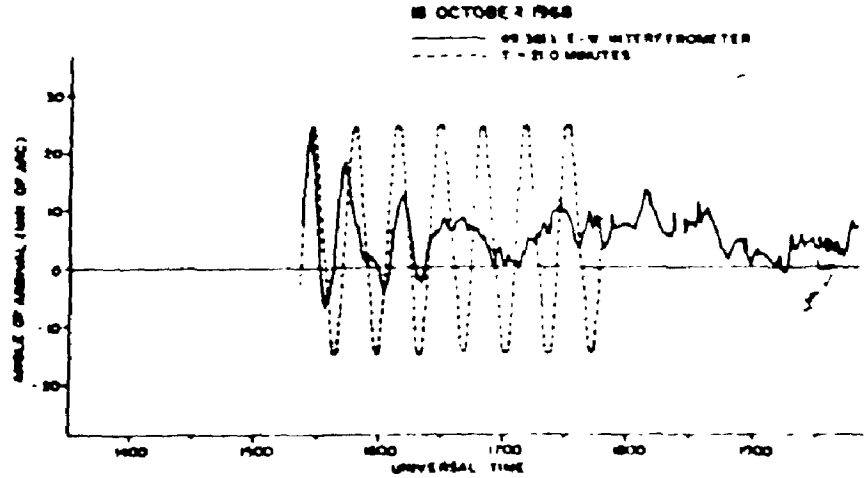

FIGURE 38

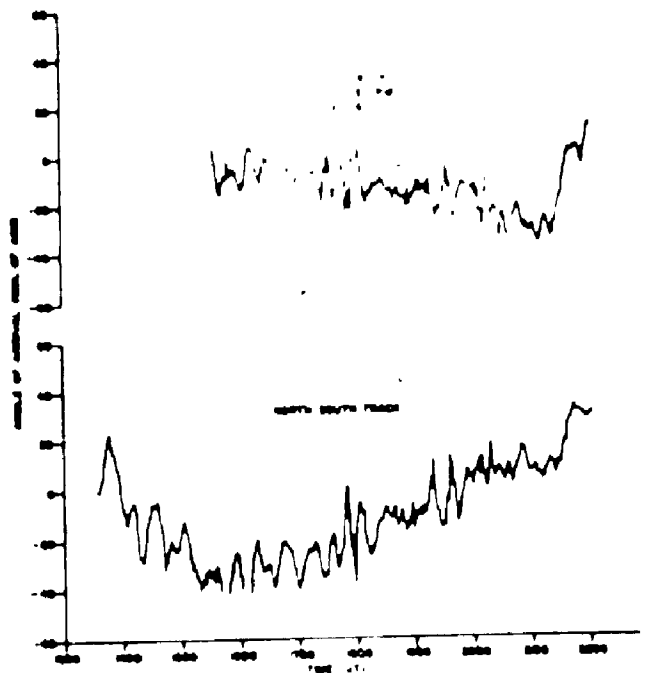

FIGURE 39· Angle-of-arrival measured by the wide E-W and N-S interferometers on 10 November 1969.

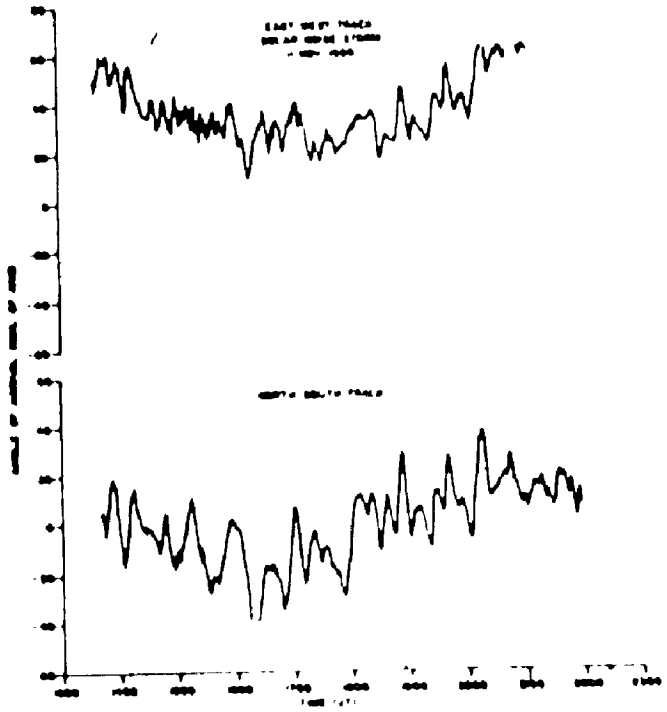

FIGURE 40 Angle-of-arrival measured by the wide E-W and N-S interferometers on 11 November 1969

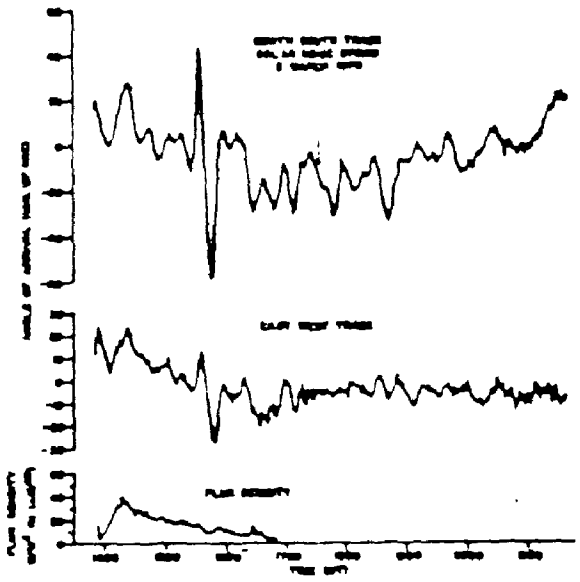

FIGURE 41: Angle-of-arrival measured by the wide E-W and N-S interferometers and the solar flux density recorded by the wide E-W interferometer on 2 March 1970.

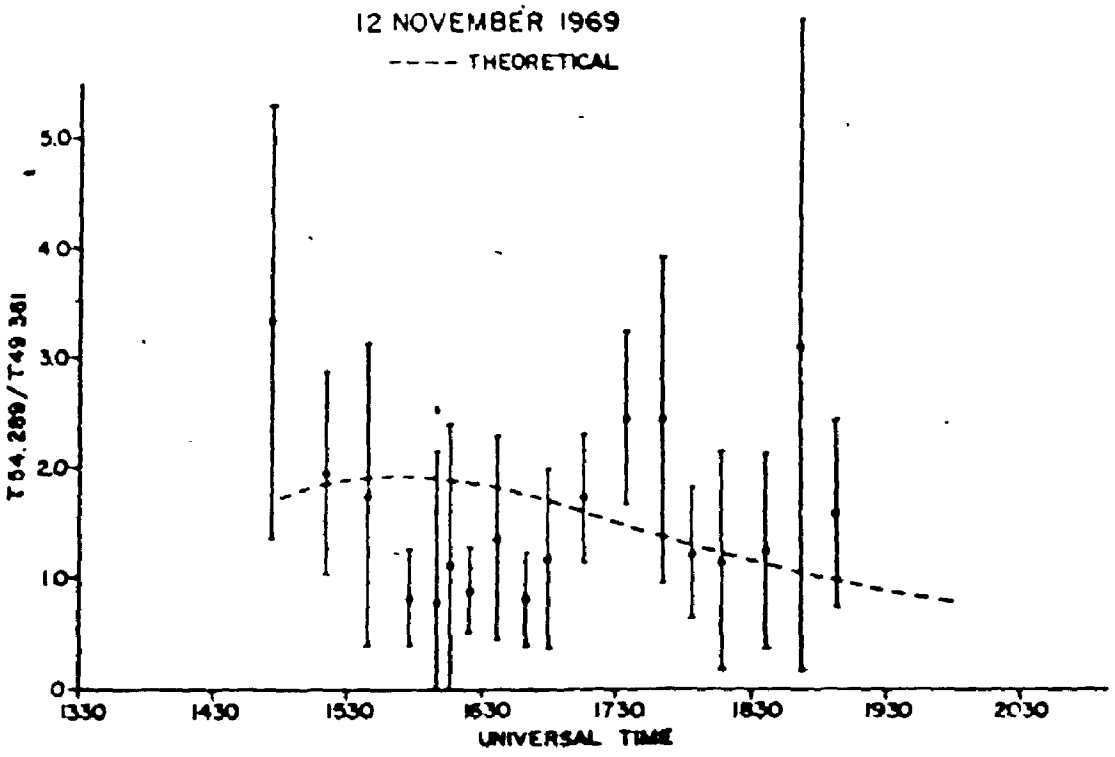

FIGURE 42: Ratio of the Amplitudes of scintillations measured by the N-S and E-W interferometers on 12 November 1969 versus universal time.

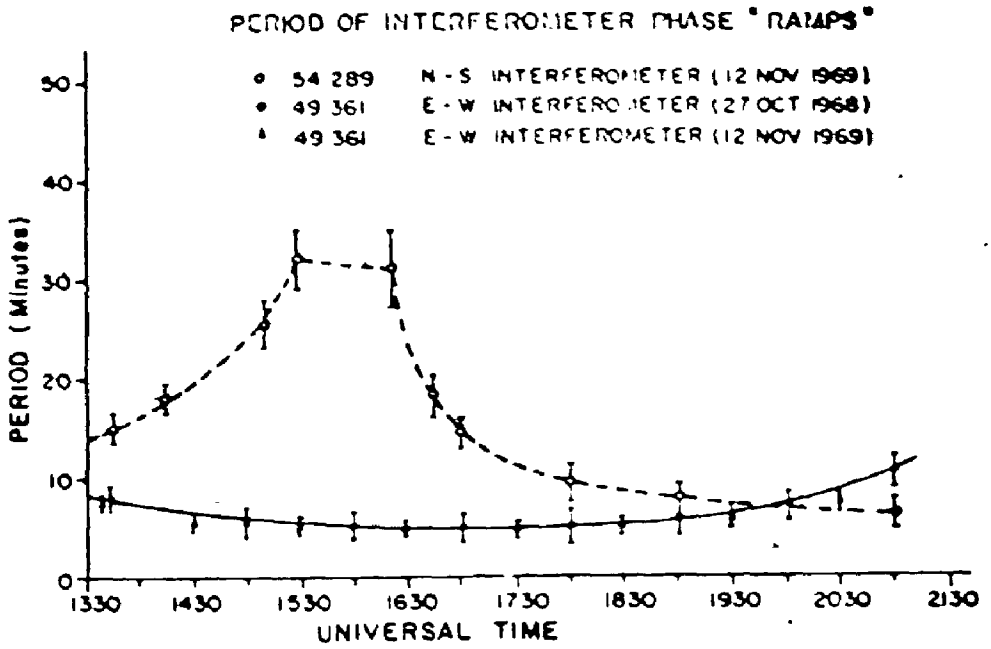

FIGURE 43 Period of phase ramps for the N-S and E-W interferometers.

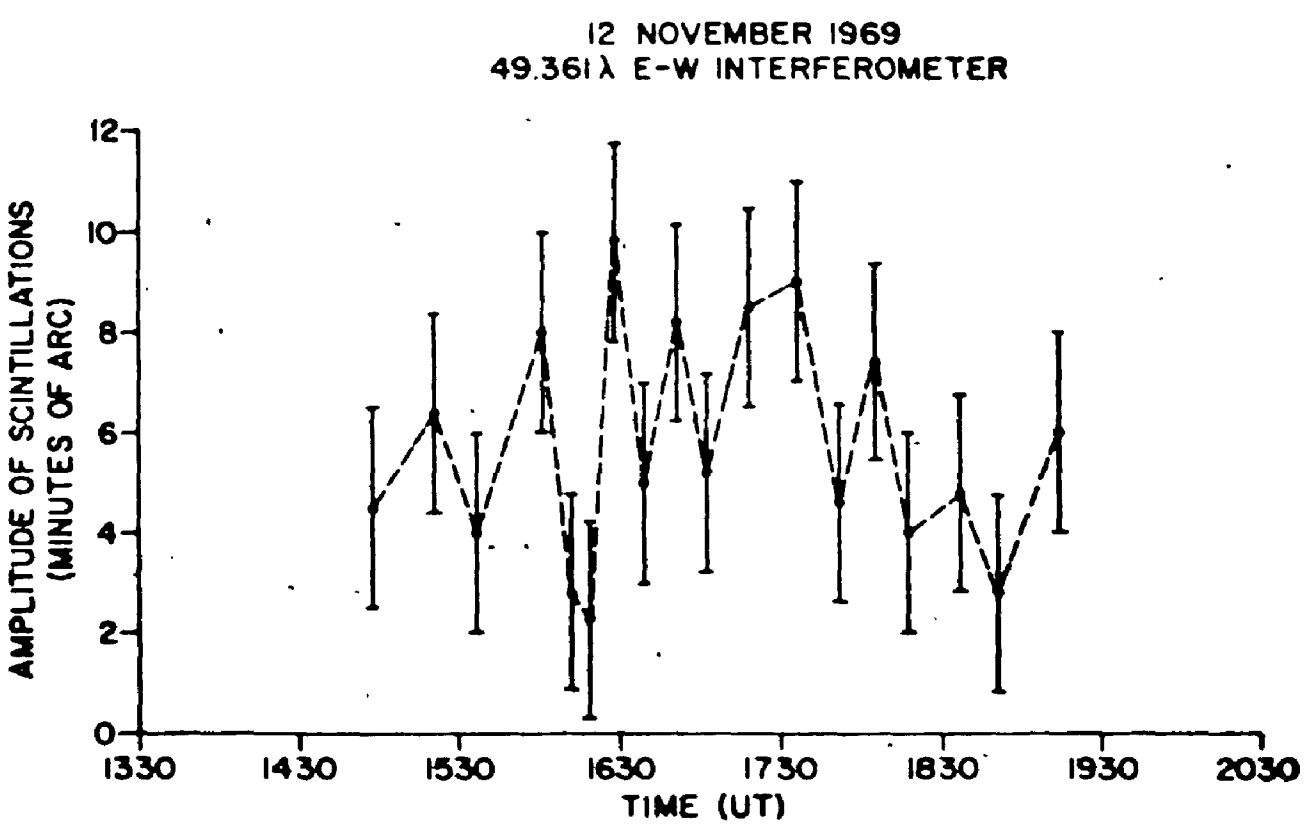

FIGURE 44 Amplitude of scintillations measured by wide E-W interferometer on November 12, 1969 versus universal time.

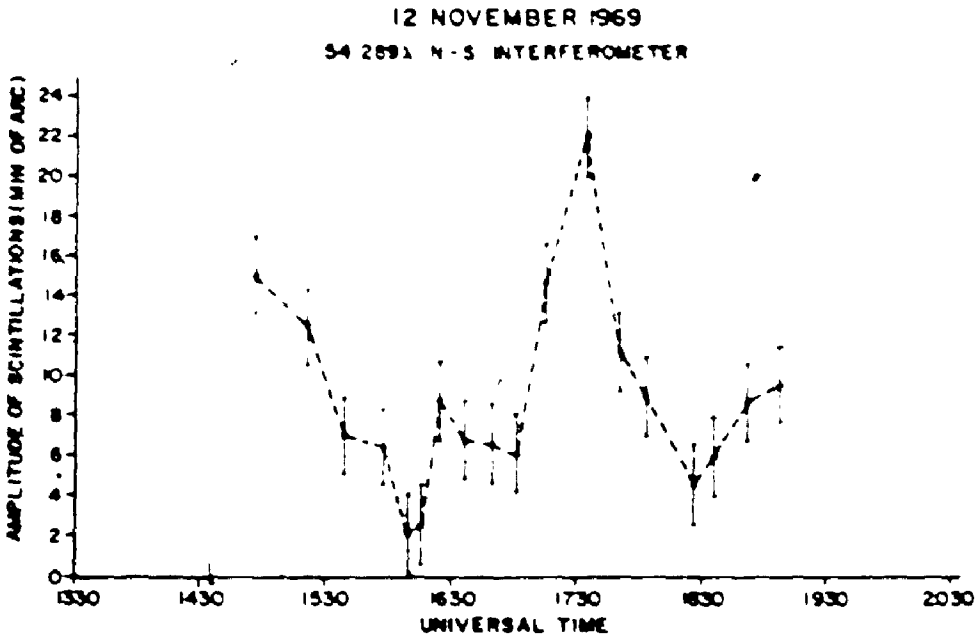

Fig 45 Magnitude of the scintillations measured by the E-W interferometer on November 12, 1961 versus universal time

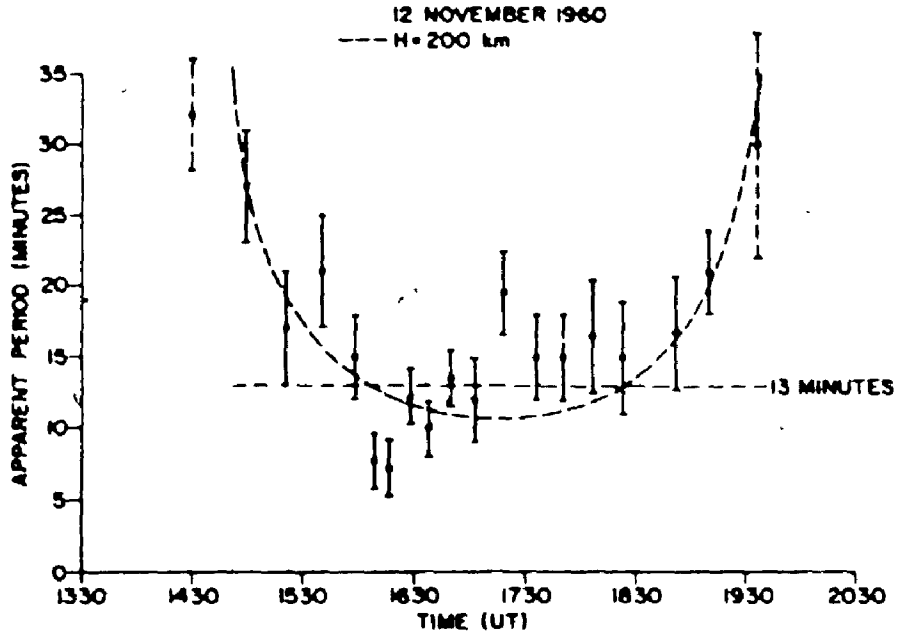

Fig 46 Apparent period of scintillations observed on November 12, 1960 versus universal time

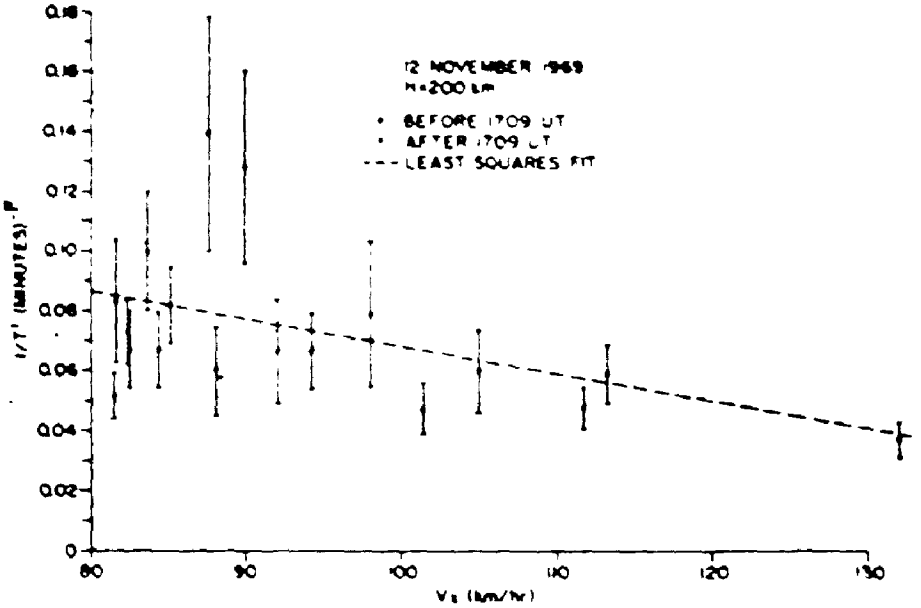

Fig. 47 Plot of the inverse of the apparent period of the November 12, 1969 scintillations versus the west component of the velocity of the solar line of sight through the 200 km level.

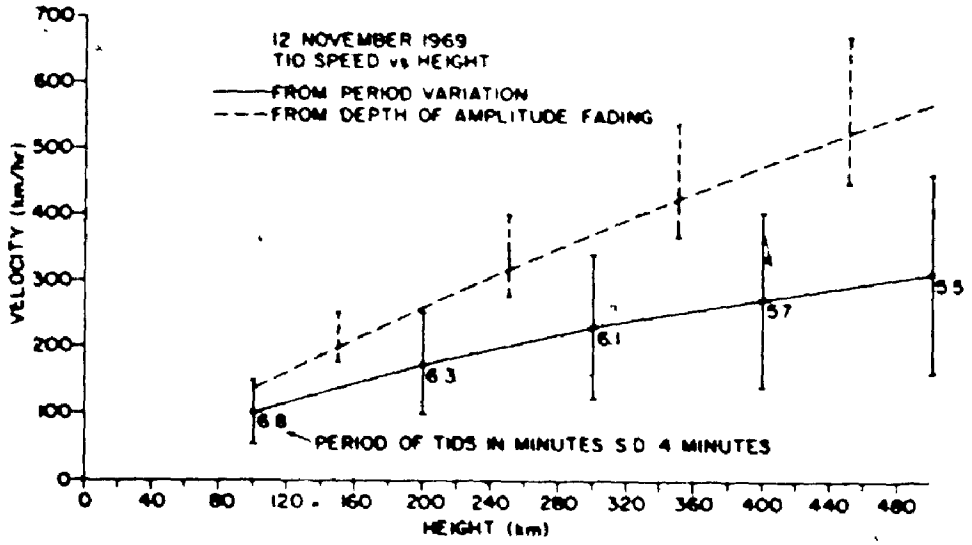

Fig. 48 Speed of the S-W TID observed on November 12, 1969 versus altitude. Solid curve was derived from the observed long term variation in the apparent period. Numbers on the curve give the TID period in minutes. Dashed curve was obtained from a correlation of the amplitude and angle of arrival scintillation.

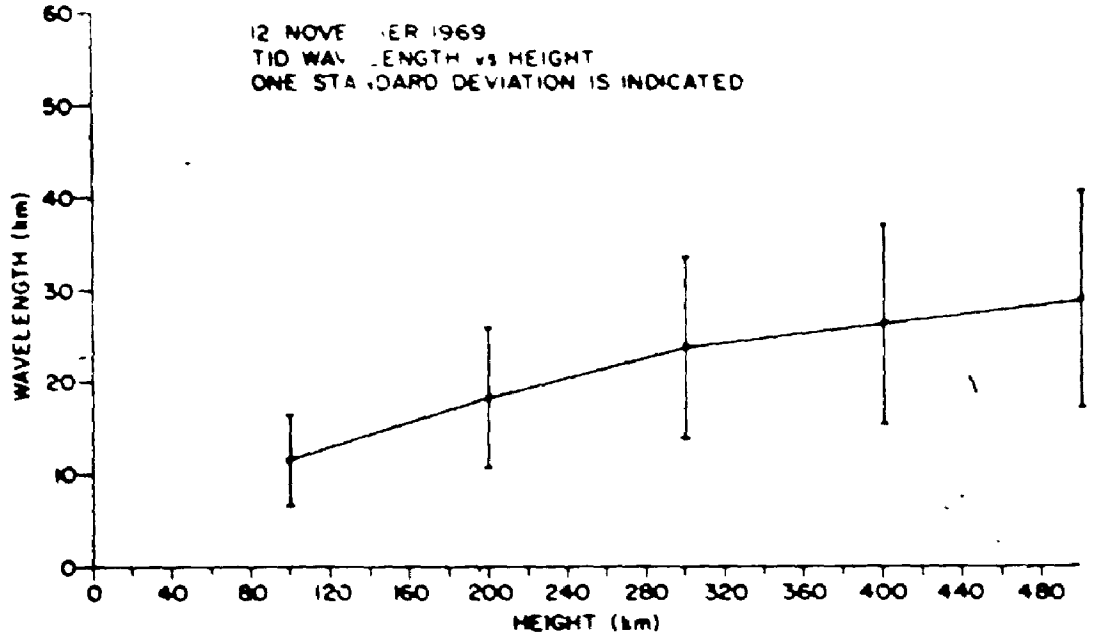

Fig 49 Wavelength of E-W TIDs observed on November 12, 1969 versus altitude

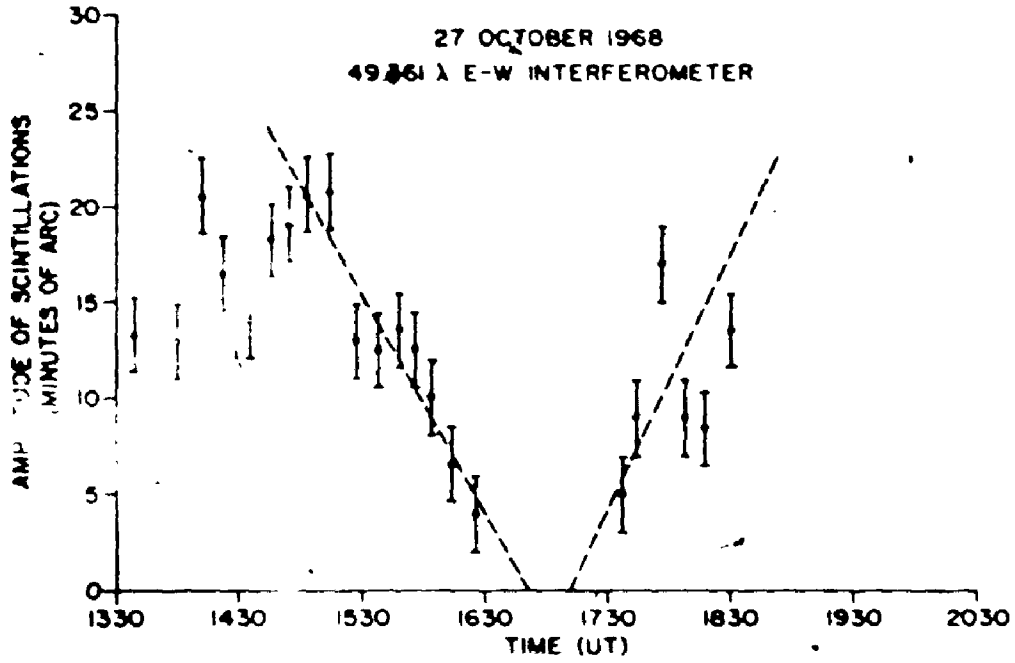

Fig 50 Amplitude of scintillations measured by wide E-W interferometer on October 27, 1968, versus universal time

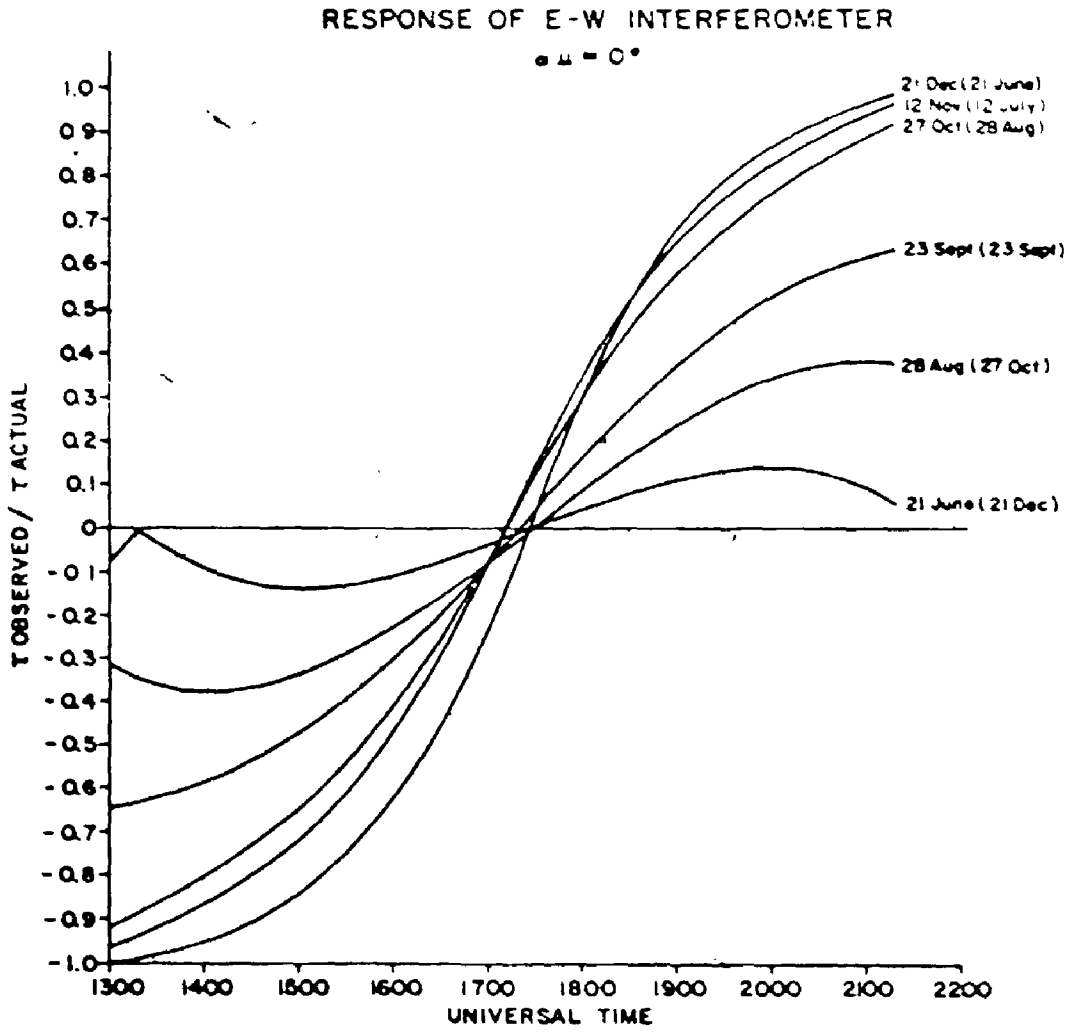

FIGURE 51: Response of the E-W interferometers versus universal time for a number of days throughout the year with the observer located at London, Ontario. The dates indicated in the brackets refer to an observer on the same meridian as London but at 43° S latitude.

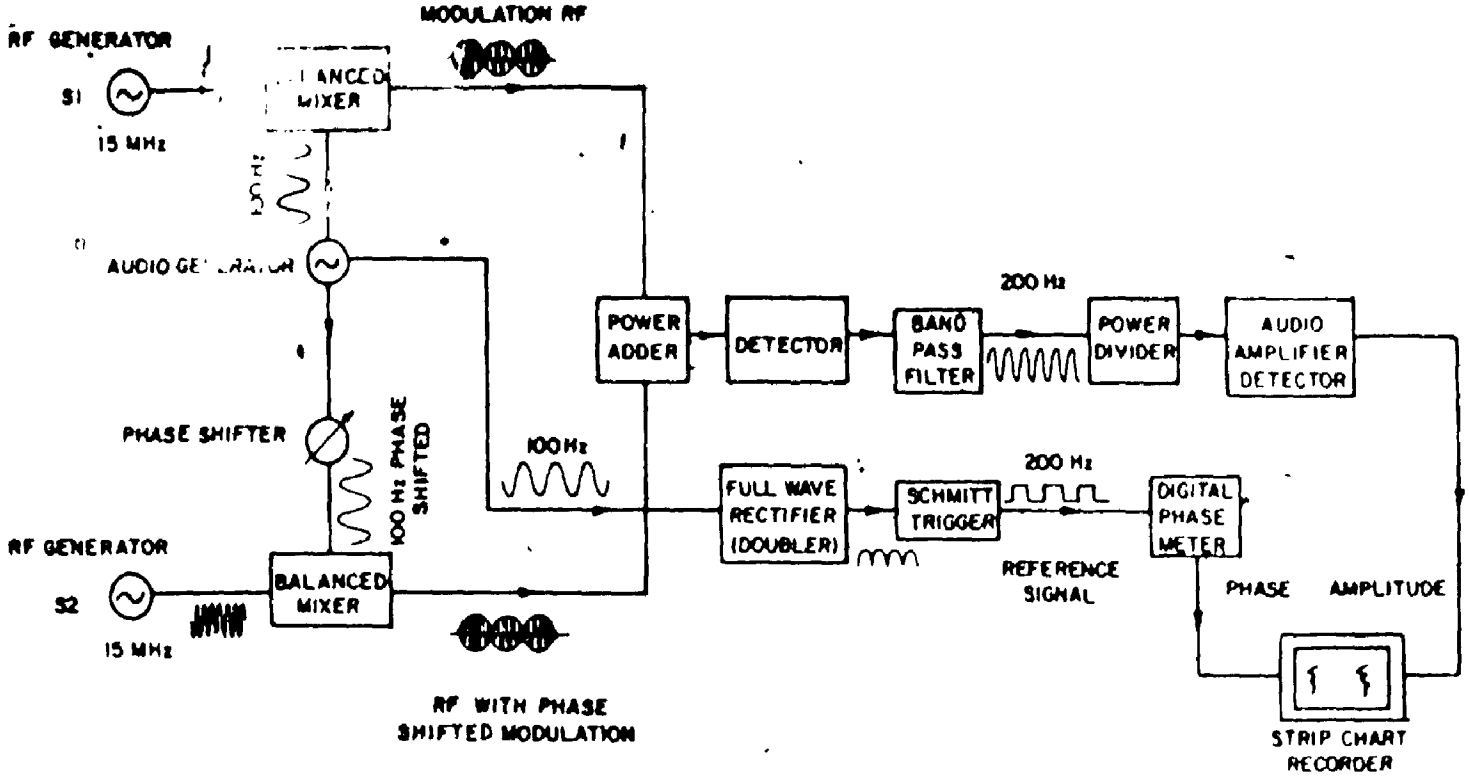

FIGURE 52: Schematic of instrumentation used to simulate an interferometer monitoring two sources.

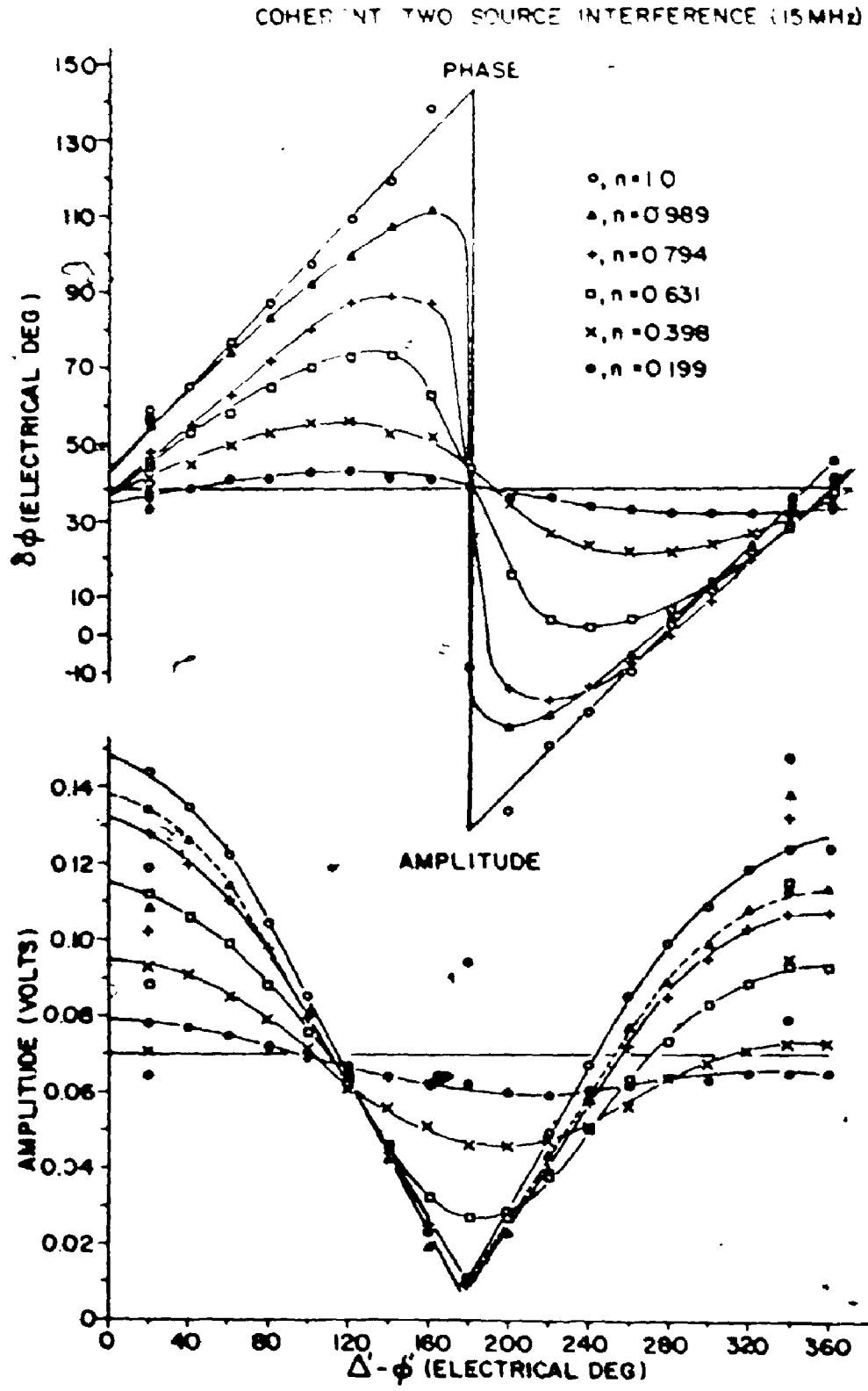

FIGURE 53: Amplitude and phase variations for two coherent sources.

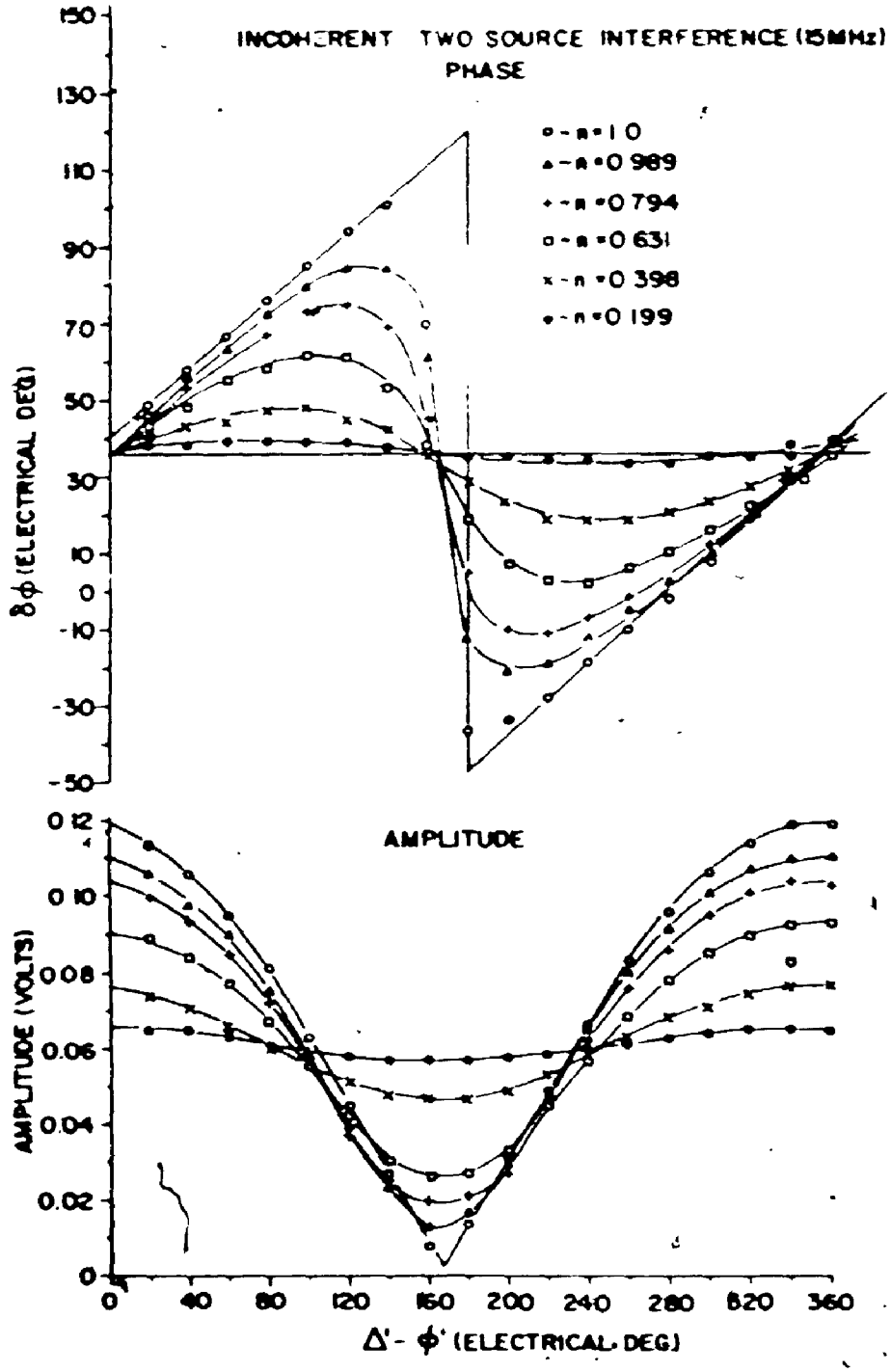

FIGURE 54: Amplitude and phase variations for two incoherent sources.

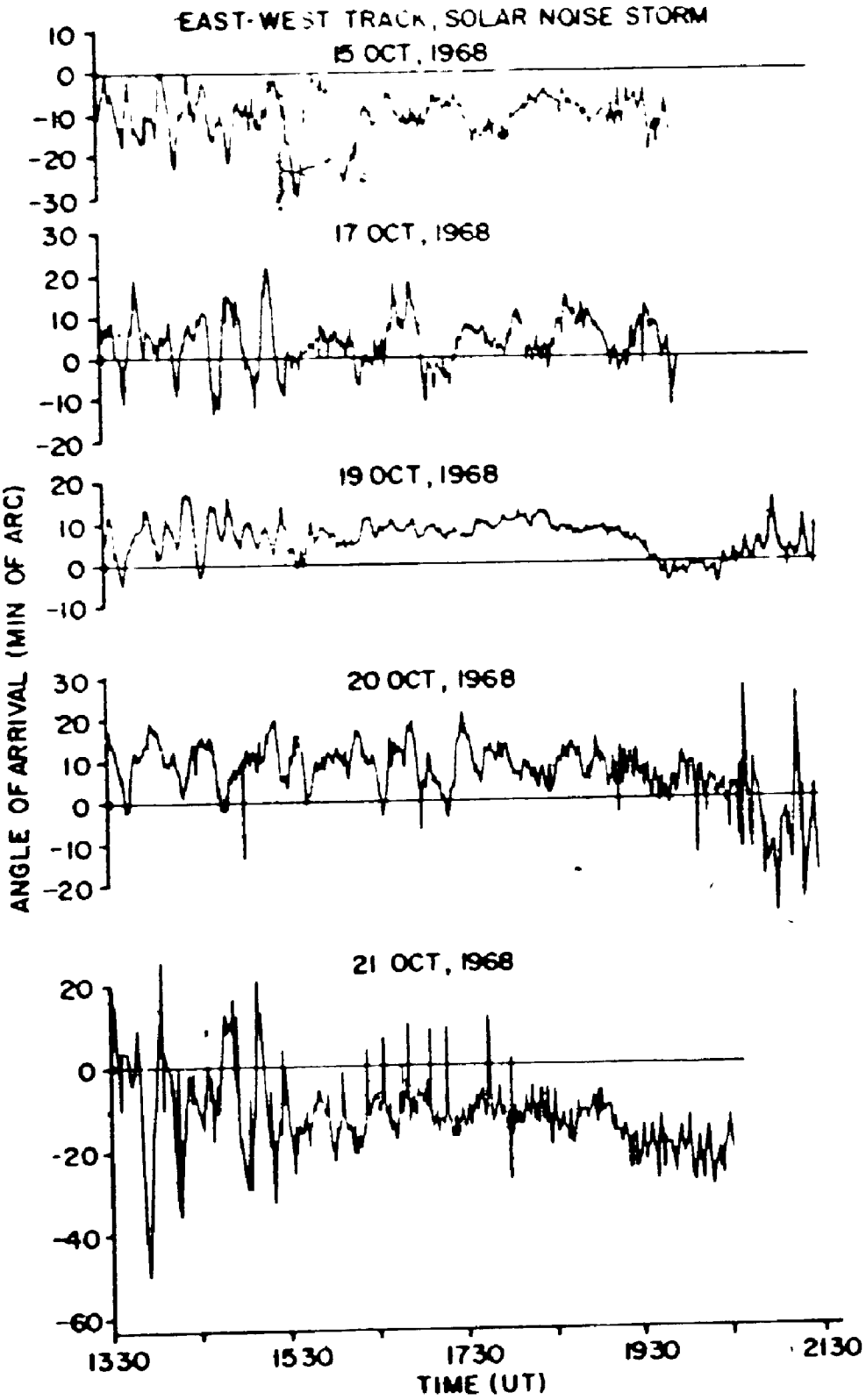

FIGURE 55: Angle-of-arrival measured by the wide E-W interferomter on 15, 17, 19, 20 and 21 October 1968

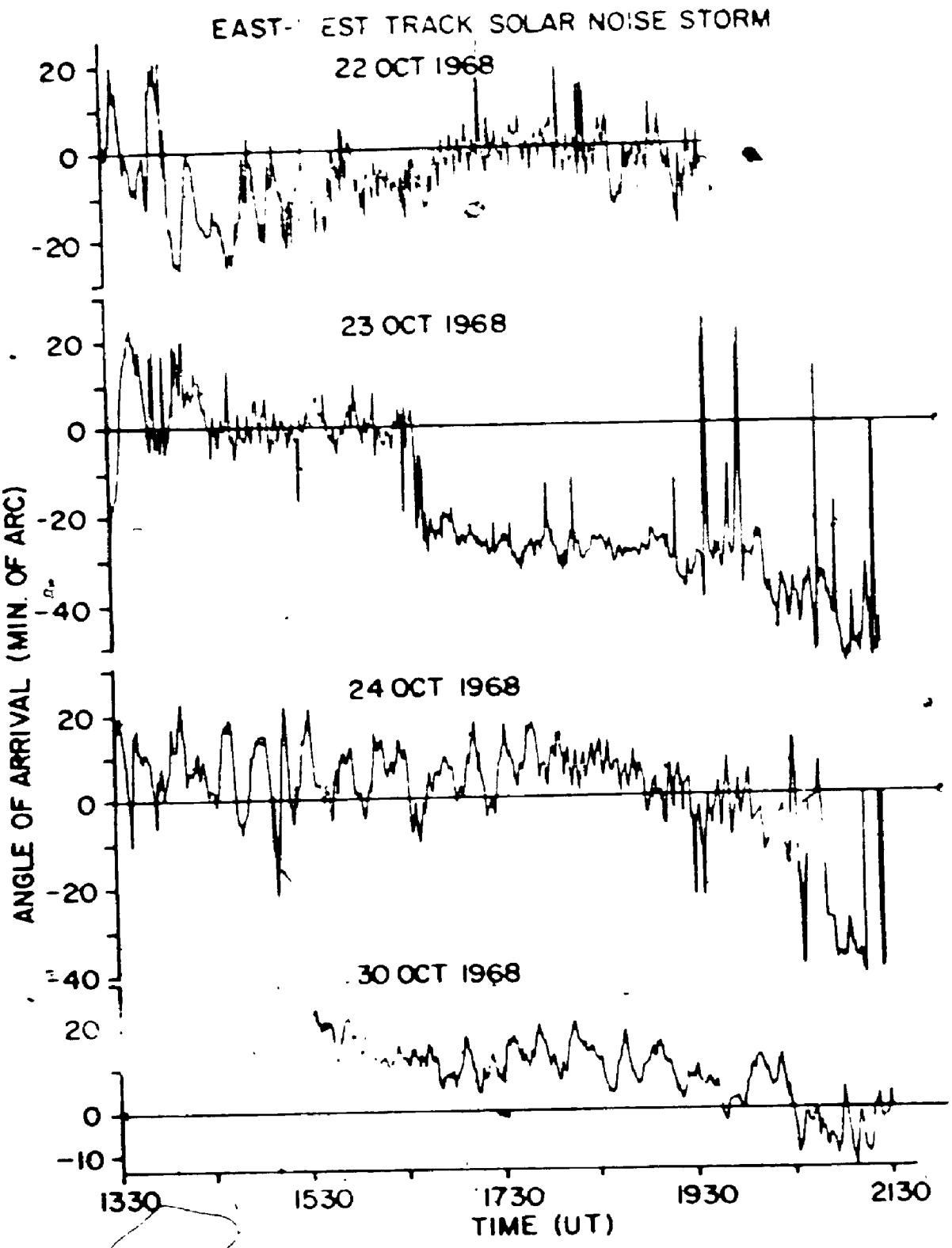

FIGURE 56: Angle-of-arrival measured by the wide E-W interferometer on 22, 23, 24 and 30 October 1968.

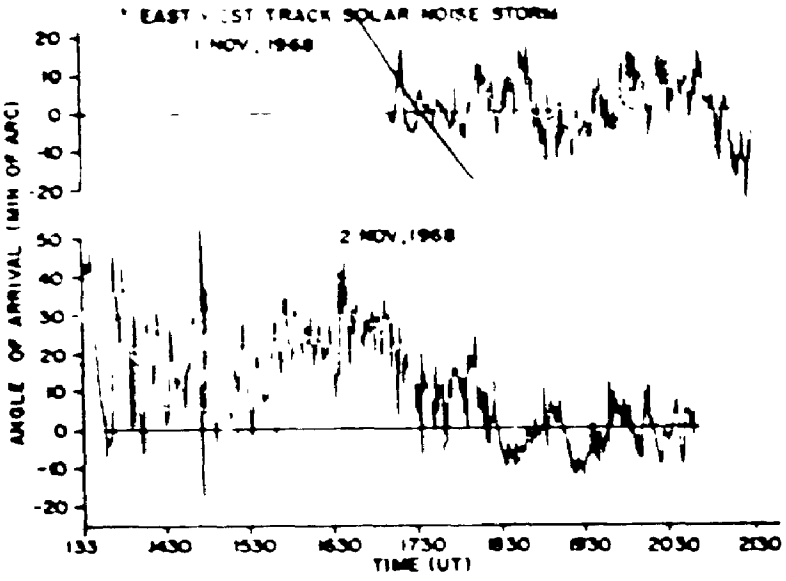

FIGURE 57: Angle-of-arrival measured by the wide E-W interferometer on 1 and 2 November 1968.

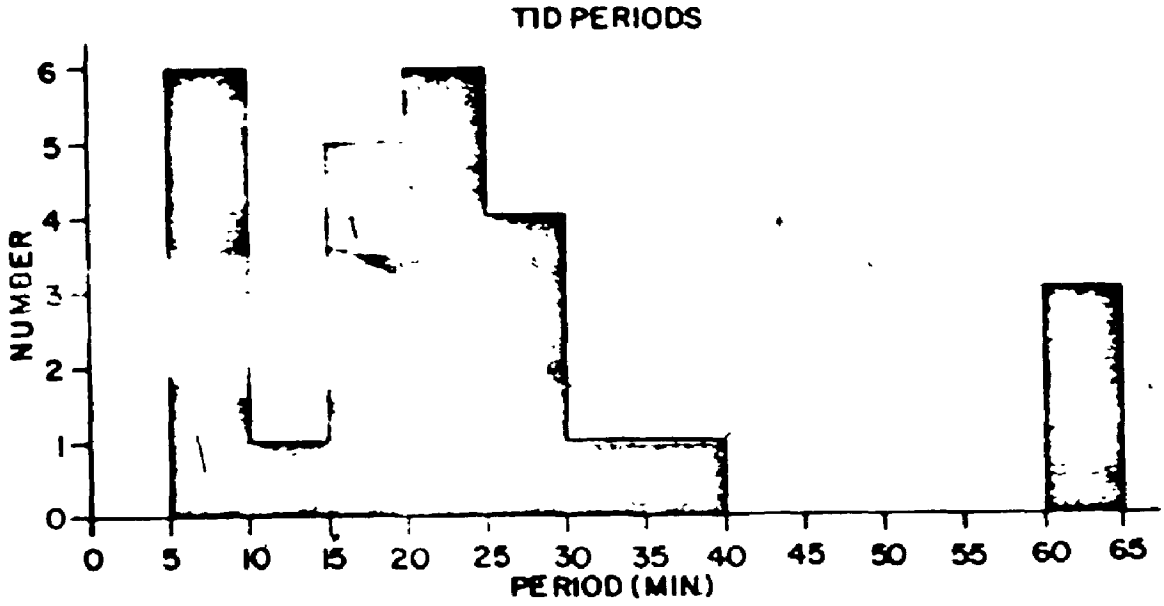

FIGURE 58: Histogram of observed TID periods.